Doctoral Degree Reviewed
by Ritsumeikan University

Development and Application of Capacitive Deionization System

（電気二重層を用いた溶液中のイオン除去システムの開発と応用）

March, 2015

2015 年 3 月

Doctoral Program in Integrated Science and Engineering
Graduate School of Science and Engineering
Ritsumeikan University

立命館大学大学院理工学研究科総合理工学専攻博士課程後期課程

ANDRES GINNO LIZANO
アンドレス　ジーノ　リザーノ

Supervisor : Professor Yoshihara Yoshinobu
研究指導教員：教授　吉原 福全

博士論文要旨

論文題名：電気二重層を用いた溶液中のイオン除去システムの開発と応用

立命館大学大学院理工学研究科
総合理工学専攻博士課程後期課程

あんどれす　じーの　　りざーの
ANDRES GINNO LIZANO

逆浸透膜法に比べてより高いエネルギー効率と低い運転コストを有する電気二重層イオン除去（CDI）法について研究を行った。我々は電気二重層イオン除去システムのために，単純で安価な親水性活性炭ベースの電極の開発を行い，その電気化学的特性を調査した。開発された電極の電気化学的プロパティは三電極サイクリックボルタンメトリー分析から，化学処理による親水性を高めることで電極の静電容量を増加できることを示した。 また，アノードとカソードの電極容量を，電極の自然電位と溶液（水）の酸化還元電位との差に基づいて定め，非対称とすることで，電気化学反応が電極面で起こらない理想的な特性を得ることができることを明らかにした。 さらに，電極のイオン除去能力は，11mS/cm の導電率で NaCl 溶液を使って評価した結果，2.5：1 の（アノード：カソード）厚み比率による電極において，0.034 モル/m^2 まで高いイオン除去能力を示した。

開発した活性炭電極を積層した CDI スタックについて，ユニポーラおよびバイポーラ接続によるイオン吸着/脱着特性を評価し，バイポーラ回路による CDI スタックがユニポーラ回路のそれに比べて，約 30 %のエネルギーで稼働出来ることを実験に明らかにした。また，イオン吸着/脱着時の処理溶液のフローについて検討を行った結果，イオン吸着時に通液処理，電極再生時にバッチ処理を行う組み合わせが最も効率的にイオンを除去・濃縮できることを明らかにした。さらに，合計 8 つの CDI セルを用いて，イオン脱着時のエネルギーを他段のイオン吸着のエネルギーとしてエネルギー回生を行う手法について検討を行い，最高 81 %のエネルギー回生率を達成した。

近年，最終処分場の埋立容量の逼迫に伴い都市ごみ焼却残渣の資源化は喫緊の課題であり，焼却灰のセメント原料化が有望視され，受入も進みつつあるが，その受入量はセメント製造時に塩素を除去する塩素バイパス装置の能力によって制限されている。焼却灰のセメント原料化の更なる促進を目的として，焼却灰の水洗による脱塩システムとその洗浄廃液のクローズド化に本研究で開発した電気二重層イオン除去システムを応用し，本方式が逆浸透圧膜(RO 膜)法など既存技術に比べてエネルギー効率および運転経費の面で優れていることを明らかにした。

Abstract of Doctoral Thesis

Title : Development and Application of Capacitive Deionization System

Doctoral Program in Integrated Science and Engineering
Graduate School of Science and Engineering
Ritsumeikan University

あんどれす　じーの　　りざーの
ANDRES GINNO LIZANO

Capacitive deionization (CDI) technique having higher efficiency and lower operation cost in comparison with the reverse osmosis technique was investigated. We have developed a simple and inexpensive hydrophilic activated-charcoal based electrode for capacitive deionizer cell system and examined its physical and electrochemical properties. The electrochemical properties of the developed electrode were characterized using a three-electrode cyclic voltammetry system, which showed that chemically modified activated-charcoal based electrodes demonstrated an increase in capacitance. An asymmetrical distribution of capacities of both electrodes was found to be ideal wherein no electrochemical reactions took place at the electrode surface. The electrode capacities were defined based on the difference between the rest potential of the electrodes and the oxidation-reduction potential of the solution. Furthermore, the ion removal capacity of the electrode was evaluated using NaCl solution with a conductivity of 11 mS/cm. The electrode with a thickness ratio of 2.5:1 (anode: cathode) exhibited high ion removal capacity up to 0.034 mol/m^2.

The ion adsorption/desorption mechanisms of CDI stack equipped with the developed activated-charcoal electrodes, having either uni-polar or bi-polar circuit structures, were evaluated. The experimental results showed that the CDI stack with a bi-polar circuit consumes 70 % less energy than of that with a uni-polar connection. As for operation of the processing fluid, a combined flow-through and batch processing operation for ion adsorption and desorption processes shows the best working efficiency for throughput. Furthermore, the energy recovery by discharging the stored energy of the ion desorbing electrode pair to another pair for ion adsorption by switching four-CDI cells for both the discharge and the charge sides was 81 % at the maximum.

In Japan, 50 million tons of municipal solid wastes (MSW) are incinerated and 10 % of residual incineration ashes are buried in landfills. However, landfills are becoming difficult and problematic due to high cost, environmental issues, lack of available land and strict laws. To promote recycling of an incineration ash as a raw material for cement plants, the closed washing system of incineration ashes for removing chloride has been investigated by applying a developed CDI system. It is demonstrated that CDI system has higher efficiency and lower operation cost in comparison with the reverse osmosis technique.

Table of Contents

CHAPTER 1

INTRODUCTION

1.1 General background

In recent years, researches related to flow-through capacitors also known as capacitive deionization (CDI) technique, has been very attractive due to the increasing worldwide demand of water purification and energy conservation[1-3]. Although it is still in its infancy, capacitive deionization accompanying with energy regeneration by charge sequestering has a potential to resolve both water and energy shortages[4,5]. Fig. 1.1 demonstrates the principle of capacitive deionization. Generally, capacitive deionization follows the electric double layer principle[6-8]. When electric potential is imposed on a porous electrode, ions are adsorbed onto the electrode pore surface layer through electrostatic interaction force between the ions and electrode without the aid of electrochemical reactions[9]. CDI is primarily affected by the ion solution concentration (aqueous electrolyte resistance), active surface area of carbon electrode (the double-layer capacitance) and the applied potential[10]. Essentially, CDI process is operated in low potentials ranging from 0.8 to 1.4 V to avoid electrochemical reactions or water electrolysis between electrode/solution interfaces. Furthermore, once the electrode reaches its maximum ion adsorption capacity and the electrode pores are saturated with ions, the adsorbed ions can be easily desorbed or discharged by simply reversing the applied potential or short-circuiting the parallel electrodes[11]. One of the key advantages in CDI is that the stored energy at the electrodes that are electrically charged can be reused for another ion adsorption/desorption process using an optimized energy recovery system. The capacitive deionization technique could be used as an alternative to other water treatment technologies. *Anderson et al.* (2010)[5] postulated that if an efficiency of over 85 % can be attained for CDI, it could become a serious competitor to reverse osmosis (RO), not only for brackish water but also for seawater desalination. The operation in CDI was regarded as an environmentally friendly operation because there is no need to use chemicals during electrode regeneration. This technique is a simple and nearly maintenance-free system. In addition, by utilizing the energy recovery system, the running cost in CDI is more cost-effective than RO. In fact, the energy needed to desalinate seawater in reverse osmosis is 3.5 to 2.5 kWh/m^3 with <30 to 40 % water recovery, whereas in CDI with 80 to 90 % water and energy recovery, would require only 2 to 1 kWh/m^3. Thus, CDI is three times more economical than RO for the treatment of 1 million gallons per day of brackish water[12].

Many researches concerning the use of CDI technique for water purification have reported, particularly on the development of electrode with novel materials that have high electrical conductivity and high ion removal capacity. Carbon aerogel is one of the promising materials for CDI due to its low electric resistance of less than 40 mΩ · cm. More recently, researchers focused on enhancing the ion removal capacity of the carbon

electrode by incorporating ion-exchange membrane and electrode-coated ion-exchange polymer[13-16]. Others focused on optimizing the CDI operation by investigating electrode reactions and ion adsorption/desorption mechanisms on the carbon electrode[17-20]. Even though the aforementioned carbon materials exhibited excellent physical and electrochemical properties with high ion removal performance for CDI application, these electrodes still suffer from their relatively complicated fabrication process. This results in a high cost of electrode material, thus limits its commercial application. *Choi* (2010)[21] has developed a relatively low-cost activated carbon powder-based electrode which composed of carbon powder and a polyvinylidenefluoride (PVDF) solution as a polymeric binder. The developed electrode exhibited good electrochemical property and ion removal capacity. Doing remarkable efforts and following the method of *Choi et al.* (2010)[2] for electrode fabrication, *Nadakatti et al.* (2011)[7] and *Hou et al.* (2012)[22] conducted investigations that aimed to enhance the electrosorption capacity by incorporating mesoporous carbon black (MCCB) and by morphological structure modification by chemical treatment.

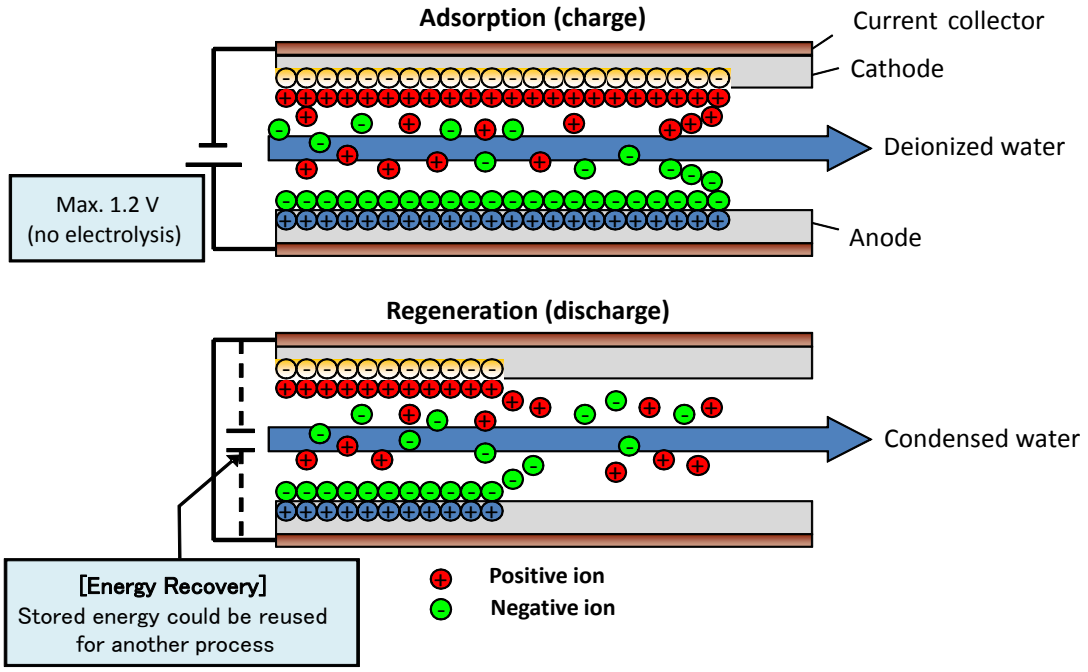

Fig. 1.1 - Capacitive deionization and electrode regeneration process.

1.2 Research objectives

Many researchers have conducted with the goal of increasing the efficiency of the CDI process, especially by experimenting many ways to increase the adsorption capacity of the electrodes. Porous carbon materials constitute very attractive electrodes for CDI processes because of their high specific surface areas and good electrical conductivities.

Specifically, the objectives of this research were to (1) fabricate a porous activated charcoal-based electrode using activated carbon powder, conductive carbon black and polymeric binder, (2) characterize the physical and electrochemical property of the electrode, (3) evaluate the ion adsorption and desorption capacity of the developed electrode, (4) design an optimized capacitive deionizer system and fabricate a CDI stack system, (5) investigate the ion adsorption and desorption performance of the CDI stack system with respect to its processing conditions, such as flow-through, batch and combination of flow-through and batch processing, (6) investigate the CDI performance of the CDI stack system depending on its polar circuit connections, (7) evaluate the ability of the CDI system to recover the energy stored in the carbon electrodes and reused for another ion adsorption process, and (8) use the developed CDI stack system to examine the ion adsorption capacity of the fabricated electrode using the prepared rinsed water from incineration bottom ash.

References

1. Andelman M. (2011) *Separation and Purification Technology*, **80**, 262-269.
2. Choi J. Y. and Choi J. H. (2010) *Journal of Industrial and Engineering Chemistry*, **16**(3), 401-405.
3. Oren Y. (2008) *Desalination*, **228**, 10-29.
4. Park K. K., Lee J. B., Park P. Y., Yoon S. W., Moon J. S., Eum H. M. and Lee C. W. (2007) *Desalination*, **206**, 86-91.
5. Anderson M., Cudero A. L. and Palma J. (2010) *Electrochimica Acta*, **55**, 3845-3856.
6. Lim J. A., Park S. P. and Choi J. H. (2009) *Desalination*, **238**, 37-42.
7. Hou C. H., Huang J. F., Lin H. K. and Wang B. Y. (2012) *Journal of the Taiwan Institute of Chemical Engineers*, **43**(3), 473-479.
8. Farmer J. C., Fix D. V., Mack G. V., Pekala R. W. and Poco J. F. (1996) *Journal of Electrochemical Society*, **143**(1), 159-169.
9. Oh H. J., Lee J. H., Ahn H. J., Jeong Y., Kim Y. J. and Chi C. S. (2006) *Thin Solid Films*, **515**(1), 220-225.
10. Foo K. Y. and Hameed B. H. (2009) *Journal of Hazardous Materials*, **170**, 552-559.
11. Park B. H., Kim Y. J., Park J. S. and Choi J. (2011) *Journal of Industrial and Engineering Chemistry*, **17**(4), 717-722.
12. Welgemoed T. J. and Shutte C. F. (2005) *Desalination*, **183**(1-3), 327-340.
13. Biesheuvel P. M. and Wal A. (2010) *Journal of Membrane Science*, **2**(346), 256-262.
14. Kim Y. J. and Choi J. H. (2010) *Water Research*, **44**(3), 990-996.
15. Lee J. B., Park K. K., Eum H. M. and Lee C. W. (2006) *Desalination*, **196**, 125-134.
16. Liang P., Yuan L., Yang X., Zhou S. and Huang X. (2013) *Water Research*, **47**, 2523-

2530.
17. Choi J. H. (2010) *Separation and Purification Technology*, **70**(3), 362-366.
18. Choi J. Y. and Choi J. H. (2010) *Journal of Industrial and Engineering Chemistry*, **16**(3), 401-405.
19. Lee J. B., Park K. K., Yoon S. W. and Park P. Y. (2009) *Desalination*, **237**, 155-161.
20. Lee J. H., Bae W. S. and Choi J. H. (2010) *Desalination*, **258**(1-3), 159-163.
21. Choi J. H. (2010) *Separation and Purification Technology*, **70**(3), 362-366.
22. Nadakatti S., Tenduklar M. and Kadar M. (2011) *Desalination*, **268**(1-3), 182-188.

CHAPTER 2

REVIEW OF RELATED LITERATURE

In order to gain more knowledge about the existing water purification technologies and to clarify that capacitive deionization could be used as an alternate to these existing one, it is imperative to review the latest technologies and the current development of the capacitive deionization technology.

2.1 Theory of Electric Double Layer (EDL)

When an external electrostatic field is imposed to the surface of the electrodes immersed in an aqueous electrolyte solution, charged ions are forced to move towards the oppositely charged electrodes. The resulting formation is known to be the electric double layers.

Studies on the concept of electric double layers started in 1879 when a chemist named of a *Herman Von Helmholtz* first developed and modeled an electric double layer in the study of colloidal suspension. Since then, studies on electric double layer had been extended until when General Electric claimed a patent in 1957 and later SOHIO in 1966. Today, high performance electric double layer capacitors are widely used[1,2].

Basically, when two porous electrodes were applied with a potential, the negatively charged electrode would attract the positively charge ions, while the negatively charge ions would be drown to positively charged electrode thus forming an electric double layer. Electric double layer phenomenon was first proposed more than 100 years ago by *Herman Von Helmholtz*. He proposed that the interface between the electrode and an electrolyte solution behaves like a capacitor, which is capable of storing electric charge. In his theory the surface charge of the electrode is balanced with a layer of oppositely charge ions as exhibited in Fig. 2.1(a)[3]. Between 1910 - 1913 *Louis George Gouy* and *David Chapman* proposed the Gouy-Chapman theory, which states the diffuse double layer model that assumed the dependence of the measured capacity on both potential and electrolyte concentration. They also assumed that the ions do not intermingle with each other[4,5].

Although the theory of Gouy-Chapman model showed considerable improvement over Helmholtz model, they failed to explain the actual capacity-potential curves found from their experiment. Fig. 2.1(b) illustrates the Gouy-Chapman model. In 1924, a simple development was obtained in the double-layer theory, which was proposed by *Otto Stern*. The Stern model was more realistic in describing the physical condition at the interface. *Stern* suggested the combination of Gouy-Chapman-Stern model which is commonly used today. This model assumed that the charge on the solution side resided partially in a compact layer (Helmholtz charge), and the remainder in a diffuse region (as in the Gouy-Chapman model) as shown in Fig. 2.1(c)[6].

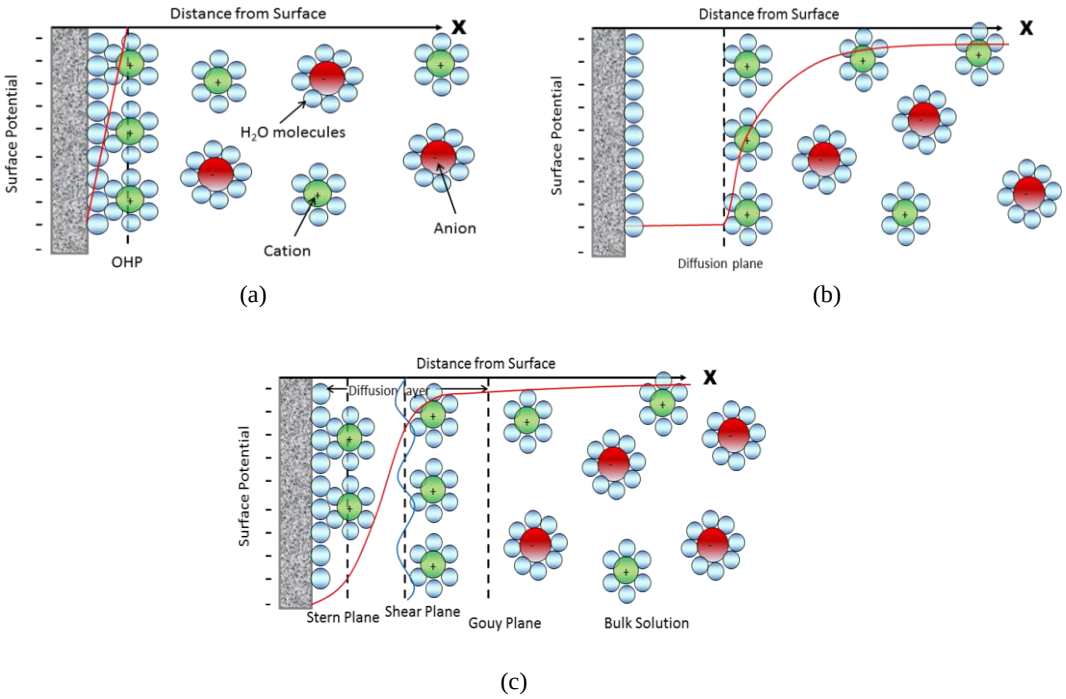

Fig. 2.1 - EDLC models: (a) Helmholtz model, (b) Gouy-Chapman model and (c) Stern model.

Both CDI and EDL capacitors perform ion adsorption (charging) and ion desorption (regeneration) processes forming an electric double layer. On the other hand, the required properties of the electrode in CDI are different from EDLC. In EDLC, the condition of the aqueous electrolyte is in stagnant state, whereas salty water solution flows between the electrodes in capacitive deionization. Therefore, electrode for CDI must acquire higher mechanical shear strength than that of EDLCs.

.

2.2 Previous works on Capacitive Deionization (CDI)

CDI was first studied in the mid 1960s and the early 1970s. The idea was first introduced by the team of *Caudle et al*. in 1966[7] who made an electrode using activated carbon powder. Later, the group of *Johnson* and *Newman*[8] performed an intensive studies and published a complete theoretical analysis of ion adsorption on porous carbon electrode[2]. The study on capacitive deionization reappears in the late 1900s by the team of *Farmer* using carbon aerogel electrodes[9-11]. They demonstrated that using higher surface area carbon electrodes ranging 400 - 1,000 m^2/g, CDI can vigorously compete with other desalination technologies such as evaporation, reverse osmosis, electrodialysis and ion-exchange. Since *Farmer* focused on developing an electrode for capacitive deionization, many researchers were exploring by studying a capacitive behavior of activated carbon, activated carbon cloth, carbon nanotubes and carbon nanofibers[2,12-25]. These material have a

large specific surface areas of about 1,000 - 2,000 m^2/g due to the volume of micro and active mesopores with a particle size ranging of 2 - 10 nm in diameter.

One major challenge in capacitive deionization is the fabrication of a carbon electrode with high hydrophilic property. In the case of activated carbon powder, hydrophobic binders were usually used, which results in lower capacity of the electrode. Various studies had been done for the fabrication of carbon electrode with high hydrophilic property. *Lim et al.* (2008)[26] increased the electrosorption capacity of the fabricated electrode by using the wet phase inversion technique. After casting the slurry on the graphite current collector, the cast film was immersed in pure water for 24 h where the exchange occurred between the solvent (NMP) and non-solvent (pure water). *Lee et al.* (2009)[27] fabricated and investigated an electrode with hydrophobic property, enhanced the carbon electrode by changing its property into hydrophilic by employing ion-exchange resin and observed 35 % enhancement in performance. In 2010, *Park* and *Choi*[28] developed a carbon electrode by using a water soluble polymeric binder, polyvinyl alcohol (PVA) and compared to a hydrophobic binder polvinylidene difluoride (PVDF). They observed that the *ac*-signal was able to charge more inner surface area in the PVA-bonded electrode because of its higher hydrophilic property than that of PVDF-bonded electrode. In the same year, *Kim* and *Choi*[29,30] fabricated a carbon electrode coated with cation-exchange polymer, crosslinked with a PVA binder with sulfosuccinic acid so as to enhance the desalination performance of capacitive deionization system. The desalination efficiency of the developed electrodes (Membrane-CDI) was enhanced by 27 - 56 % in comparison to a conventional CDI cell, depending on the processing condition. Various surface modification promises higher efficiency of the electrode. *Lee et al.* (2011)[31] reported a noble electrode prepared by embedding ion exchanger onto the surface of a carbon cloth electrode. Based on their study, the drawbacks of a membrane-CDI system enable to overcome using the developed advanced membrane CDI system (A-MCDI) by reducing the interfacial resistance between ion exchanger layer and the carbon electrode. Currently, several studies emerge largely focused on evaluation of capacitive deionization process such as system optimization and operating conditions modification to evaluate the most suitable process and explained according to theoretical principle[32-42]. More recently, studies concerning energy consumption and energy recovery during regeneration process of the CDI system have been conducted. *Dlugolecki* and *van der Wal* (2014)[43] systematically evaluated the charge and discharge mechanism according to the applied current. Also, the energy recovery at a low concentration solution was examined using a membrane CDI stack wherein exhibited energy recovery of 83 %.

In this research, the energy recovery process of the developed CDI system was conducted. We demonstrated, for the first time, how the sequestered energy of the charge cells was effectively reused for another ion adsorption process by controlling the circuit sequence of the CDI system. The energy recovery process we described in this study can be a useful guide in optimizing a CDI device operation.

2.3 Capacitive deionization and other desalination technologies

Most of the major desalination processes in the world are based on variations of evaporation and distillation. However, these thermal processes require abundant heat and huge amount of energy. Despite of large amount of energy requirement, thermal processes are still reasonable for seawater desalination since large production could be achieved with reasonable investments in capital equipment. Electrodialaysis and reverse osmosis system are more energy efficient, but require expensive and troublesome membranes. In the following sections, different desalination processes are outlined. Thermal separation techniques consist of two main categories – (a) evaporation followed by condensation of the formed water vapor and (b) freezing followed by melting of the formed ice crystals. Evaporation process is the most common in desalination, and in most cases it is tied with power generation units.

The evaporation processes include multistage flash desalination (MSF), multiple-effect distillation (MED), single-effect vapor compression, and solar distillation. Single-effect vapor compression includes mechanical vapor compression (MVC), thermal vapor compression (TVC), absorption vapor compression (ABVC), and adsorption vapor compression.

Multistage flash distillation has a sequence of spaces called stages, each containing a heat exchanger and condensate collector. The sequence has a cold end and a hot end while in-between stages have intermediate temperatures. The stages have various pressures corresponding to the boiling points of water at the stage temperatures. After the hot end, there is a container called the brine heater. The total evaporation product for all the stages is approximately 15 % of the flowing in the system, depending on the range of temperatures used. Increase of scale formation and corrosion may take place with increasing temperature. 120 ˚C appears to be a maximum, even though scale avoidance may require temperatures below 70 °C.

Multiple-effect distillation is a process of distillation frequently used for seawater desalination. It consists of multiple stages or “effects” and each of these stages, the feed water is heated by steam in tubes. Some of the water evaporates, and this stream flows into the tubes for the next stage, and continuously heating and evaporating. The energy supplied is reused to evaporate more water, but the process takes much longer time. The amount of water distilled per stage is directly proportional to the amount of energy transport.

Membrane water treatment systems were originally used only in desalination. These membranes used for water treatment are usually thin sheet materials that are able to separate contaminants based on properties such as size or charge of ions. Using membranes specifically reverse osmosis (RO) and nanofiltration could be a good technology for small scale water treatment in a variety of contaminants. However, this technology produces large quantity of concentrated waste water than most other water treatment technologies in as much as 15 % of the total treated water volume[44].

Reverse osmosis (RO) is the process of forcing a solvent from a region of high solute concentration through a semi-permeable membrane to a region of low solute concentration by applying a pressure in excess of the osmotic pressure. This has a dense barrier layer in the polymer matrix where most separation takes place. The membrane was designed to

allow only water to pass through this dense layer, while preventing the passage of solutes such as Na^+ and Cl^- ions. RO system is generally classified according to pressure used such as, 800 - 1,500 psi (lb/in^2) for sea water, 400 - 600 psi for standard pressure, 200 - 300 psi for low pressure and 45 - 150 psi for nanofiltration. The minimum energy required for desalinating brackish water with 1,500 - 2,000 ppm TDS has been estimated to be about 2.1 - 3.1 Wh/gal (2.0 - 2.9 kJ/L)[13].

In electrodialysis (ED), ionic impurities are separated from the water by an imposed electric potential that forces the ions to migrate through the ion exchange membrane. However, electrodialysis has limitation in comparison with reverse osmosis. In electrodialysis, low molecular weight ions could be removed from the solution while high molecular weight ionic components are not significantly removed. In addition, oxygen and hydrogen take place by electrolysis at the anode and cathode. Electrodialysis reversal (EDR) is another version of ED with period of voltage reversal in order to decrease the scale formation and fouling. Periodically, the direction of ion flow is reversed by reversing the polarity of applied electric current. According to *Farmer* (1995)[9] it was assumed that the required energy for EDR per 1,000 ppm TDS (total dissolved solids) was about 2.0 Wh/gal (1.9 kJ/L), with additional 2.5 Wh/gal (2.4 kJ/L) for the pump and an allowance of 5 % for instrumentation. Hence, it was estimated that the required energy to desalinate a 1,500 - 2,000 ppm TDS was approximately 5.8 - 6.8 Wh/gal (5.5 - 6.5 kJ/L) for brackish water and about 76 Wh/gal (72 kJ/L) for seawater.

Capacitive deionization (CDI) technology is a new exciting method of removing ionic components from the solution specifically for seawater and brackish water. This technology can also be used for various applications such as water softening, because it could adsorb divalent ions which include Mg and Ca, removal of nitrates, ammonium ions from brackish water, treating brackish water containing oil compound and removal of ionic metals with high molecular weight such as ferric ions from water[29,30,45,46]. CDI is a non-membrane technology which is capable for desalinating seawater and treats ionic liquids. This technology uses low energy as compared with other technologies since the occurrence of faradaic reaction must not be observed. This technology may be classified as energy efficient. In addition, CDI is environmentally friendly because no secondary wastes are formed during regeneration process. Table 2.2 shows the required energy for desalination technology. From the previous studies, capacitive deionization indicated advantage from other technologies, specifically from membrane processes. The energy required to desalinate and treat seawater as well as brackish water is approximately 16 - 32 Wh/gal and 0.2 - 0.4 Wh/gal, respectively[11]. Further discussion on capacitive deionization will be tackled in Chapter 3.

Table 2.2 - Energy requirement for desalination technology.

Desalination Technology	Energy Requirement*
Mechanical Vapor Compression (MVR)	6.6 kW/m^3 (25 Wh/gal) – Sea Water
Multiple Effect Distillation with Mechanical Vapor Compression (MED-MVR)	7.9 – 10.8 kWh/m^3 (30-41 Wh/gal) – Sea Water
Multiple Effect Distillation with Thermal Vapor Compression (MED-TVR)	56.8 – 83.2 kWh/m^3 (215-315Wh/gal) – Sea Water
Multi Stage Flash Evaporation (MFE)	84.5 kWh/m^3 (320 Wh/gal) – Sea Water
Reverse Osmosis (RO) (Depending on energy recovery)	6.6 – 9.3 kWh/m^3 (25-35 Wh/gal) – Sea Water 2.3 kWh/m^3 (8.5 Wh/gal) – Brackish Water
Electrodialysis	2.03 kWh/m^3 (7.7 Wh/gal) – Brackish Water
CDT (Include Energy Recovery)	4.2-8.5 kWh/m^3 (16-32 Wh/gal) – Sea Water 0.05-0.1 kWh/m^3 (0.2-0.4 Wh/gal) – Brackish Water

*Brackish Water TDS: 800 - 3,200 mg/L and Seawater TDS: 35,000 mg/L
Adopted from Welgemoed and Schutte (2005)[13]

References

1. Pandolfo A. G. and Hollenkamp A. F. (2006) *Journal of Power Sources*, **157**, 11-27.
2. Oren Y. (2008) *Desalination*, **228**, 10-29.
3. von Helmholtz H. (1853) *Journal Analytical Physical Chemistry*, **89**, 211-233.
4. Gouy G. (1910) *Journal of Physics*, **9**, 457-468.
5. Chapman D. L. (1913) *Philosophical Magazine and Journal of Science*, **25**(148), 475-481.
6. Stern O. (1924) *Z Elektrochem Angew. Journal of Physical Chemistry*, **30**, 508-516.
7. Caudle D. D., Tucker J. H., Cooper J. L., Arnold B. B. and Papastamataki A. (1966) Electrochemical demineralization of water with carbon electrodes, Research Report, Oklahoma University Research Institute.
8. Johnson A. M. and Newman J. (1971) *Journal of Electrochemical Society*, **118**(3), 510-517.
9. Farmer J. C., Fix D. V., Mack G. V., Pekala R. W. and Poco J. F. (1995) UCRL-JC-121405.
10. Farmer J. C., Fix D. V., Mack G. V., Pekala R. W. and Poco J. F. (1996) *Journal of Electrochemical Society*, **143**, 159-169.
11. Farmer J. C., Bahowick S. M., Harrar J. E., Fix D. V., Martinelli R. E. and Vu A. K. (1997) *Energy Fuels*, **11**, 337-347.
12. Wada H., Nohara S., Furukawa N., Inoue H., Sugoh N., Iwasaki H., Morita M. and ,

Iwakura C. (2004) *Electrochemica Acta*, **49**, 4871-4875.
13. Welgemoed T. J. and Schutte C. F. (2005) *Desalination*, **183**, 327-340.
14. Xu B., Wu F., Chen R., Cao G., Chen S., Zhou Z. and Yang Y. (2008) *Electrochemistry Communications*, **10**, 795-797.
15. Yan C., Zou L. and Short R. (2012) *Desalination*, **290**, 125-129.
16. Peng Z., Zhang D., Shi L. and Yan T. (2012) *Journal of Material Chemistry*, **22**, 6603-12.
17. Nie C., Pan L., Liu Y., Li H., Chen T. and Lu T. (2012) *Electrochim Acta*, **66**, 106-109.
18. Dai K., Shi L., Fang J., Zhang D. and Yu B. (2005) *Materials Letters*, **59**, 1989-1992.
19. Li H., Pan L., Zhang Y., Zou L., Sun C. and Zhan Y. (2010) *Chemical Physics Letters*, **485**, 161-166.
20. Zhang D., Shi L, Fang J., Dai K. and Li X. (2006) *Materials Chemical Physics*, **97**, 415-419.
21. Presser V., Heon M. and Gogotsi Y. (2011) *Advanced Functional Materials*, **21**, 810-833.
22.Wang X. Z., Li M. G., Chen Y. W., Cheng R. M., Huang S. M. and Pan L. K. (2006) *Electrochemical Solid-State Letters*, **9**, E23-E26.
23. Dai K., Shi L., Zhang D. and Fang J. (2006) *Chemical Engineering Science*, **61**, 428-433.
24. Zhang D., Yan T., Shi L., Peng Z., Wen X. and Zhang J. (2012) *Journal of Material Chemistry*, **22**, 14696-14704.
25. Li H., Pan L., Lu T., Zhan Y., Nie C. and Sun Z. (2011) *Journal of Electroanalytical Chemistry*, **653**, 40-44.
26. Lim J. A., Park N. S., Park J. S. and Choi J. H. (2008) *Desalination*, **238**, 37-42.
27. Lee J. B., Park K. K., Yoon S. W. and Park P. Y. (2009) *Desalination*, **237**, 155-161.
28. Park B. H. and Choi J. H. (2010) *Electrochemica Acta*, **55**, 2888-2893.
29. Kim Y. J. and Choi J. H. (2010) *Water Research*, **44**, 990-996.
30. Kim Y. J. and Choi J. H. (2010) *Separation Purification Technology*, **71**, 70-75.
31. Lee J. Y., Seo S. J., Yun S. H. and Moon S. H. (2011) *Water Research*, **45**, 5375-5380.
32. Suss M. E., Baumann T. F., Bourcier W. L., Spadaccini C. M., Rose K. A., Santiago J. G. and Stadermann M. (2012) *Energy Environmental Science*, **5**, 9511-9519.
33. Porada S., Sales B. B., Hamelers H. V. M. and Biesheuvel P. M. (2012) *Journal of Physical Chemistry Letters*, **3**, 1613-1618.
34. Haro M., Rasines G., Macias C. and Ania C. O. (2011) *Carbon*, **49**, 3723-3730.
35. Lee J. K., Kim Y. E., Kim J., Chung S., Ji D. and Lee J. (2011) *Journal of Industrial Engineering Chemistry*, **18**, 763-766.
36. Porada S., Bryjak M., van der Wal A. and Biesheuvel P. M. (2012) *Electrochimica Acta*, **75**, 148-156.
37. Li H., Nie C., Pan L. and Sun Z. (2011) *Shanghai International Nanotechnology Cooperation Symposium*, pp. 110-113.
38. Peng Z., Zhang D., Shi L., Yan T., Yuan S., Li H., Gao R. and Fang J. (2011) *Journal of Physical Chemistry*, **115**, 17068-17076.
39. Bouhadana Y., Avraham E., Noked M., Ben-Tzion M., Soffer A. and Aurbach D. (2011) *Journal of Physical Chemistry*, **115**, 16567-16573.

40 Biesheuvel P. M., Zhao R., Porada S. and van der Wal A. (2011) *Journal of Colloid Interface Science*, **360**, 239-248.
41. Avraham E., Noked M., Bouhadana Y., Soffer A. and Aurbach D. (2010) *Electrochimica Acta*, **56**, 441-447.
42. Noked M., Avraham E., Soffer A. and Aurbach D. (2009) *Journal of Physical Chemistry*, **113**, 21319-21327.
43. Dlugolecki P. and van der Wal A. (2013) *Environental Science & Technology*, **47**, 4904-4910.
44. Ettoune H. M., Dessouky E., Hisham T. and Imad A. (1999) *Chemical Engineering Progress*, **5**(9), 43-54.
45. Nadakatti S., Tenduklar M. and Kadar M. (2011) *Desalination*, **268**(1-3), 182-188.
46. Seo. S. J., Jeon. H., Lee. J. K., Kim. G. Y., Park. H. N., Lee. J. and Moon. S. H. (2010) *Water Research*, **44**(7), 2267-2275.

CHAPTER 3

DEVELOPMENT OF ACTIVATED CHARCOAL ELECTRODE

3.1 Introduction

Among the components in the CDI system, the electrode is the most crucial part because in order to fabricate the electrode especially when using activated charcoal powder, the electrode must obtain its optimum compositions. There are several considerations in electrode fabrication. First, the electrode must exhibit high mechanical shear strength for longer cyclic life. Second, the electrode must possess high hydrophilic property. This means that the electrode must be wettable enough to achieve higher ion adsorption capacity. Even if the fabricated electrode has high surface area but its active surface area does not come in contact with the aqueous solution, the active surface area would be useless and the adsorption capacity of the electrode would be low. And last, the electrode must have a high surface area with particularly active mesopore area for higher accommodation of ions.

An electrode in this study was fabricated by mixing activated charcoal powder (ACP), conductive carbon black (CCB), binder and a solvent. Recently, carbon aerogel was used as a carbon electrode for CDI, which exhibited high specific surface area of about 400 - 1,100 m^2/g with an electric resistance of less than 40 $m\Omega \cdot cm$. However, this electrode suffers from relatively complicated manufacturing process and a high manufacturing cost. On the other hand, ACP has been known as an inexpensive and good active material with high specific surface area of 1,000 - 2,000 m^2/g. Nevertheless, it is essential for ACP to compactly hold together using polymeric binder in order to manufacture the electrode. Accordingly, due to the addition of polymeric binder, the electric resistance of the electrode may be increase, which could be a cause of lower capacitance. The use of polymeric binder may increase the hydrophobicity of the electrode which would result in lower adsorption of ions. Conductive carbon black was used as electrically conductive material to improve the electrical conductivity of the electrode.

Moreover, the electrode for capacitive deionization must exhibit the following characteristics:

1. Large specific surface area available for ion capturing.
2. High electrical conductivity.
3. Fast response of the entire surface area to ion adsorption/desorption process changes.
4. Chemical and electrochemical stability and ability to tolerate voltage changes
5. Flexible for fabrication according to the designed requirements.
6. Low tendency for scaling, bi-fouling and organic fouling.

3.2 Materials and Methods

3.2.1 Fabrication of activated charcoal electrode

The carbon electrodes were fabricated by mixing activated charcoal powder (ACP, Dainen Corp., Japan, specific surface area: 1,964 m^2/g), conductive carbon black (CCB, Nippon Graphite Industries Ltd., Japan, SP-270, average particle size: 4 μm, BET surface area: 250 m^2/g), polyvinylidene difluoride (PVDF, Kureha Corp., Japan, W#1100) or polyvinyl-alcohol (PVA) and N-methyl-2-pyrrolidone (NMP, Nacalai Tesque Inc., Japan, 99.5 %). PVDF or PVA and NMP were used as the polymeric binder and organic solvent, respectively. As can be seen in Fig. 3.1, the screen printing technique was performed by directly pouring the slurry on a screen to form a solid activated charcoal electrode. The electrode was dried at room temperature for 24 h, followed by subsequent drying for 2 h each at 50 °C in a constant temperature oven and vacuum oven to evaporate all organic solvents in the electrode pores. The thickness of the dried electrode was then measured. The microstructures of the carbon electrode were modified by soaking it in alkaline electrolyzed water (pH 12) (Tanah Process Ltd., Japan) for 24 h. Hereafter, the electrode was washed by deionized water many times. Several electrode compositions were tried and evaluated using different polymeric binders such as Polytetrafluoroethylene (PTFE), Polyvinyl butyral (PVB), Styrene-butadiene (SBR), Polyvinylidene difluoride (PVDF) and Polyvinyl alcohol (PVA). In this study, PVDF and PVA showed better binding property particularly when the electrode was attached at a graphite sheet current collector. Also, various ACP: CCB: Binder compositions were used. Of all compositions tried, 15 % PVDF or PVA exhibited high ion removal efficiency and high mechanical strength. Details of the experiment are described elsewhere[1,2]. Thus, after a series of electrode fabrication it was found that the optimum composition of the electrode was 75 % ACP: 10 % CCB: 15 % PVDF or PVA mainly due to its high mechanical stability. The efficiency of the fabricated electrodes was evaluated using a manufactured single unit cell capacitive deionizer. To date, there has been no publication which used screen printing technique to manufacture carbon electrode for capacitive deionization process. Table 3.1 shows the novelty of the electrodes fabricated in previous studies.

Table 3.1. - Comparison of electrode compositions and physical characteristics from previous works.

Electrode	Park et al. (2007)	Nadakatti et al. (2011)	This study
Materials	ACP:CCB:PTFE	ACP:MCCB:PE	ACP:CCB:PVDF
Composition	84:12:4	70:10:20	75:10:15
Solvent	isopropyl alcohol	ultrapure water	NMP
Method	roll press	mold and compression	screen print
Anode thickness [μm]		300	70 - 550
Cathode thickness [μm]		300	220

ACP: activated charcoal powder, CCB: conductive carbon black, MCCB: mesoporous conductive carbon black, PVDF: polyvinylidene difluoride, NMP: N-methyl-2-pyrrolidone, PE: polyethylene

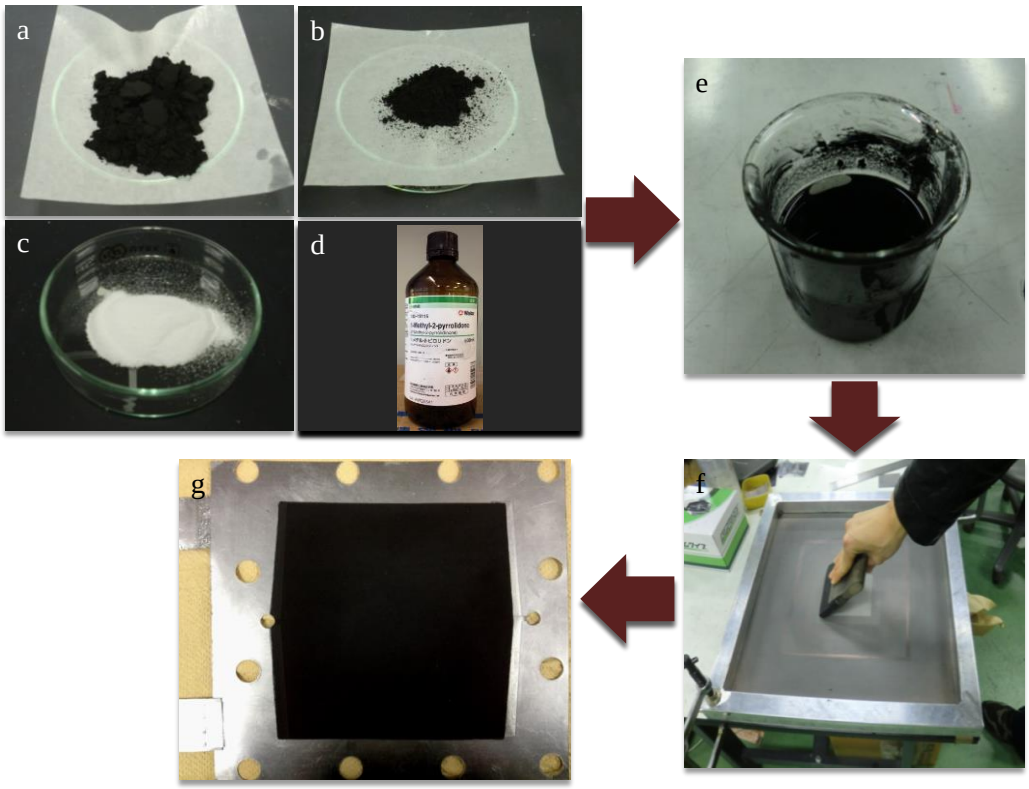

Fig. 3.1 - Active carbon-based electrode development: (a) activated charcoal powder (ACP), (b) conductive carbon black (CCB), (c) polymeric binder, (d) organic solvent (NMP), (e) carbon slurry, (f) screen printing and (g) active carbon-based electrode.

3.2.2 Physical characterization of the developed electrode

A scanning electron microscopy (SEM) (Keyence, Japan) was used to evaluate the physical microstructure of the developed activated charcoal electrode. Before analysis, the carbon electrode was dried in a constant-temperature oven at 50 ºC to ensure that the electrode is completely dry. The specimen was analyzed with an acceleration voltage of 5 kV and magnification of 230x. To assess the hydrophilic property of the developed electrode, approximately 0.5 mL of water was dropped on the electrode surface layer while capturing it using a high resolution camera. For deeper understanding regarding the developed electrode pore microstructure, nitrogen adsorption-desorption measurements were performed using an Autosorb 1 (Quantachrome Corp.) analyzer system at -196 ˚C (77 K). The specific surface areas of the carbon electrodes were measured using Brunauer-Emmett-Teller surface area analysis (BET).

3.2.3 Electrochemical characterization of the developed electrode

A galvanostatic charge and discharge instrument (Hokuto Denko Corp.) was used to examine the capacitance of the prepared electrode as a function of the applied voltage. A constant current of 100 mA was supplied to a pair of activated charcoal electrode, while the set maximum voltages ranging 0.8 - 1.5 V so as to complete the ion adsorption (charge) process. During ion desorption (discharge) process, the current was limited to 100 mA. In order to evaluate the effect of the ionic solution as well as the effect of *IR* drop on the electrode capacitance, the prepared NaCl solutions having ion concentrations ranging from 0.004 mol/L to 0.15 mol/L were prepared and used.

The resistance [Ω] was calculated according to the following equations:

$$R_{Expt.} = \frac{V}{I} \tag{3.1}$$

$$R_{NaClSol`n} = \frac{1}{\sigma} \cdot \frac{\ell}{\mathrm{A}} \tag{3.2}$$

where, R_{Expt} [Ω] represents the resistance calculated from the resulted *IR* drop evaluation experiment. The resistance of the solution was obtained using eq. (3.2) where σ [S/m] is the NaCl ion conductivity, ℓ [m] the distance between parallel electrode, and A (m^2) the effective area of the electrode.

The electrochemical properties of the fabricated carbon electrodes were characterized by three-electrode CV measurements using a potentiostat (HAL 3001, Hokuto Denco, Japan) at a 5 mV/s potential sweep rate in a 3.5 % NaCl solution at 25 ºC. A silver/silver chloride (Ag/AgCl) saturated KCl electrode was used as a reference electrode. By keeping the potential sweep rate 1/(dV/dt) constant, the capacitance *C* can be directly calculated as follows:

$$C = \int \frac{dt}{dV} \tag{3.3}$$

where i is the current, t time, and V voltage.

Fig. 3.2 illustrates the experimental set-up and schematic set-up of a three-electrode system when conducting a cyclic voltammetry analysis.

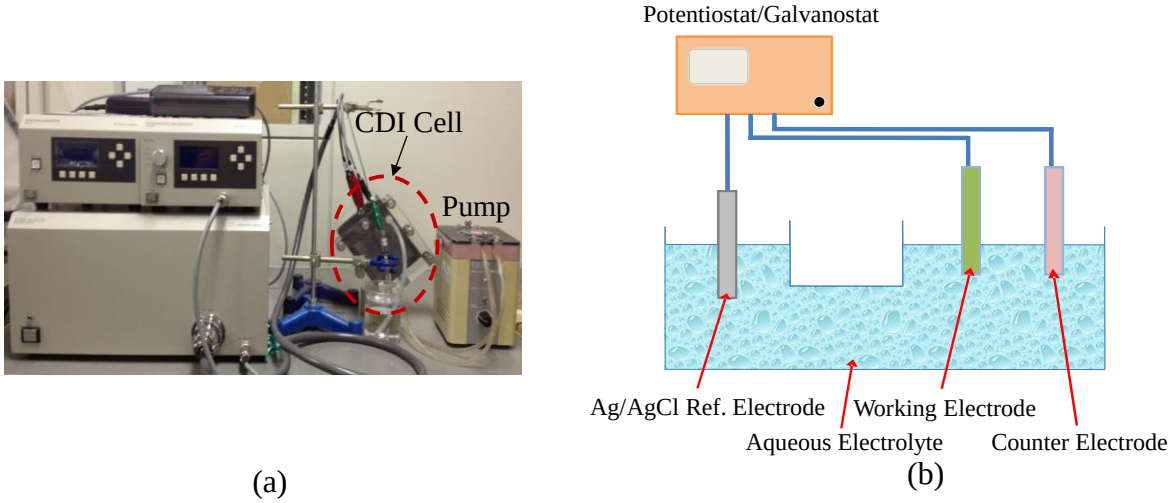

Fig. 3.2 - Cyclic voltammetry (a) experimental set-up and (b) schematic set-up of a three-electrode system.

3.3 Results and Discussion

3.3.1 Physical characterization of the developed electrode

3.3.1.1 Scanning Electron Microscopy (SEM) analysis

Figs. 3.3(a) and (b) show the SEM micrographs of the electrode surface and cross-sectional views, respectively. As shown in the figure, the electrode is permanently attached to a graphite sheet as a current collector, and the ACP is effectively bound together with agglomerated small and large pore sizes, thus a uniform electrode layer was formed. In fact, when the electrodes were rubbed by hand, the ACP did not fall off. Also, when the electrodes were placed in flowing water, the ACP easily got wet and remained intact.

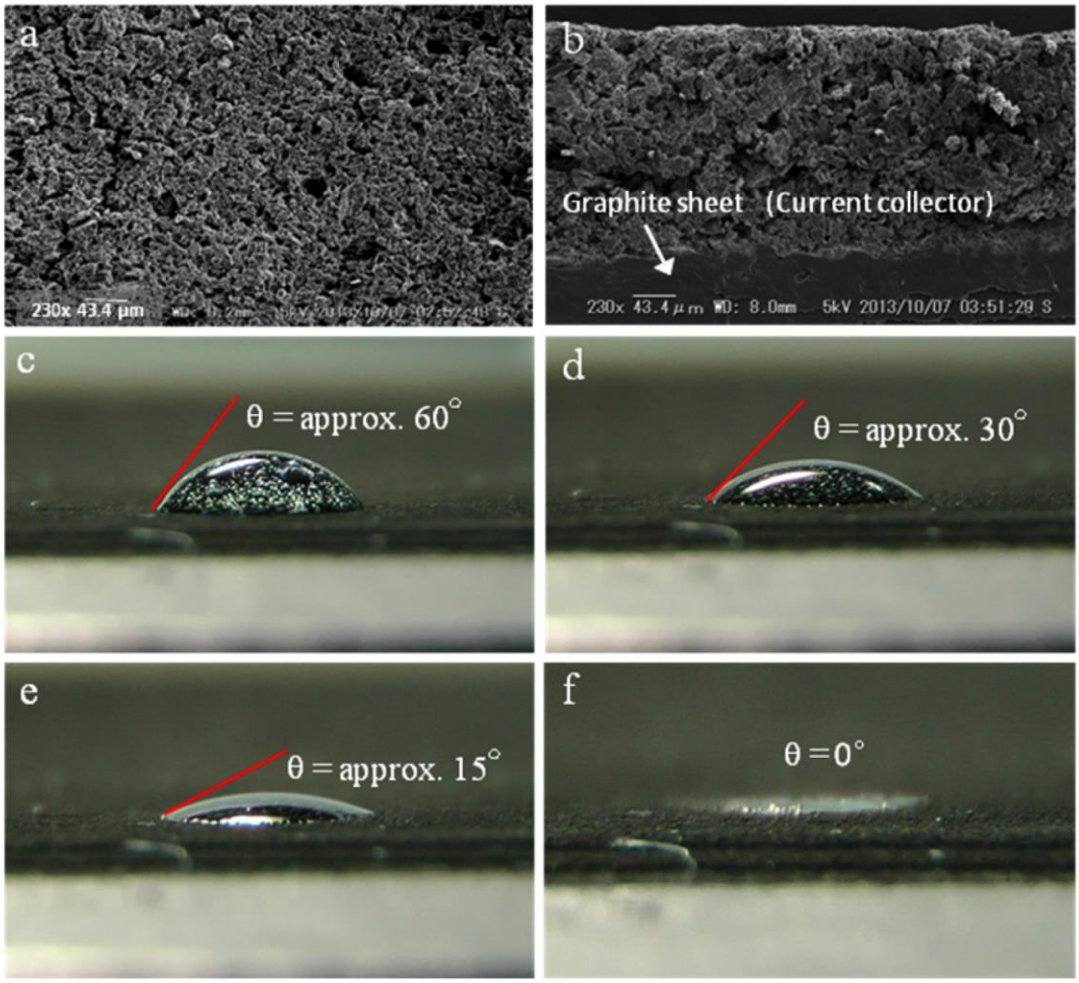

Fig. 3.3 - SEM (230x magnification) micrographs of developed electrode: (a) surface and (b) cross-sectional views. Contact angle images of a drop of water on the electrode at different times: (c) 1, (d) 2, (e) 3, (f) 4s.

3.3.1.2 Hydrophilic property evaluation

A high ion adsorption capacity electrode with a high hydrophilic property is ideal because it affects the total effective areas for ion accommodation during capacitive deionization process. As shown in Figs. 3.3(c) to (f), the water droplet on the electrode changes its contact angles by the time; it was dropped and immediately absorbed after 4 s. This indicates a high hydrophilic property of the carbon electrode. It is known that carbon functional groups such as carboxyl and carbonyl, and a hydroxyl group enhance the hydrophilic property of the electrode[5]. The contact angle observation and SEM micrographs validate that the fabricated electrode possesses strong hydrophilic property as well as a high mechanical strength.

3.3.1.3 Surface area analysis (BET method)

The surface structure analysis would give us direct information about the effective area of the carbon electrode. Theoretically, the capacitance of the carbon electrode is proportional to its specific surface area. However, only the surface of the pores that the ions can access can contribute to the double layer capacitance. Therefore, mesopores are more useful than micropores especially for ionic liquid electrolyte with larger ions. The carbon aerogel, carbon nanotubes and porous carbon were types of electrode materials used for CDI[6,7]. Although these carbon materials were prepared by various methods to have highly mesoporous structure, their capacitance is still not satisfactory due to their low specific surface area. Consequently, the carbon electrode for high performance should have high surface area, large pore volume and high hydrophilic property. Therefore, it is important to fabricate an electrode with pores that are large enough for the ions to access completely, but small enough to ensure a large surface area[8,9]. As shown in Fig. 3.4, the surface area of the carbon electrode increases along with increasing electrode thickness. The same trend was observed in ion removal capacity evaluation as shown in Fig. 3.5, wherein the ion removal capacity is strongly related with the electrode surface area and the electrode thickness. On the other hand, alkali-treated carbon electrode (PVDF 140 μm) illustrated higher surface area even though it is thinner than with the electrode with 150μm thickness. This result agrees well with its ion removal performance.

Fig. 3.5 shows a summary of the capacitive deionization performance evaluations. As expected, the electrode pair with the anode/cathode thickness ratio of $\delta_{anode}/\delta_{cathode}$ = 2.5 exhibited the highest ion adsorption capacity. The initial ion conductivity (11 mS/cm) was reduced to 9.73 mS/cm (0.034 mol/m^2), 9.97 mS/cm (0.026 mol/m^2) and 10.57 mS/cm (0.011 mol/m^2) for $\delta_{anode}/\delta_{cathode}$ = 2.5, 1.1 and 0.7, respectively, after repetitive charge and discharge processes. The change in ion conductivity indicates the adsorption and desorption of ions at the electrode's pores. The ion removal capacity of the alkali-treated carbon electrode (soaked in alkaline-electrolyzed water) was also analyzed. The $\delta_{anode}/\delta_{cathode}$ thickness ratio of electrode was 0.6 while indicated an ion removal capacity of 0.022 mol/m^2. Hence, it is relatively higher than the $\delta_{anode}/\delta_{cathode}$ = 0.7 thickness ratio. This result suggests that it is possible to increase the ion removal efficiency of the developed electrode by microstructure modification.

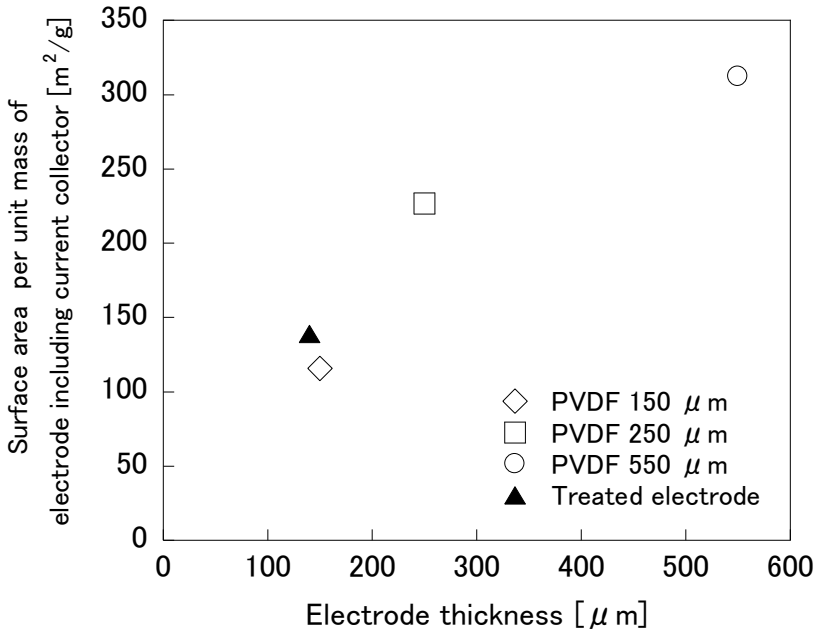

Fig. 3.4 - Specific surface area of carbon electrode per unit mass of electrode including current collector with respect to electrode thickness.

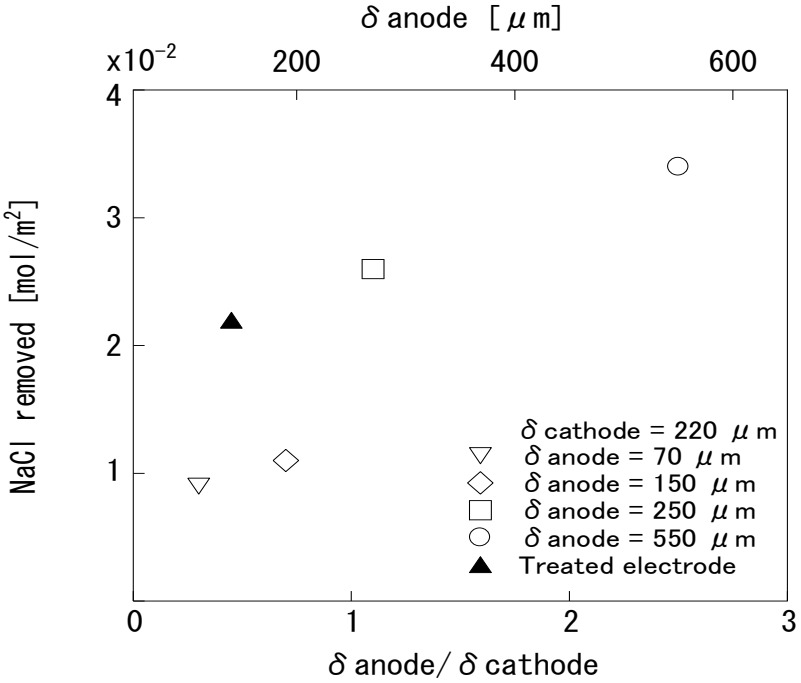

Fig. 3.5 - Capacitive deionization measurements of the carbon electrodes with various thickness (δ) ratios for 0.11 mol/L (11 mS/cm) NaCl aqueous electrolyte.

3.3.2 Electrochemical characterization of the developed electrode

3.3.2.1 Capacitance of the electrode as a function of applied voltage

Fig. 3.6 shows the variation of the electrode charge and discharge capacity at different maximum voltages. It clearly shows that the electrode has capability of adsorbing and desorbing ions. Also, the fabricated carbon electrode performance varies depending on its set maximum voltages for ion adsorption. Since oxidation and reduction potentials should be considered as important parameters in CDI process, it is essential to determine the highest maximum voltage where the electrode could sustain without chemical reactions.

3.3.2.2 Capacitance of the electrode as a function of ionic concentration of the solution

The fabricated carbon electrode was evaluated according to its specific capacitance and *IR* drop (voltage drop) at various NaCl solution concentrations as shown in Fig. 3.7. This was done to evaluate the resistance between electrode/electrolyte interfaces. In this experiment, the galvanostatic charge and discharge instrument was set to open circuit for 60 s after completing the charge cycle to examine the *IR* drop of the carbon electrode.

It shows that the *IR* drop decreases as the concentration of the NaCl solution increases. Table 3.2 shows the summary of the carbon electrode performance. Using eqs. (3.1) and (3.2), the calculated resistance agreed with the resistance resulted from the *IR* drop evaluation experiment.

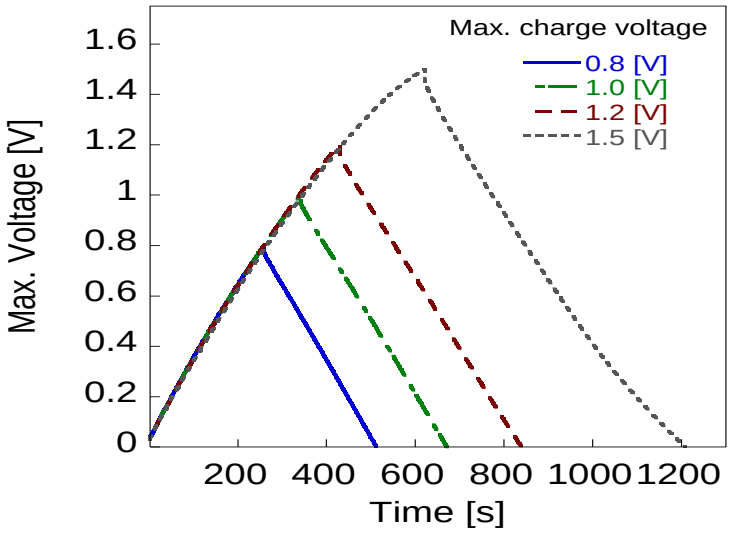

Fig. 3.6 - Capacitance evaluation of fabricated carbon electrode at different maximum voltages for 0.15 mol/L NaCl solution.

Hence, the concentration of the ionic solution affects the charging performance of the CDI cell. Therefore, it is essential to reduce the distance between a pair electrode at low concentration to control the resistance between the electrode/electrolyte interfaces. The resistance of the ionic solution at low concentration is high due to the low electrostatic force between ions in the solution.

Table 3.2 - Electrode performance and IR drop on various NaCl solution concentration.

NaCl concentration [mol/L]	Capacitance [F/m^2]	Charge [C]	IR Drop [V]	$R_{Expt.}$ [Ω]	$R_{NaClSol`n}$ [Ω]
0.004	388	1	0.308	3.078	3.086
0.010	1080	6	0.129	1.286	1.234
0.030	1378	10	0.042	0.423	0.412
0.150	1668	13	0.013	0.134	0.082

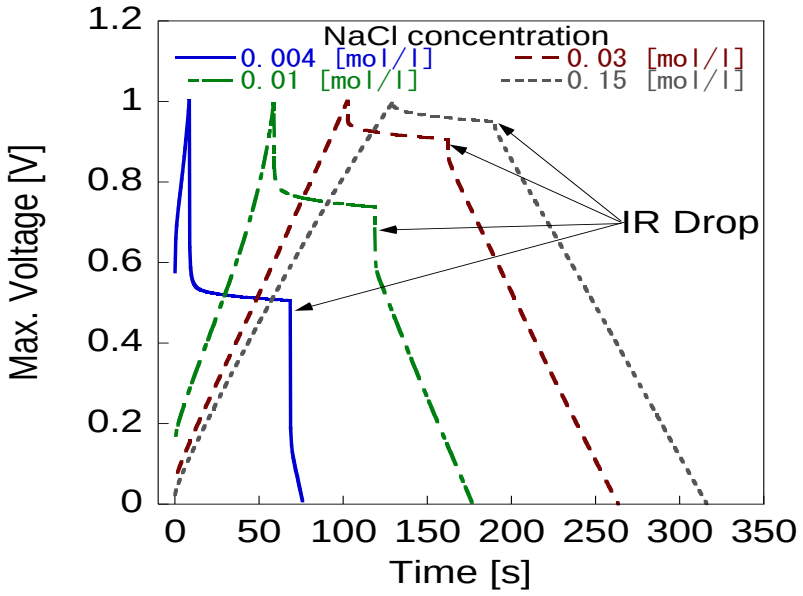

Fig. 3.7 - Capacitance and *IR* drop evaluation of fabricated carbon electrode at various electrolyte concentrations.

3.3.2.3 Cyclic Voltammetry (CV) evaluation

An ideal capacitor would demonstrate a rectangular shaped cyclic voltammograph wherein no oxidation/reduction will occur between electrode/electrolyte interfaces. Accordingly, it is known that the distortion of cyclic voltammograph is mainly caused by faradaic current and the charging resistance of the porous carbon electrode. Thus, smaller the resistance of the electrode, the more the cyclic voltammograph approaches to a rectangular shape. Fig. 3.8 shows an example of the electrode reactions when applied by an oxidation/reduction potential. Since the decomposition of water into hydrogen and oxygen may take place under the cell potential of 1.23 V. Therefore, capacitive deionization process should be carried out at a maximum potential of 1.2 V or lower. The chemical reaction formula of water electrolysis are represented in eqs. (3.4), (3.5) and (3.6).

Electrolysis of Water (H_2O)

Overall reaction: $2H_2O\ (l) \rightarrow 2H_2\ (g) + O_2\ (g)$ (3.4)

Reduction at cathode: $2H_2O\ (l) + 2e^- \rightarrow H_2\ (g) + 2OH^-\ (aq)$ (3.5)

Oxidation at anode: $2H_2O\ (l) \rightarrow O_2\ (g) + 4H^+\ (aq) + 4e^-$ (3.6)

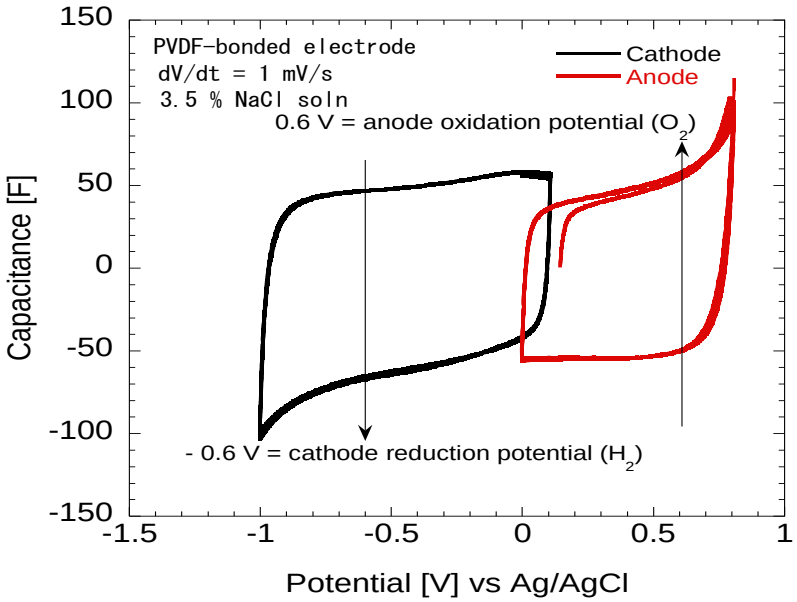

Fig. 3.8 – Oxidation/reduction evaluation of the prepared PVDF-bonded electrode.

As shown in Fig. 3.8, the anode oxidation takes place at a potential around 0.6 V while the cathode hydrogen reduction takes place at around - 0.6 V, in which the cyclic voltammographs of both electrodes deviated resulted to a distorted cyclic voltammographs. This indicates that the electrolysis of water did not occur within the potential margin of 1.2 V.

3.3.2.4 CV evaluation of the Polyvinylidene diflouride (PVDF)-bonded electrode

In these experiments, a carbon electrode (220 µm thick) was used as the auxiliary electrode (counter electrode) to carry out the cyclic voltammetry measurements.

As shown in Fig. 3.9, the capacities of the electrodes in potential windows from 0.2 - 0.6 V varied with increasing working electrode thickness. The capacitances of the carbon electrodes were as follows: 12, 28, 46, 57 and 88 F for carbon electrodes with thicknesses of 70, 150, 250, 290 and 550 µm, respectively. Since the rest potential (RP) of the fabricated carbon electrodes was around 0.14 - 0.20 V, the CV measurement started from 0.2 V. The results demonstrate that as the thickness increases, the capacitance also increases. Higher capacitance could indicate better electrosorption performance. In this evaluation, cyclic voltammographs show rectangular shape, which indicates that ions were adsorbed in a form of electrical double layer without chemical reactions within electrode/electrolyte interfaces. Nevertheless, CV of 550 µm thick electrode illustrated a rectangular shape with a little deviation, mainly due to the slow transient of ions into the high resistance micropores.

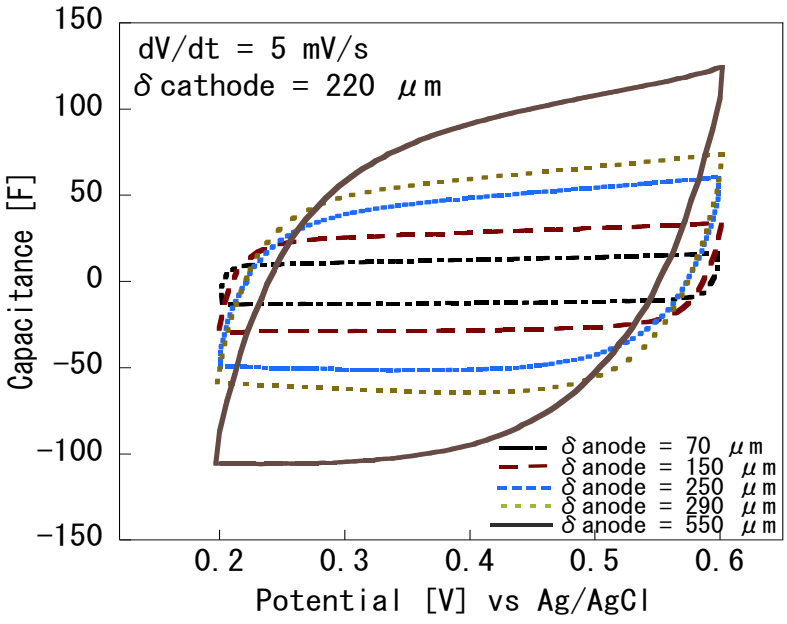

Fig. 3.9 - CV measurements of prepared carbon electrodes with different thicknesses.

3.3.2.5 CV comparison in PVDF and Polyvinyl Alcohol (PVA)-bonded electrodes

Cyclic voltammetry evaluations were conducted at 52 mS/cm NaCl solution conductivity. The potential window starts from 0.2 - 0.6 V since the developed electrode rest potential ranges from 0.14 to 0.20 V. Fig. 3.10 presents the CV measurements of the PVDF and PVA-bonded carbon electrodes at potential scan speed of 5 mV/s. Here, it is worthy of noting that the thickness of the carbon electrode affects its capacity. The capacitance of the PVDF-bonded carbon electrode shows the following trend: 88, 57, 46, 28 and 12 F for the electrode with thickness of 550, 290, 250, 150 and 70 μm, respectively. On the other hand, the PVA-bonded carbon electrode capacitance shows the following trend: 85, 44, 17 and 10 F for the electrodes with thickness of 340, 140, 80 and 40 μm, respectively. It is noticeable that the PVA-bonded electrode has higher capacitance than the PVDF-bonded electrode. For example, in the case of the 550 μm thick PVDF-bonded electrode its capacitance is almost equal to the 340 μm thick PVA-bonded electrode. Additionally, cyclic voltammograph illustrates that 550 μm thick PVDF-bonded electrode is steeper indication of high resistance. Consequently, the capacitance of the 140 μm thick PVA-bonded electrode is 36% higher than the capacitance for 150 μm thick PVDF-bonded electrode. This phenomenon indicates that the capacitance of the PVDF-bonded electrode was not proportional to its thickness and several high surface area micro-pores were not utilized for ion adsorption.

Investigation on the wettability (hydrophilic property) of the PVDF and PVA-bonded electrodes was also conducted. Figs. 2.11(a) and (b) demonstrate the SEM micrographs of the carbon electrodes. From here, PVA-bonded carbon electrode seems to have more pores than the PVDF-bonded electrode, since they were analyzed under the same acceleration voltage of 5 kV and magnification range of 230x.

Accordingly, the wettability of the carbon electrodes was characterized by measuring a water droplet on the carbon electrode surface layer as presented in Fig. 3.11(c) to (d). In previous experiment, in the case of PVDF-bonded electrode, the water droplet was absorbed after 4 s, whereas PVA-bonded electrode adsorbed the water droplet immediately. These results validate that the PVA-bonded electrode has better hydrophilic property than the PVDF-bonded electrode. Water soluble polymer like PVA can be a good candidate for increasing the hydrophilic property of the hydrophobic carbon electrode, as PVA is known to have a good membrane-forming properties and good chemical and thermal stability[10].

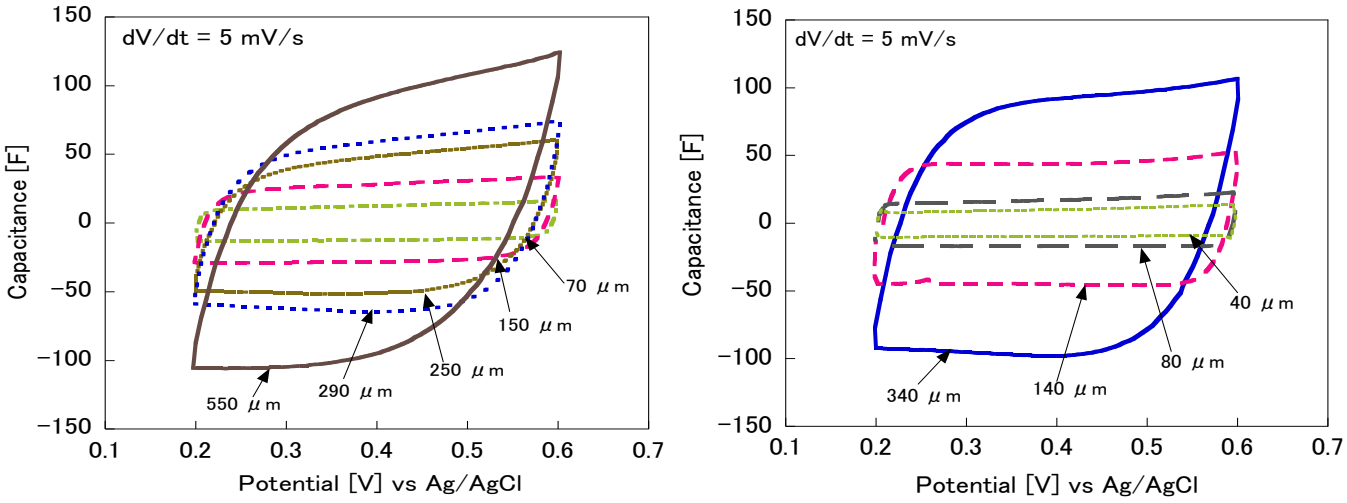

(a) (b)

Fig. 3.10 - CV measurements of prepared carbon electrodes with different thicknesses (a) PVDF-bonded carbon electrode and (b) PVA-bonded carbon electrode.

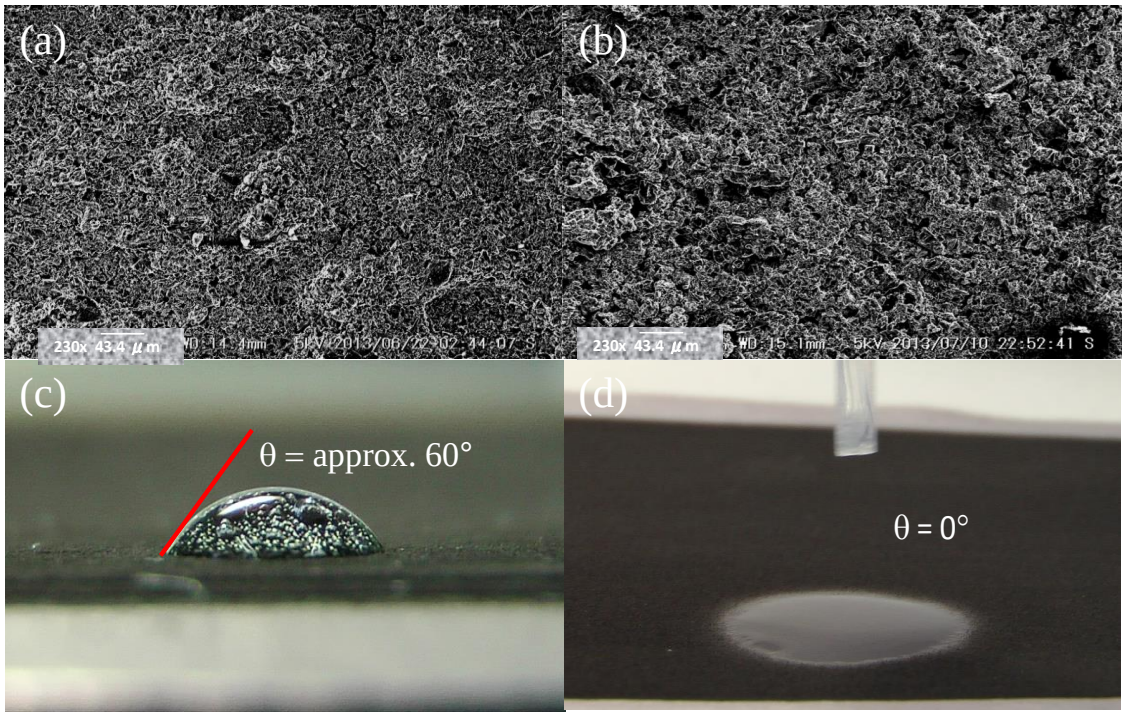

Fig. 3.11 - SEM micrographs of (a) PVDF-bonded carbon electrode and (b) PVA-bonded carbon electrode. Contact angle images of a drop of water on the (c) PVDF-bonded carbon electrode and (d) PVA-bonded carbon electrodes.

3.3.3 Comparison of non-treated and chemically modified electrode

As illustrated in Fig. 3.12, the electrochemical behaviors of non-treated and alkali-treated carbon electrodes were evaluated. The capacitance was calculated from the electrode rest potential to its peak current. The CV analysis was conducted in the potential range of −0.6−0.6 V with a scan speed of 10 mV/s for a 3.5 % NaCl solution. *Choi* and *Choi* (2010)[11] reported that the capacitance of carbon electrode can be slightly decreased as the amount of PVDF binder increases. This is because the PVDF polymeric binder is hydrophobic and could decrease the accessibility of the transient ions at the electrode pores. On the other hand, polymeric binder can be useful in preventing oxidation/reduction reaction at the surface of the electrode. To overcome the problem mentioned above, the electrode was treated with alkaline electrolyzed water. Previous works have modified their electrodes using strong base such as potassium hydroxide (KOH)[3]. The capacitance increased after soaking the electrode into alkaline electrolyzed water in which OH^- ions are abundant.

The rest potential of the carbon electrode was changed after alkali treatment from 0.17 V reduced to 0.018 V where the capacitance was increased up to 1.7 times. Moreover, as shown in Fig. 3.12, the cyclic voltammograph of the non-treated carbon electrode exhibited a slight distortion within negative potentials, which was assumed to be related to pseudo-Faradaic reaction between electrode/solution interfaces. In contrast, weak pseudo-capacitance was not observed in cyclic voltammograph of the alkali-treated electrode not only in the same potential range but also at lower potentials. This implies that some hydrophobic area of the carbon electrode was transformed into a more hydrophilic one,

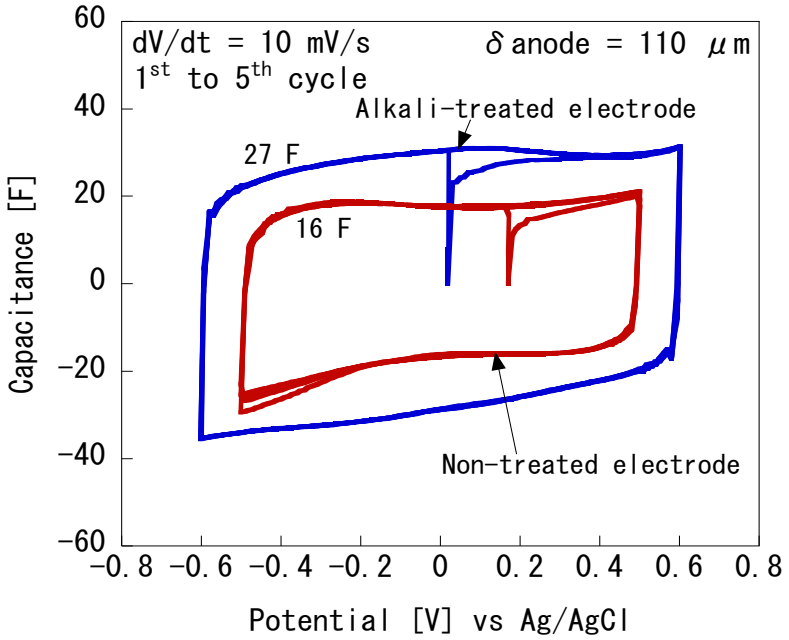

Fig. 3.12 - Effects of chemical treatment using electrolyzed water on capacitance.

mainly because of the effect of OH^- functional groups. Although the BET surface area analysis of alkali-treated electrode exhibited a slight improvement as can be seen in Fig. 3.4, its ion removal capacity was increased significantly as can be seen in Fig. 3.5. This indicates that since the hydrophilicity of the developed carbon electrode was enhanced by alkaline treatment, its effective surface area was also increased. In principle, even though the surface area of the carbon electrode is high, however if the liquid could not access through the carbon electrode meso and micro pores, high surface area is insignificant.

To examine further the electrode transformation phenomenon, ion-removal performance of the non-treated and alkali-treated carbon electrodes has been evaluated. In the case of the non-treated electrode, from 450 μS/cm of NaCl solution conductivity, it was reduced to an average conductivity of 190 μS/cm. The ion removal efficiency was 57 %.

On the other hand, treated carbon electrode exhibited an ion removal efficiency of 81 % (from 407 to 90 μS/cm). The result from ion removal evaluation is in good agreement with the cyclic voltammetry measurement. The ion removal efficiency, electrode capacity, and effective surface area of alkali-treated carbon electrode were higher than those of the non-treated carbon electrode. These results indicate that the property of the carbon electrode could transform from some hydrophobic surface area to a more hydrophilic property using alkaline electrolyzed water. This leads to increased ion removal efficiency.

3.3.4 Developed activated charcoal electrode capacity balance

The charge and discharge behaviors of the fabricated electrodes were determined by connecting the galvanostatic charge/discharge instrument to the potentiostat/galvanostat instrument as demonstrated in Fig. 3.13. The currents for the charge and discharge processes were kept constant at 100 mA, while the potentiostat/galvanostat instrument simultaneously was recording the charge/discharge data from the anode. The effective area of the paired carbon electrode was 90 mm x 90 mm.

Fig. 3.14 shows the oxidation/reduction potential of water against the standard Ag/AgCl electrode potential and the standard hydrogen electrode (SHE) potential, wherein the electrolysis of water takes place under a 1.23 V or more electrode gap. As mentioned above, the rest potential of the fabricated carbon electrodes was around 0.14 - 0.20 V, therefore, the anode has only a 0.42 - 0.48 V margin in potential against the oxidation. On the other hand, the cathode has a 0.75 - 0.80 V margin against the reduction. If the same electrode is used having the same capacities for anode and cathode, oxidation takes place around 0.84 - 0.96 V (0.42 - 0.48 V x 2), which results in a voltage loss wherein the potential gap up to the electrolysis of water (1.23 V) is not fully utilized for ion capturing. To compensate for this asymmetrical potential gap at anode and cathode, a pair of carbon electrodes with different capacities or different thicknesses would be more effective for capacitive deionization. The charging and discharging behaviors of the fabricated electrodes were studied in 0.11 mol/L NaCl solution, and were performed using the potentiostat and galvanostatic charge/discharge instrument.

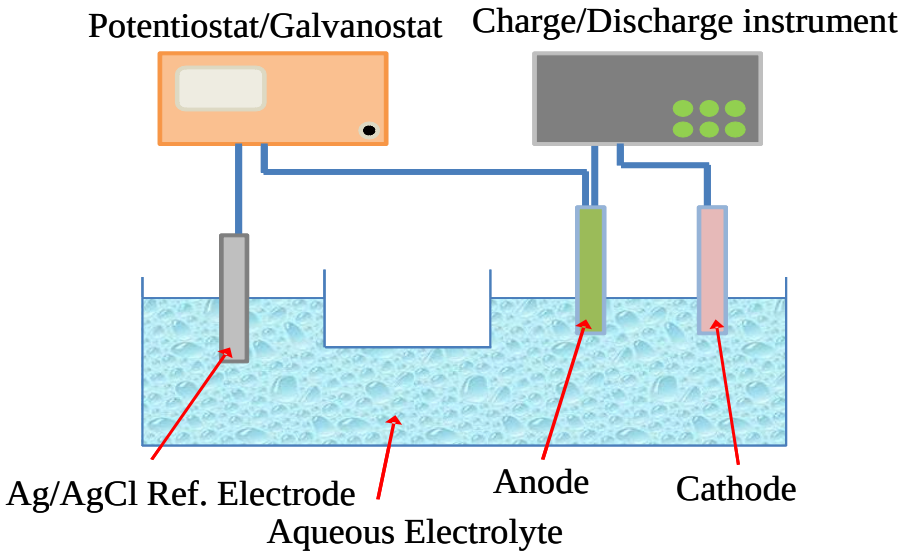

Fig. 3.13 - Schematic drawing of electrochemical set-up for voltage distribution analysis.

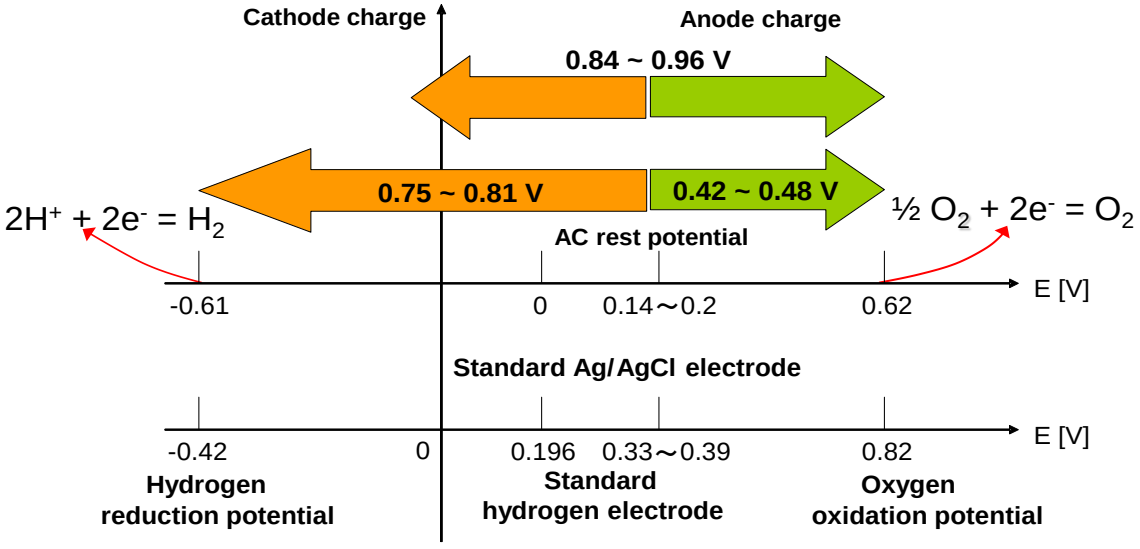

Fig. 3.14 - Oxidation-reduction potential standard for the developed electrodes.

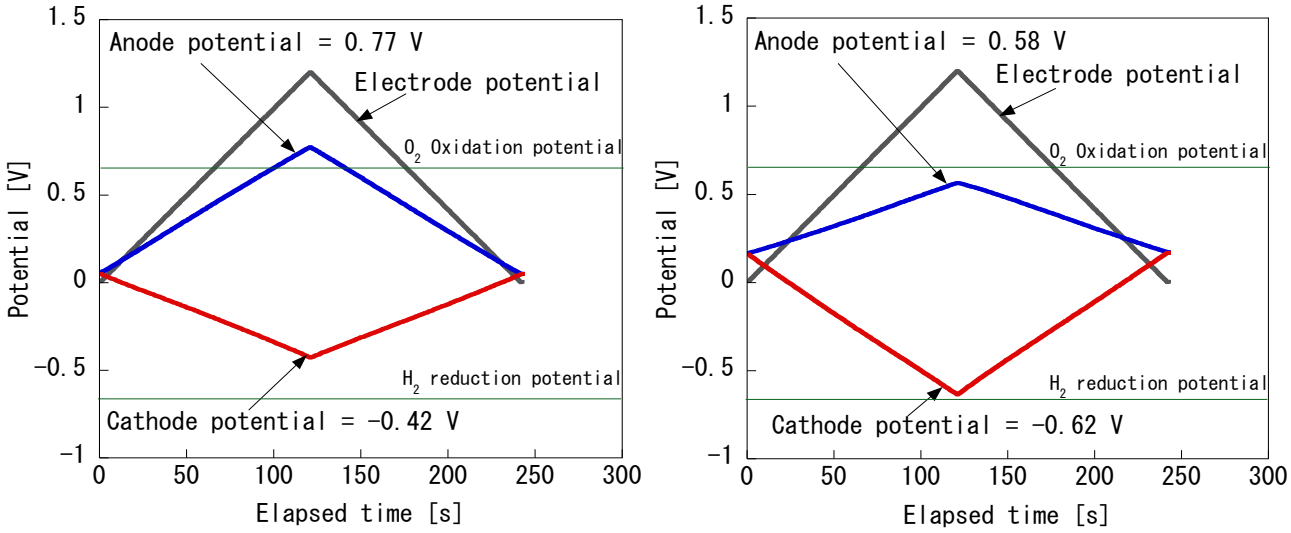

Fig. 3.15 - Charge and discharge behavior of electrode with (a) $\delta_{anode}/\delta_{cathode}$ = 1.1, (b) $\delta_{anode}/\delta_{cathode}$ =2.5 and $\delta_{cathode}$=220 μm.

As presented in Fig. 3.15(a), in the case of a 1.1 thickness ratio of anode and cathode ($\delta_{anode}/\delta_{cathode}$), the charging potential of the anode exceeds the oxidation potential. Thus, oxidation takes place at the anode and the ion adsorption capacity is limited. On the other hand, for $\delta_{anode}/\delta_{cathode}$ = 2.5 as presented in Fig. 3.15(b), neither the anode nor the cathode potentials exceeded the oxidation/reduction potentials. This indicates that electrochemical reaction or electrolysis of water did not take place. Therefore, $\delta_{anode}/\delta_{cathode}$ = 2.5 is an ideal pair for effective capacitive deionization. Different anode:cathode ratios were examined and the results are summarized in Table 3.3.

Table 3.3 - Summary of charge/discharge behavior at various anode:cathode ratios.

Anode:Cathode ratio	Anode potential [V]	Cathode potential [V]
0.3:1 (70:220 [μm])	0.94	−0.25
0.7:1 (150:220 [μm])	0.84	−0.29
1.1:1 (250:220 [μm])	0.77	−0.42
1.3:1 (290:220 [μm])	0.73	−0.46
2.5:1 (550:220 [μm])	0.58	−0.62

References

1. Andres G. L., Shiyoukei Y., Yoshihara Y. and Tanahashi M. (2013) *Sustainability of Water Resources and Environmental Solutions to Climate Change*, Philippine Water Works Association, March 20-22, 2013, Manila, Philippines, pp. 98-104.
2. Andres G. L., Yano N., Shiyoukei Y., Yoshihara Y. and Tanahashi M. (2013) *The 5th IWA-ASPIRE Conference and Exhibition*, International Water Association, September 8-12, 2013, Daejeon, South Korea, 09A3-1.
3. Park K. K., Lee J. B., Park P. Y., Yoon S. W., Moon J. S., Eum H. M. and Lee C. W. (2007) *Desalination*, **206**(1-3), 86-91.
4. Nadakatti S., Tenduklar M. and Kadar M. (2011) *Desalination*, **268**(1-3), 182-188.
5. Seo. S. J., Jeon. H., Lee. J. K., Kim. G. Y., Park. H. N., Lee. J., Moon. S. H. (2010) *Water Research*, **44**(7), 2267-2275.
6. Farmer J. C., Fix D. V., Mack G. V., Pekala R. W. and Poco J. F. (1995) *Journal of Electrochemical Society*, **143**(1), 159-169.
7. Welgemoed T. J. and Shutte C. F. (2005) *Desalination*, **183**(1-3), 327-340.
8. Pandolfo A.G. and Hollenkamp A.F. (2006) *Journal of Power Sources*, **157,** 11-27.
9. Xu B., Wu F., Chen R., Cao G., Chen S., Zhou Z. and Yang Y. (2008) *Electrochemistry Communications*, **10**(5), 795-797.
10. Park B. H., Kim Y. J., Park J. S. and Choi J. (2011) *Journal of Industrial and Engineering Chemistry*, **17**(4), 717-722.
11. Choi J. Y. and Choi J. H. (2010) *Journal of Industrial and Engineering Chemistry*, **16**(3), 401-405.
12. Shiyoukei Y., Andres G. L., Ando Y., Yoshihara Y. and Mukai A. (2013) *The 34th National City Cleaning Meeting*, pp.105-107. *(in Japanese)*

CHAPTER 4

OPTIMIZATION OF OPERATING PARAMETERS AND ENERGY RECOVERY OF THE CDI SYSTEM

4.1 Introduction

We previously reported[1] that the potential margin against oxidation and reduction was mainly influenced by the electrode rest potentials (RP). For instance, since the RP of the developed activated charcoal electrode is around 0.14 - 0.20 V, the anode has only a 0.42 - 0.48 V margin in potential against oxidation, whereas the cathode has a 0.75 - 0.81 V margin against reduction. If the same electrode is used having the same capacities for the anode and cathode, oxidation takes place around 0.84 - 0.96 V (0.42 - 0.48 V x 2), which results in a voltage loss wherein the potential gap up to the electrolysis of water (1.23 V) is not fully utilized for ion capturing. To compensate for this asymmetrical potential gap at the anode and cathode, a pair of activated charcoal electrode with different capacities or different thicknesses would be more effective for capacitive deionization.

Comparison of mono- and bi-polar connections in CDI operation for the treatment of NaCl has been reported by *Lee et al.*[2]. In their report, they used a carbon cloth as the electrode and investigated the advantages of a bi-polar circuit over a uni-polar circuit structure on CDI. Although they studied the voltage distribution, details on this aspect were sparse.

To the best of our knowledge, there have been no published papers showing results of the energy recovery on the capacitive deionization process using activated charcoal-based electrodes. In this study, an extensive examination of the suitable operating conditions on the capacitive deionization process was systematically performed. We have outlined below the specific aims of this chapter:

- We developed an activated charcoal electrode using inexpensive activated charcoal powder. A simple fabrication technique by screen-printing was utilized to form the solid carbon electrode. Although the polar circuit structure has been studied by *Lee et al.*[2] using carbon cloth, in this study the polar circuit connection utilizing a multiple CDI stack equipped with an developed activated-charcoal based electrode was investigated. Hence, the ion adsorption capacity of the CDI stack with respect to the polar circuit connection and its operating conditions was examined.
- Ion adsorption mechanisms of the CDI stack with uni-polar and bi-polar connections were examined extensively and compared based on their voltage distribution.
- The change in pH of the solution during ion adsorption and desorption processes was analyzed.
- A systematic investigation on a combined flow-through and batch capacitive deionization process was conducted.

- Finally, this study clarifies the energy recovery upon discharging the stored energy of the ion desorbing electrode pair to another pair for ion adsorption. For example, a pair of carbon electrodes having stored energy (charged cell) was connected to another pair of electrodes (uncharged cell) in parallel circuit. Ideally, 50 % of the stored energy will be regenerated on the other electrode pair and utilized for another ion adsorption process.

4.2 Materials and Methods

4.2.1 Capacitive deionizer (CDI) stack system design and fabrication

To evaluate the ion adsorption and desorption capacity of the developed electrodes, a capacitive deionizer single unit cell comprising of a pair of the developed carbon electrode was designed and fabricated. Basically, a capacitive deionizer system is compose of (a) a pair of carbon electrodes, (b) graphite sheet where the carbon electrode was attached to act as a current collector, (c) a separator inserted between the two electrodes as a non-conductive separator to prevent short circuits and used as a pathway of the flowing electrolyte, (d) a spacer and (e) a retaining plates used to hold the electrodes. In this experiment, a 58-μm thick separator was made of PET net material and a spacer made of plastic material with a thickness of 1 mm to maintain the distance between the pair of electrodes. The retaining plates were made of acrylic material. In this design, the spacer also acts as a gasket to prevent water leakage wherein only the effective area of the carbon electrode will be exposed to ionic liquid. The schematic design and a photo of a pilot size capacitive deionizer single cell is shown in Fig. 4.1. Fig. 4.2 shows the schematic design of the retaining plate and spacer. The effective area of the carbon electrode was (0.09 m x 0.09 m) 0.0081 m^2. As can be seen in Fig. 4.1(b), the capacitive deionizer was positioned wherein the influent and effluent were horizontally linear. This was done to make sure that all exposed areas of the carbon electrode will be wetted since the ionic electrolyte is flowing from the bottom to the top.

The capacitive deionizer comprising of a five-pair carbon electrodes was fabricated to form a capacitive deionizer (CDI) stack system having five-flow channels. Here, the system structure of the CDI stack was assembled having asymmetrical capacities (δ anode: δ cathode = 0.2 mm: 0.1 mm). Although adjusting the electrode thickness could elevate its ion adsorption capacity, in this experiment, thin electrode was used so as to decrease the electrode ohmic resistance. Therefore, transient ions could easily adsorb and desorb within low and high resistance electrode pores. This time, the apparent effective area of each carbon electrode pair was approximately (0.18 m x 0.18 m) 0.0324 m^2. The inter-electrode distance was controlled using acrylic spacer with a thickness of 1.5 mm. The internal volume of the CDI stack was approximately 300 mL. Fig. 4.3 presents schematic design of (a) a retaining plate, (b) a spacer, (c) a photo of the prepared carbon electrodes in different sizes, and (d) schematic representation of the CDI stack unit.

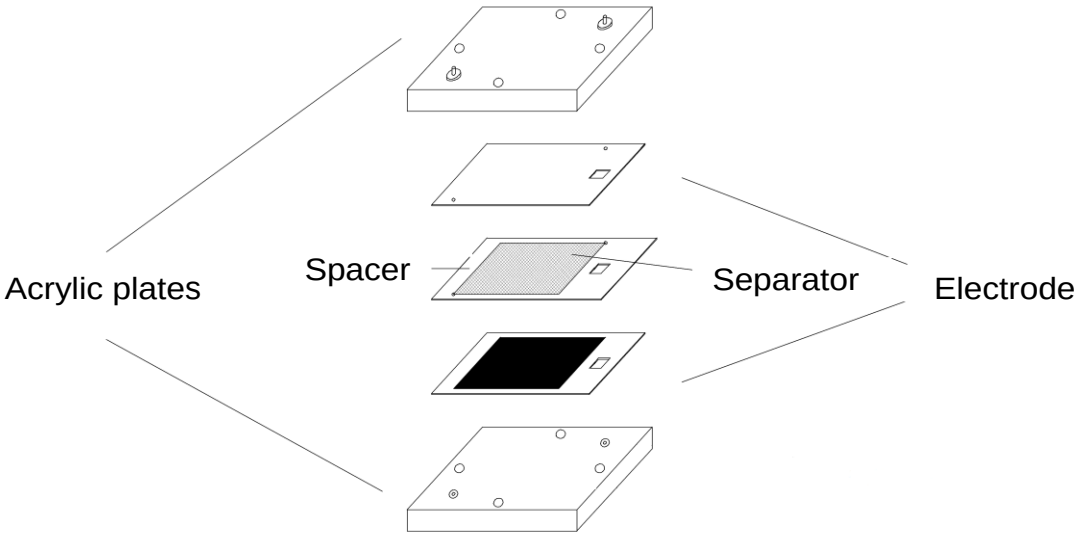

(a)

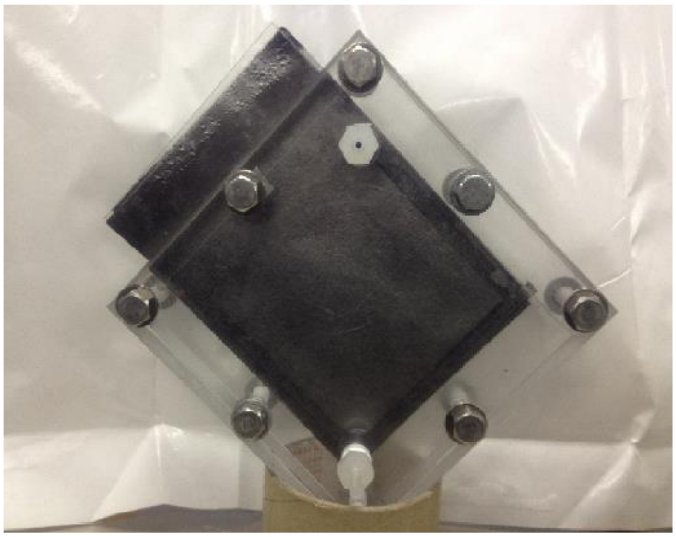

(b)

Fig. 4.1 - Pilot size capacitive deionizer system: (a) schematic design and (b) photo of CDI single cell.

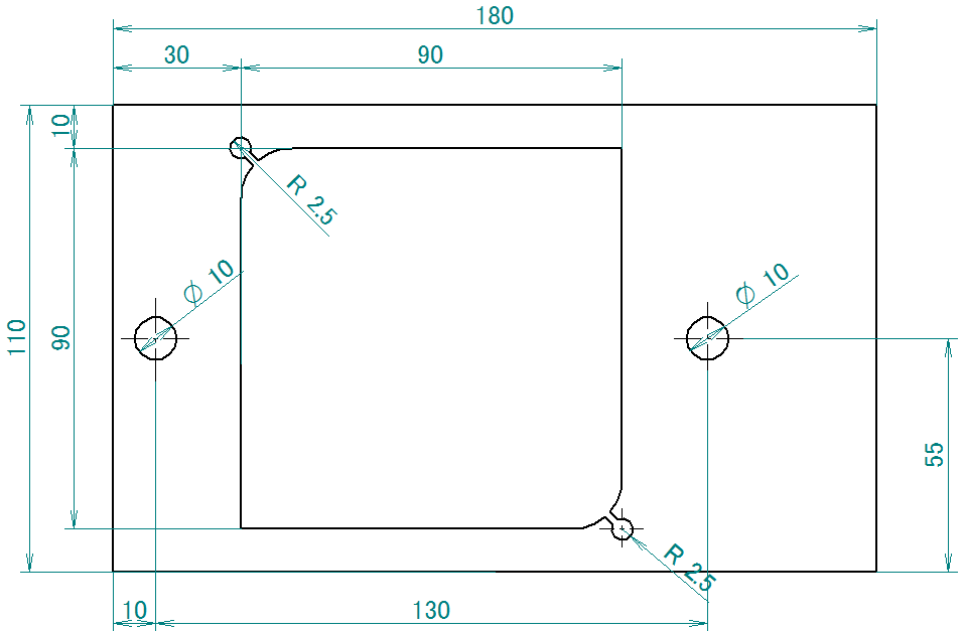

(a)

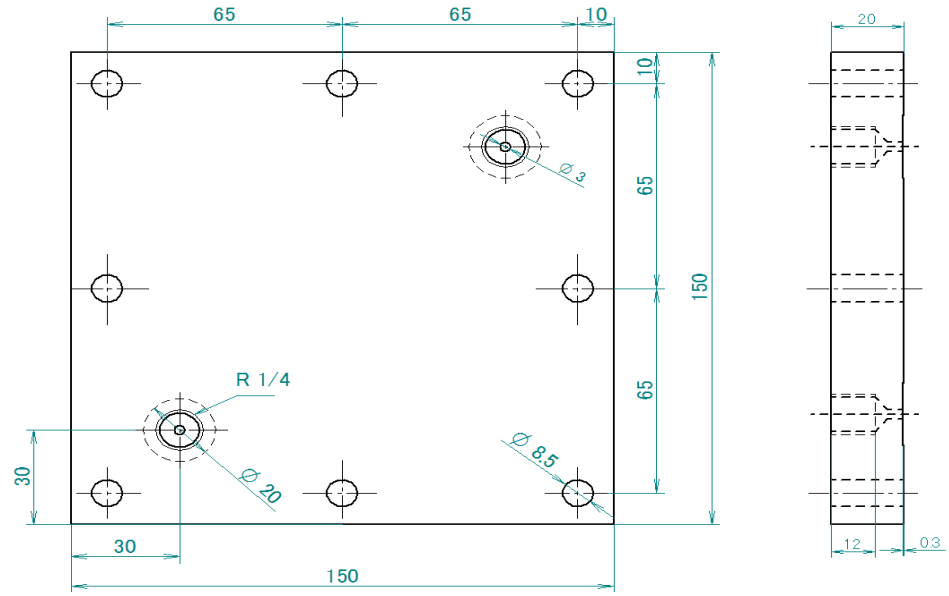

(b)

Fig. 4.2 - Schematic design of pilot size: (a) retaining plate and (b) spacer.

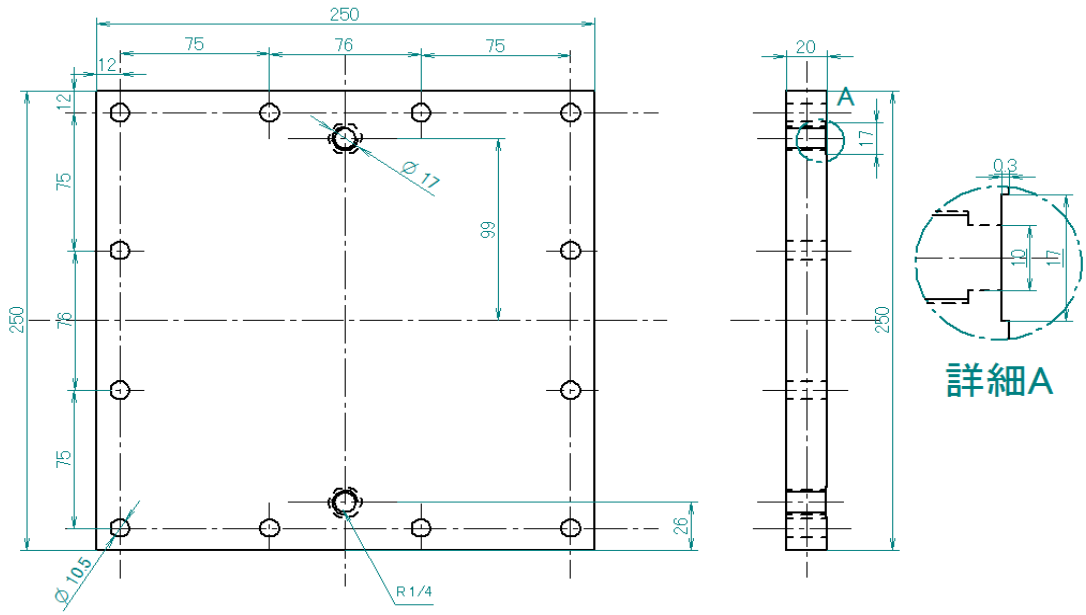

(a)

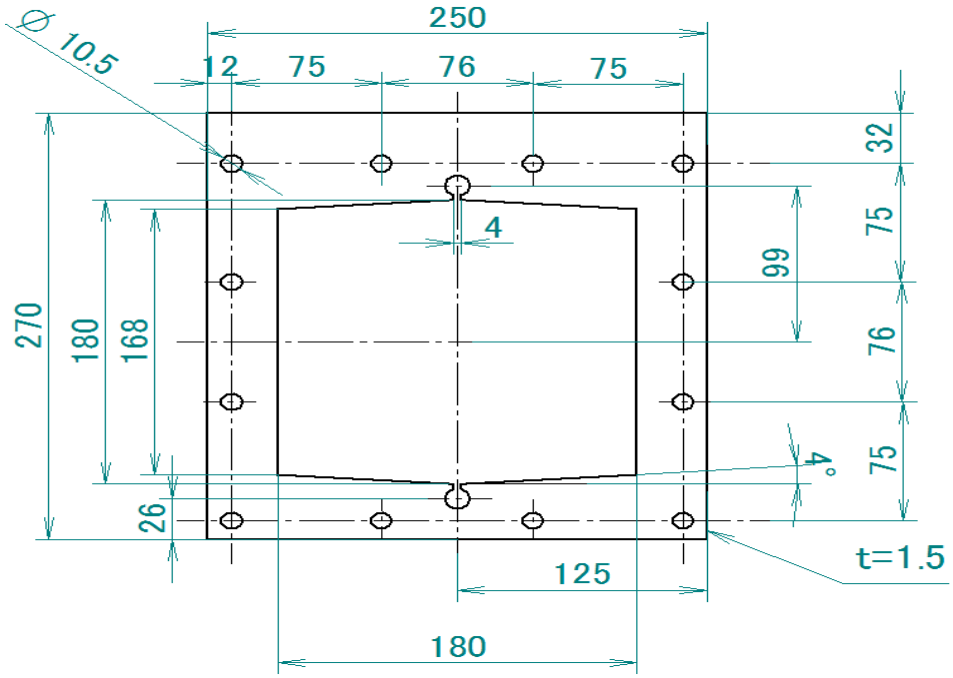

(b)

Fig. 4.3 - Schematic design of (a) retaining plate, (b) spacer, (c) photo of the carbon electrodes and (d) CDI stack system.

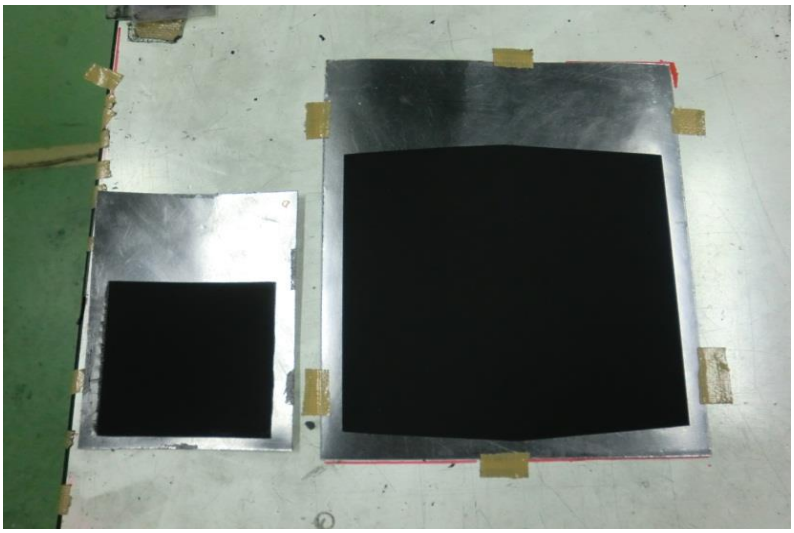

(c)

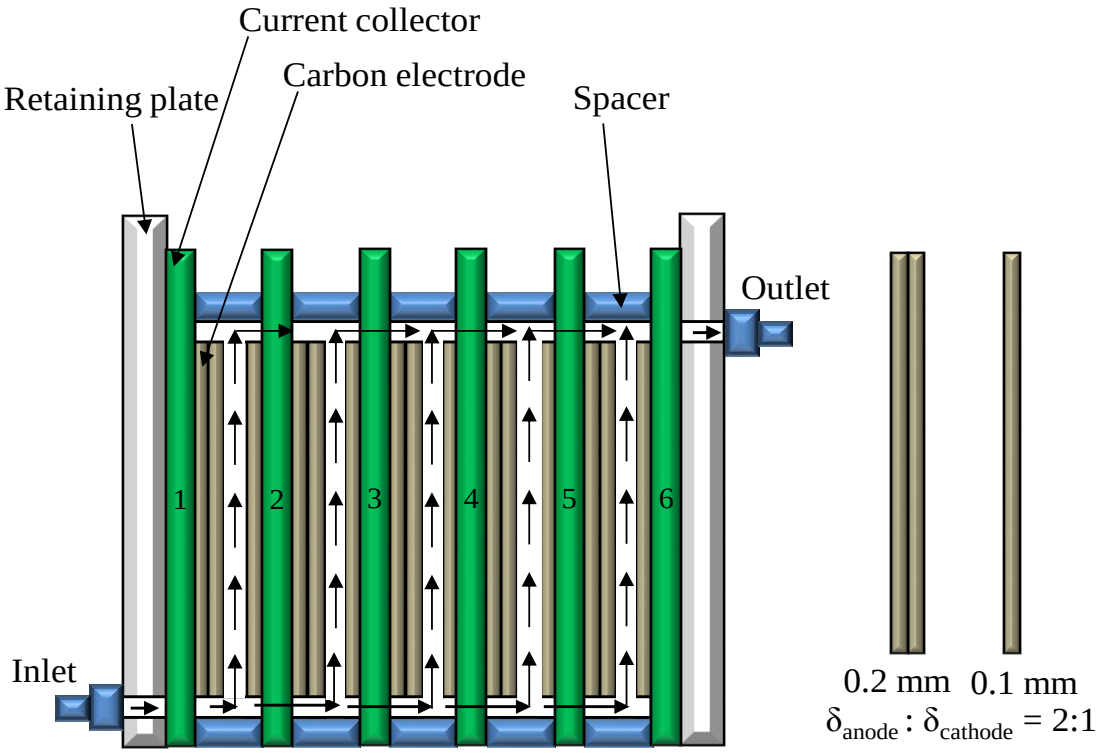

(d)

Fig. 4.3 (continued) - Schematic design of (a) retaining plate, (b) spacer, (c) photo of the carbon electrodes and (d) CDI stack system.

4.2.2 Conductivity/pH meter standard calibration

During capacitive deionization experiments, the change in ion conductivity of the ionic liquid was monitored using a conductivity electrode probe attached to a conductivity/pH meter (Laqua F-74, HORIBA, Japan) as shown in Fig. 4.4(a). The accuracy of the ion conductivity probe and chloride electrode was evaluated based on its linear calibration curve as presented in Figs. 4.4(b) and (c), respectively. All calibration standards were measured under automatic temperature calibration mode at 25 °C. The chloride calibration was performed in a four-point calibration curve using the commercial potassium chloride (KCl) calibration standard.

(a)

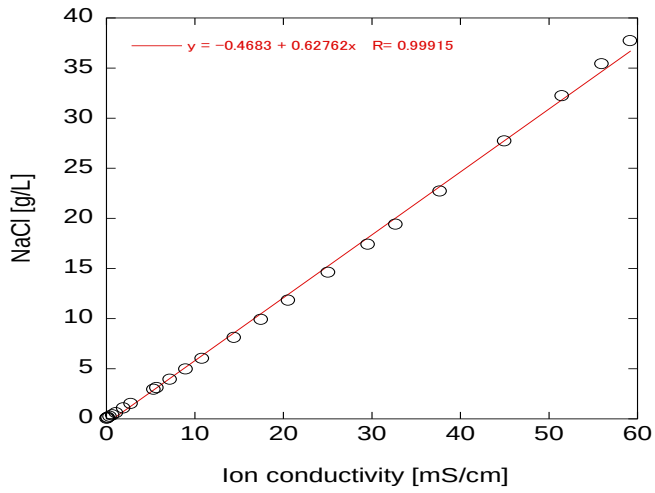

(b)

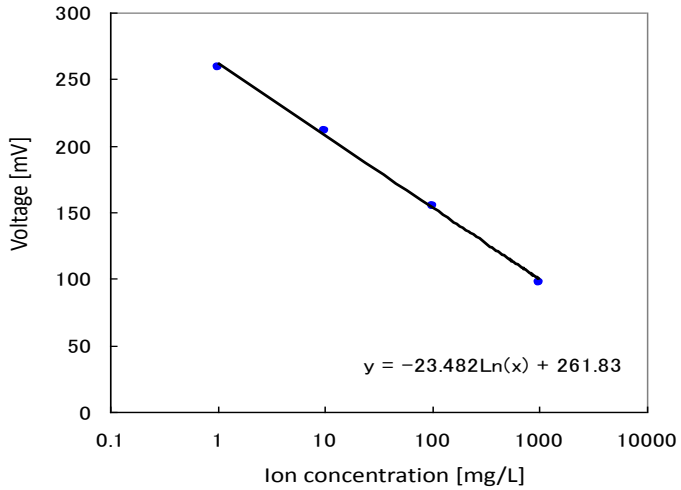

(c)

Fig. 4.4 - (a) Conductivity/pH meter. Linear calibration curve of (b) ion conductivity electrode and of (c) chloride electrode.

4.2.3 Capacitive deionization performance of the CDI single unit cell

The ion adsorption capacity of the developed carbon electrode was evaluated in a batch processing. As can be seen in Fig. 4.5, the CDI system was composed of a fabricated capacitive deionizer cell, a tube pump, and a charge/discharge instrument used as power supply. The NaCl solution was kept flowing for several times to ensure that all effective surface areas of the parallel electrode were wetted. Before the evaluation starts, the ion conductivity of the feed solution was measured to check if the influent and effluent solution were identical. The CDI cell was charged at a maximum voltage of 1.2 V by applying constant current voltage of 100 mA until the electrode was saturated with ions. The voltage was maintained constant for about 120 s until the current in the CDI cell reached 10 mA before the product was collected. A 20 mL charged processed solution was gathered from the CDI cell. The electrode regeneration process was carried out by applying a constant current of −100 mA until the CDI cell voltage reached to 0.0 V. The processed solutions were thoroughly mixed before measuring the ion conductivity using an ion conductivity probe attached to the pH /conductivity meter.

The ion adsorption and desorption performance of the developed carbon electrode was evaluated according to its ion adsorption capacity per electrode effective area β [mol/m^2] given by the following equation:

$$\beta = \frac{\Delta C_i \, \mathrm{x} \, \omega}{A} \tag{4.1}$$

where, ΔC_i, change of initial to final ion concentration ($C_o - C$) (mol/L), ω, amount of processed solution (L), and A, effective area of carbon electrode (m^2).

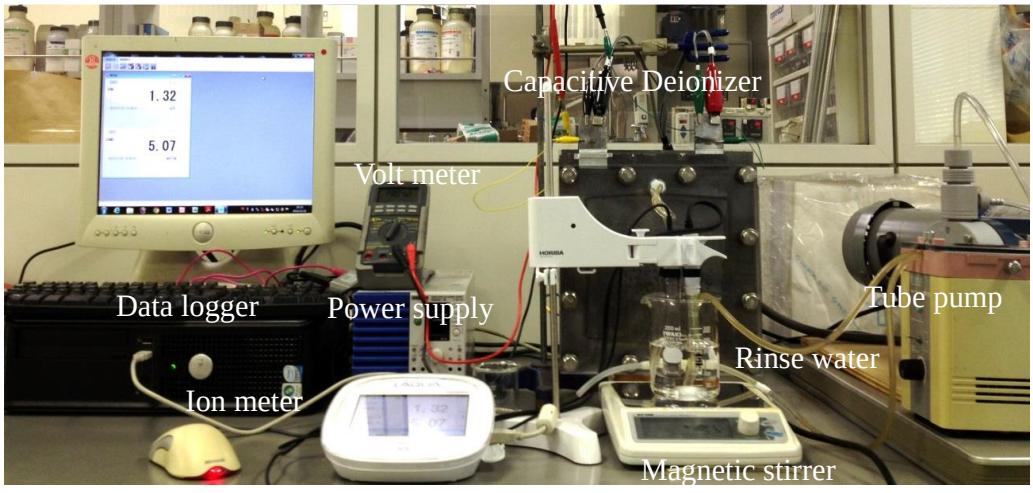

Fig. 4.5 - Capacitive deionization experimental set-up photo.

4.2.4 Capacitive deionization performance of the CDI stack system

A simple and inexpensive hydrophilic activated charcoal-based electrode was fabricated in a similar manner as in our previous work[1]. Briefly, screen printed carbon electrodes were made from a mixture of activated charcoal powder, conductive carbon black, polyvinyl alcohol and *N*-methyl-2-pyrrolidone. In the present work, the capacitive deionizer comprising five pairs of activated charcoal electrodes was fabricated to form a capacitive deionizer (CDI) stack having five flow channels. As proposed in the previous paper[1], the system structure of the CDI stack was assembled having asymmetrical capacities with a thickness ratio δanode: δcathode = 2:1 as illustrated in Fig. 4.6. Although adjusting the electrode thickness will increase the ion adsorption capacity, thin electrodes were used for easy fabrication. In addition, thin electrodes possess low resistance compared to thick electrodes. Therefore, transient ions could easily adsorb and desorb within low and high resistance electrode pores.

The ion adsorption/desorption performance of the CDI stack was evaluated with respect to the operating conditions and its polar circuit connections. The circuit connections of the CDI stack were designed as uni-polar and bi-polar so as to study their optimum operations in the capacitive deionization process. In the case of the uni-polar connection, the supplied voltage at the parallel electrode was limited to 1.2 V [Fig. 4.6(a)]. On the other hand, the CDI stack with the bi-polar connection comprising five electrode pairs was supplied with 6 V (1.2 V * 5 = 6 V) at both ends of the current collectors [Fig. 4.6(b)]. The ion adsorption/desorption performance of the CDI stack was carried out in a flow-through process using a prepared NaCl solution with initial ion conductivity of 5.5 mS/cm. 500 mL of feed water was constantly flowing using a gear pump whilst the changes in ion conductivity and hydrogen concentration (pH) were simultaneously measured using an

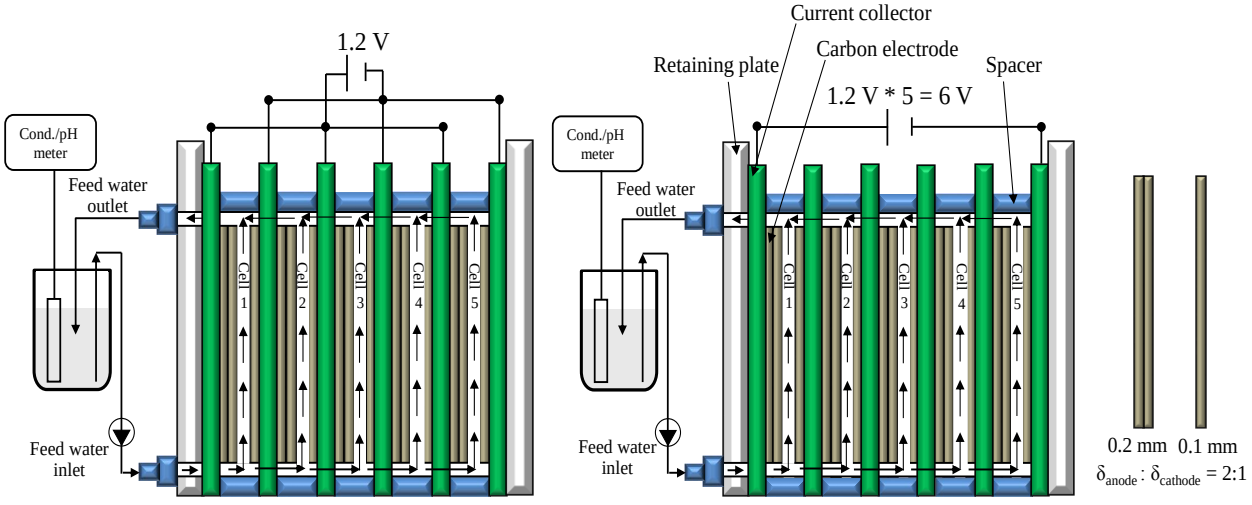

(a) Uni-polar connection (b) Bi-polar connection

Fig. 4.6 - Schematic description of the CDI stack with (a) uni-polar and (b) bi-polar circuit connections. Electrode pairs have asymmetrical capacity.

online ion conductivity and pH probe (pH/conductivity meter, Laqua F-74, HORIBA, Japan) with an interval time of 2 s. For accuracy, the relationship between ion conductivity and ion concentration was determined based on their linear calibration. The pH probe was calibrated with a three-point calibration using commercial pH calibration standards.

Since the system flow rate is considered to be one of the more significant parameters for optimized CDI operation, flow rates ranging 100 - 600 mL/min were used and compared with respect to the change in feed water ion conductivity. Moreover, experiments relating to the processing conditions were conducted. Batch processing, flow-through processing and a combination of flow-through and batch processing were compared.

In flow-through processing, the feed water was constantly re-circulated in the CDI stack throughout the ion adsorption and desorption processes while the change of the feed water ion conductivity was continuously monitored. Before proceeding to ion adsorption/desorption experiments, the solution was flowed through the CDI stack until the ion conductivities of influent and effluent were identical. In the case of batch processing, the solution was flowed into the CDI stack and kept inside during the ion adsorption process. Hereafter, deionized water (processed water) was collected and its ion conductivity was measured. The electrode regeneration (ion desorption) was executed in batch processing by filling the CDI stack with new water (initial ion conductivity of unprocessed water: 5.5 mS/cm) while holding its electric potential constant. Electrode regeneration was carried out by short-circuiting the parallel electrodes. Finally, the concentrated solution was collected and its ion conductivity was measured. The combined flow-through and batch processing was carried out using both the flow-through process for ion adsorption and batch process for ion desorption.

4.2.5 Energy recovery on the CDI system

To examine the energy recovery process of the CDI system, eight unit-capacitive deionizer cells comprising a pair of activated charcoal electrodes were fabricated prior to energy recovery experiments. A program was developed specifically for this study using a National Instrument LabView program for automatic circuit conversion, wherein the circuit connections of each CDI cell could be varied depending on the desired operating conditions.

As demonstrated in Fig. 4.7, the four-CDI cells connected in parallel circuit could be shifted into a series circuit connection by using a solid-state-relay (SSR). Since the ion adsorption and desorption operations during energy recovery could vary, a solenoid valve was used, wherein treated water or concentrated solution could automatically discharge from the CDI cells. Using the computer program and SSR, energy recovery processing could be carried out in multiple CDI units. Ideally, the energy recovery ratio R_{Eideal} is the ratio of electric charge at the charge side (cell recovering the energy) to the discharge side (cell passing the energy) given as follows:

$$R_{Eideal} = \frac{n^2}{n^2 + 1} \tag{4.2}$$

where n is the unit number of both the discharge and charge cells. Therefore, if n = 1, R_{Eideal} = 0.5; n = 2, R_{Eideal} = 0.8; n = 3, R_{Eideal} = 0.9; and n = 4, R_{Eideal} = 0.94.

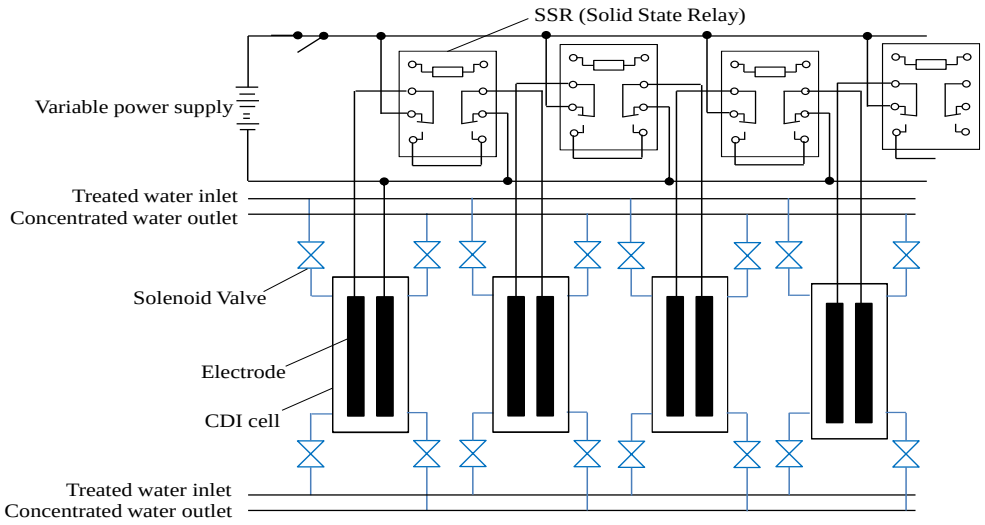

Fig. 4.7 - Circuit conversion of CDI cells from parallel to series connection using the SSR (solid state relay).

The energy recovery rate, R_E, based on the experimental results was analyzed according to the following equation:

$$R_E = \frac{\int_0^t V_c i_c dt}{\int_0^t V_d i_d dt} \tag{4.3}$$

where V_d and V_c are the voltages at both the discharge and charge cells, i_d and i_c are the current at both the discharge and charge cells with respect to time t.

The ion adsorption recovery ratio R_I, was calculated based on the amount of adsorbed ions when the CDI stack was fully charged over the amount of adsorbed ions using the recovered energy and given by:

$$R_I = \frac{ion\ adsorbed(charge\ side)}{ion\ adsorbed(discharge\ side)} \tag{4.4}$$

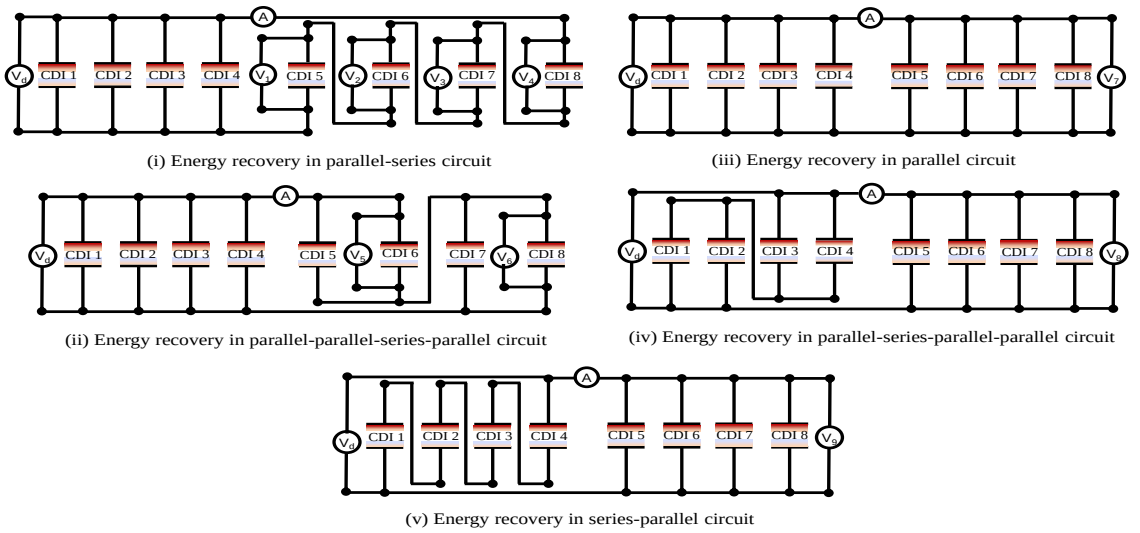

Fig. 4.8 - Energy recovery processing on CDI depending on the circuit structures (i) – (v).

The eight unit-capacitive deionizer cells were utilized as follows: CDI cells 1-4 were charged to 1.2 V, while the other four-CDI cells (CDI 5-8) were kept uncharged. Initially, the circuit structure of the CDI cells 1-4 was in a parallel circuit for balanced distribution of voltage in each cell. By the time the CDI cells 1-4 were in discharge mode, the circuit connection was automatically shifted into a series circuit, whereas CDI cells 5-8 were then connected to the discharge cells (CDI cells 1-4 = V_d) to absorb their stored energy for reuse in another ion adsorption process. It is at this moment that the energy recovery process begins. To examine the energy recovery process on the CDI system, various circuit structures were designed to realize the most efficient energy recovery processing as presented in Fig. 4.8. Various circuit sequences were used for the purpose of investigating the capability of the CDI to recover energy from the discharge cells, e.g., energy recovery processing circuit sequences [v], [i, ii, v], [i, iii, v], [i, iv, v], [ii, iii, v], [ii, iv, v], [iii, iv, v], and [i, ii, iii, iv, v].

4.3 Results and Discussion

4.3.1 Capacitive deionization performance of PVDF and PVA-bonded electrode

The developed PVDF and PVA-bonded carbon electrode were used to form a CDI single unit cell. The ion adsorption capacities of the developed electrodes were performed in batch condition electrosorption process with 0.011 mol/L NaCl solution. The capacitive deionization operating condition was described in section 4.2.3. Fig. 4.9 shows the ion adsorption performances of PVDF and PVA-bonded carbon electrodes. The result illustrates linear form indication that the electrode effective surface area was effectively used with respect to the electrode thickness, which also suggests that oxidation/reduction reactions did not take place during capacitive deionization process. Meanwhile, the PVA-bonded

electrode shows higher ion removal capacity than the PVDF-bonded electrode. For instance, with δanode: δcathode = 80 μm: 40 μm and 140 μm: 80 μm, PVA-bonded electrode is 5 μmol/m^2 higher and 2 μmol/m^2 higher than the PVDF-bonded electrode, respectively. Thus, improvement of ion adsorption is greatly affected by the hydrophilicity of the carbon electrode wherein the liquid accessible area of the PVA-bonded electrode was high. Carbon electrode with high hydrophilicity enhances the electrosorption capacity since it helps the mobility of the transient ions from aqueous solution into the electrode active surface area.

Polymeric binder was used in order to join the activated carbon particles and electric conduction material particles, and in itself does not have the ability to adsorb ions. Therefore, the fewer binder content is desirable, and it is guessed that the performance of an electrode changes remarkably with its hydrophilicity.

In this research, the required least amount of the binder was defined from the mechanical strength of the fabricated electrode as well as its flexibility and the tolerance to high flow flux of flowing water.

Moreover, in the case where PVdF or PVA was used as a binder to form the carbon electrode wherein PVA-bonded carbon electrode exhibited higher ion adsorption capacity in comparison with the PVDF-bonded carbon electrode. Thus, the ion adsorption performance result agrees well with the wettability property results in Chapter 3.

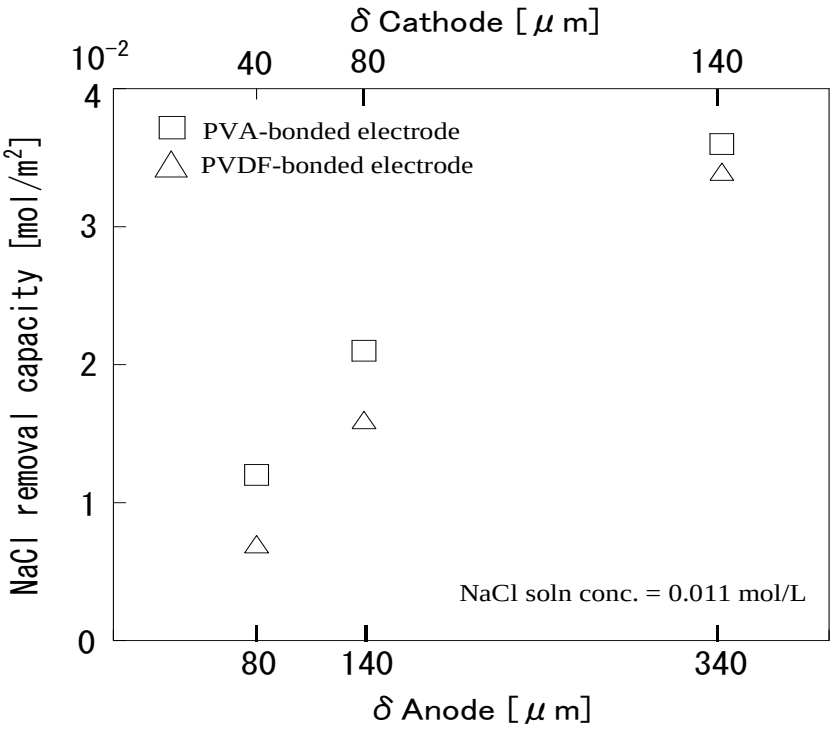

Fig. 4.9 - Ion removal capacity of PVDF and PVA-bonded carbon electrodes.

4.3.2 Investigations for the optimum system flow rate

The CDI stack having a bi-polar connection was used to investigate the ideal flow rate for a high efficient capacitive deionization process. Fig. 4.10 presents the ion conductivity changes of the feed water as a function of time using different flow rates. Clearly, the change of feed water ion conductivity does not directly influence the ion adsorption and desorption performance of the CDI stack even though the feed water flow rate varied.

Although these experiments were conducted in a multiple cycle process, the ion adsorbed capacity was observed to be relatively constant. Thus, the trend of average ion adsorbed capacity was nearly constant even though the flow rate varied as shown in Fig. 4.11. The only distinction was the feed water ion conductivity log time interval changes as the flow rate became faster. Other research has suggested that the ion adsorption efficiency depends on the residence time of the ions on the electrode when applying an electric potential for increased desalination efficiency and more time for mass transfer is required. Nevertheless, consideration of the proportionality between the size of the system and the system flow rate should be taken into account. In this study, it was revealed that flow rates ranging from 100 - 600 mL/min exhibited no significant effect on the electrode ion adsorption capacity. Therefore, flow rates within this range could be used for capacitive deionization evaluation.

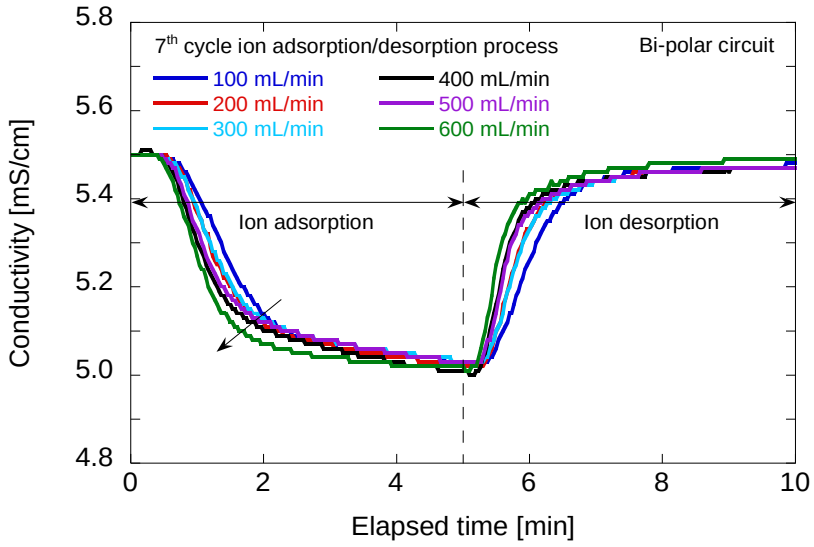

Fig. 4.10 - Ion adsorption and desorption evaluation of CDI stack with varying flow rates ranging from 100 to 600 mL/min.

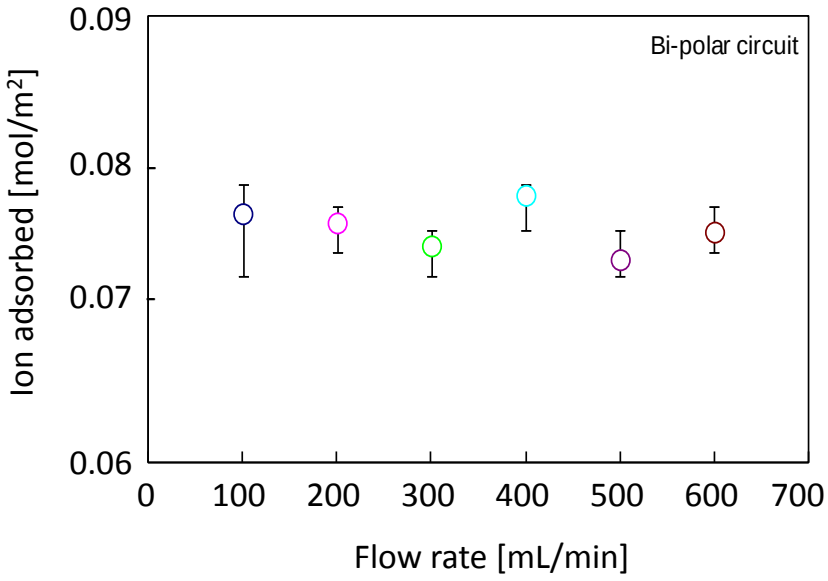

Fig. 4.11 - Average ion adsorption capacity of CDI stack with varying flow rate.

4.3.3 Comparison on the CDI performance of the CDI stack system having uni- and bi-polar connections

A voltage-current profile will indicate the saturation period of the electrodes and the energy consumed during the capacitive deionization process. Figs. 4.12(a) and (b) show the voltage-current profiles of the CDI stack designed with uni-polar and bi-polar connections, respectively. In the case of a CDI stack with uni-polar connection upon polarization, even though the set limit current was 10 A, the current started from 1.33 A then decreased gradually until the ion adsorption process was finished and a final current of 0.10 A was indicated. In this evaluation, the test intervals for the ion adsorption and desorption processes were limited to 20 min each to evaluate the electrode maximum saturation capacity. In contrast, in the CDI stack with bi-polar connection, the current was dramatically decreased from 5.67 to 0.03 A in less than 3 min and then remained constant. The current indicates the ionic saturation of the electrodes and these results validate that the ion saturation time in the bi-polar connection is faster than that of the uni-polar connection. It is clear that the ion adsorption process in the bi-polar system can be executed in a shorter period. Shorter execution times indicate higher work efficiency.

Observed pH and conductivity changes of the feed water in the CDI stack are depicted in Fig. 4.13. The ion adsorption and desorption performance of the CDI stack depending on its circuit connection was evaluated with a flow-through processing capacitive deionization using the prepared NaCl solution.

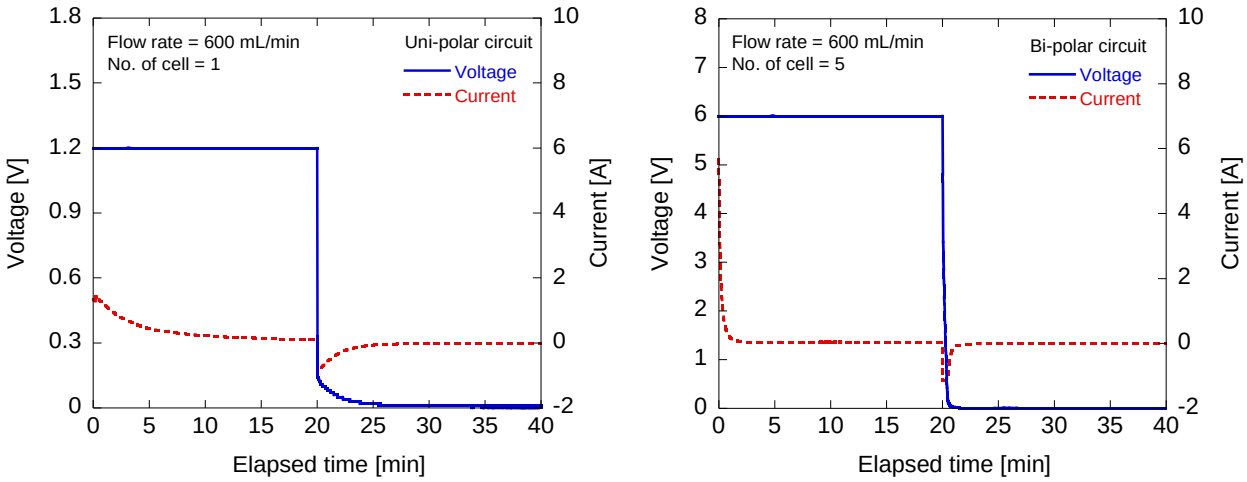

(a) Uni-polar connection (b) Bi-polar connection

Fig. 4.12 - Voltage-Current profiles of the CDI stack with (a) uni-polar and (b) bi-polar connections.

Fig. 4.13(a) shows the ion adsorption and desorption performance of the CDI stack depending on its polar circuit connection. As expected, the CDI stack with bi-polar connection adsorbed ions more quickly than that of the uni-polar one, wherein the change of feed water ion conductivity decreased dramatically, an indication that the ions were quickly adsorbed onto the electrodes which were saturated in less than 5 min.

On the other hand, a gradual decrease of ion conductivity was observed in the uni-polar connection even though the system flow rate for both operations was the same (600 mL/min). Taking into account the energy consumption with respect to the operating time per unit volume of the processed water, the capacitive deionization process in the CDI stack with the bi-polar connection is more advantageous than the CDI stack with the uni-polar connection. The energy consumed in the uni-polar and bi-polar connections on the CDI stack up to saturation time was calculated to be 72 and 21.6 J, respectively, for a 20 min ion adsorption process. The ion adsorption capacity of the CDI stack with the bi-polar connection was 0.096 mol/m^2 for 20 min. This is higher than the CDI stack with uni-polar connection having an ion adsorption capacity of 0.085 mol/m^2.

Undoubtedly, CDI with the bi-polar connection demonstrated higher ion adsorption capacity and consumed 70 % less energy than that of the uni-polar connection. These results suggest that the bi-polar connection would be ideal to achieve higher ion adsorption capacity in a shorter cycle time and consume lower energy in the capacitive deionization process.

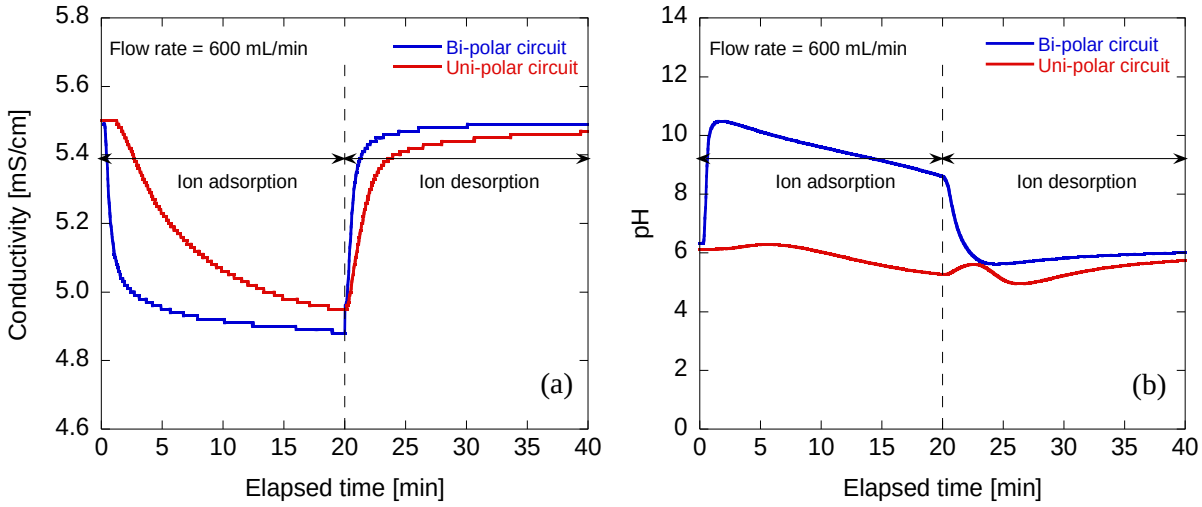

Fig. 4.13 - Capacitive deionization performance of the CDI stack with uni-polar and bi-polar circuit connections. (a) Change of feed water ion conductivity and (b) pH change of the feed water during ion adsorption and desorption processes.

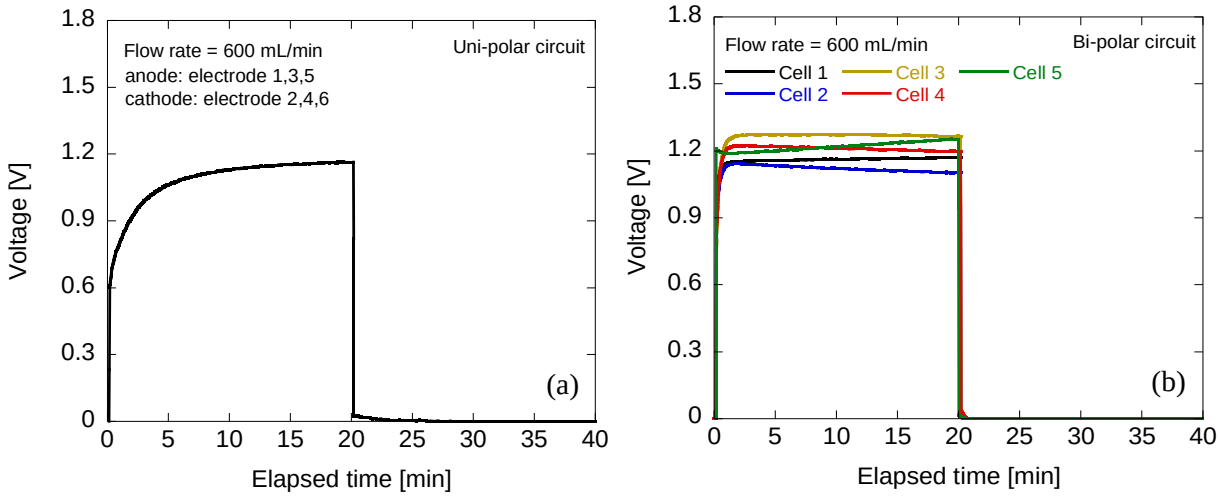

Fig. 4.14 - Voltage distribution profiles of the CDI stack having (a) uni-polar and (b) bi-polar connections.

Fig. 4.13(b) presents the pH change of the NaCl solution during capacitive deionization. The pH profiles varied depending on the CDI stack polar circuit connection. The uni-polar connection exhibited no significant change in pH of the flowing NaCl solution, whereas in the case of the bi-polar connection, the pH of the feed water increased dramatically when the voltage was supplied, from the initial pH

6.3 to the final pH 10.4. This is an indication that the feed water has become alkaline. It is clear that the period where the feed water conductivity changes during the ion adsorption process correlates directly with the period where the pH of the flowing solution changes. This phenomenon denotes that hydrogen cations (H^+) were adsorbed onto the cathode faster than the sodium cations (Na^+)[3]. This can be expected because it is known that the hydrogen cation ionization energy (1312 kJ/mol) is approximately 2.65 times higher than the sodium cation ionization energy (495.8 kJ/mol. Thus, hydrogen cations were adsorbed onto the cathode initially, then replaced by sodium cations. Even though there was an increased pH of the feed water, the amount of adsorbed hydrogen cations was small enough to affect the total ion adsorption capacity of the activated charcoal electrodes. Notably at the end of the cycle, the pH value of the feed water returned to its initial pH, signifying that the concentrations of hydrogen cations (H^+) and hydroxide anions (OH^-) were intact in the solution. Both uni-polar and bi-polar connections could be considered as chemical reaction-free capacitive deionization processes and the change in the pH was essentially caused by separation of ions via electrostatic energy.

To rationalize the adsorption and desorption mechanisms of the electrodes, voltage distributions of the CDI stack depending on the polar circuit connection were investigated. Fig. 4.14 illustrates the voltage distribution profiles of the CDI stacks having bi-polar and uni-polar connections. In the bi-polar connection, high voltage (6.0 V) was applied at both ends of the current collectors to induce stronger electrostatic forces between electrode/solution interfaces, which leads to faster adsorption of ions. Interestingly, although the voltage was applied only at the ends of the current collectors, the voltage of each cell was likely distributed equally as demonstrated in Fig. 4.14(a). The slight difference in the voltage distributions was attributed largely to the uneven thickness of the electrodes because the electrodes were manually screen printed. On the other hand, the CDI stack with uni-polar connection presumably demonstrated equal distribution of the voltage to anode (0.6 V) and cathode (−0.6 V) as presented in Fig. 4.14(b). The gradual increase of cell voltage agrees with the flowing current during the ion adsorption process [refer to Fig. 4.12(a)], wherein ions were gradually adsorbed onto the electrodes. This feature was validated by the change of ion conductivity over time of the feed water as well as the change in pH. Uni-polar connections in nature are capable of distributing voltage, therefore slower adsorption of ions occurs in comparison to bi-polar connections. As *Lee et al.*[2] reported, a CDI stack having a bi-polar circuit structure is more favourable for adsorbing ions electrostatically onto the electrode surface although there is a voltage-balancing problem between one cell and another of the CDI stack. In contrast, this study revealed that the voltage distribution between electrode cells was likely even. Even though the pH of the feed water increased during the ion adsorption process, the electrode capacity was effectively utilized for ion capturing rather than pseudo capacity due to oxidation/reduction reactions.

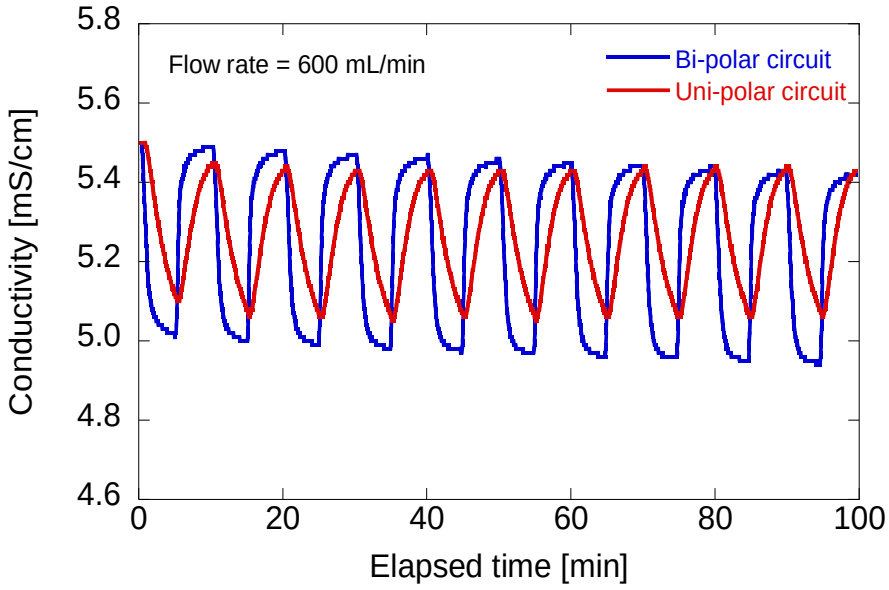

Fig. 4.15 - Multi-cycle capacitive deionization of CDI stack system having uni-polar and bi-polar connections.

A multiple cycle capacitive deionization process was executed using the CDI stack with uni-polar or bi-polar connection as shown in Fig. 4.15. The ion adsorption and desorption were carried out over a span of 10 min based on the previous experiment shown in Fig. 4.13, where the CDI stack with bi-polar connection was saturated with ions in less than 5 min. Here, the CDI stack with bi-polar connection exhibited higher ion adsorption capacity than the uni-polar connection with the short period of ion adsorption and desorption. There was a gradual decrease in feed water ion conductivity with both connections, which was mostly caused by the impregnated ions in the electrode pores. Therefore, no significant decrease in capacitive deionization efficiency was observed even up to the 10^{th} ion adsorption/desorption cycle. The electrode ion adsorption capacity and the consumed energy were maintained throughout the cycle. Ultimately, this experiment revealed that the developed activated charcoal electrode has high durability and reproducibility.

4.3.4 Comparison on CDI performance of batch, flow-through and combined flow-through and batch processing

During the ion adsorption process, ions from the ionic water are adsorbed onto the electrode active pores, forming an electric double layer (EDL). The operating conditions play a crucial role, affecting the ability of the electrode to capture ions or the mobility of the transient ions. This study examined the ion adsorption/desorption

Table 4.1 – Summary of ion adsorption/desorption performances of the CDI stack with respect to the processing condition and polar circuit connections.

Capacitive deionization process on NaCl			
Uni-polar [1.2 V]			
Electrode capacity	Batch process	Flow-through process	Combined process
Ion adsorbed [mol/m^2]	0.101	0.085	0.083
Ion desorbed [mol/m^2]	0.060	0.080	0.117
Bi-polar [6 V]			
Electrode capacity	Batch process	Flow-through process	Combined process
Ion adsorbed [mol/m^2]	0.116	0.096	0.091
Ion desorbed [mol/m^2]	0.061	0.094	0.131

performance of the CDI stack depending on the processing conditions, namely batch processing, flow-through processing and a combination of flow-through and batch processing. Batch processing and flow-through processing both have strong advantages and disadvantages when utilized in the capacitive deionization process. To determine which of these three processes would be desirable for our purpose, the ion adsorption and desorption performances of the CDI stack system equipped with five-pairs of activated charcoal electrodes were investigated with both uni-polar and bi-polar connections.

The schematic procedures of batch processing and flow-through processing were described in section 4.2.4. Table 4.1 presents a summary of the ion adsorption and desorption performances under different processing conditions. In the case of batch processing, the bi-polar connection shows higher adsorption capacity than that of the uni-polar connection. In addition, it is obvious that the ion desorbed capacity for both uni-polar and bi-polar connections was less than that of the ion adsorbed capacity. The primary reason for this phenomenon is that after the ion adsorption process, the water was withdrawn from the CDI stack, leaving a fraction of the processed water. For instance, the internal volume of the CDI stack in this experiment was around 300 mL but when the water was withdrawn from the system, the amount collected was only 225 mL, and about 75 mL or 25 % of the solution remained inside the CDI stack. Since the volume capacity of the CDI was 300 mL, and a constant volume was pumped into the CDI, the residual water (low concentration solution) retained inside combined with the newly-filled water for the regeneration process. This resulted in lower ion conductivity of the regeneration product (ion desorbed).

On the other hand, flow-through processing shows better performance than batch processing with respect to the amount of processed solution. Desorbed ions were approximately equal to the ions adsorbed. Consequently, for both processing conditions, the CDI stack with bi-polar connection exhibited higher ion adsorption capacity, which agreed with the previous result shown in Fig 4.13. Therefore, it is concluded that a bi-polar connection with a flow-through processing condition shows favourable capacitive deionization performance.

It can be seen from the results of our experiment shown in Table 4.1 that the CDI stack with bi-polar connection and flow-through processing was the ideal operating condition. However, from a practical viewpoint, the amount of water used for the ion desorption process should be minimal. Since flow-through processing will be utilized for the ion adsorption process, the effect of inter-electrode distance is irrelevant and the amount of processed water will be large. In contrast, it was thought that batch processing would be an ideal operation since it consists of a single process. The electrode capacity (mol/m^2) in this operation should be large enough to achieve a target removal of ions in 0.1 mol/m^2 NaCl solution. This could be achieved by controlling the thickness of the electrode or by reducing the inter-electrode distance[1]. In batch processing, the inter-electrode distance plays a significant role since it controls the resistance of the ionic solution[4,5]. Therefore by maintaining an inter-electrode distance of 1 mm, the target ion removal may be achieved. However, it was observed in the batch processing operation that diffusion of ions takes place when the water was newly-filled into the CDI stack during the regeneration process. This could influence the performance of the electrodes resulting in decreased ion adsorption capacity. Consequently, the range of ion concentration of salt water (0.5 to 30 grams of salt per liter) and the drawbacks of batch processing were taken into account. As presented in Table 4.1, in the case of batch processing, the CDI with bi-polar connection shows relatively higher ion adsorption capacity of 0.116 mol/m^2 in comparison to the uni-polar connection with ion adsorption capacity of 0.101 mol/m^2. These experiments were carried out using a synthetic NaCl solution and the amount of adsorbed Na^+ and Cl^- ions in either the uni-polar or bi-polar connection achieved the target ion adsorption capacity (0.1 mol/m^2) using batch processing. In contrast, the ion desorbed capacity was not identical to the ion adsorbed capacity because a fraction of water remained inside the system accompanied by the impregnated ions in the electrode pores (high resistance pores) when the water was withdrawn from the CDI stack.

In order to alleviate the problems from the batch or flow-through process, a combination of flow-through and batch processing was utilized using the fabricated CDI stack, and investigations on its ion adsorption/desorption performance using the combined processing were carried out. In the case of flow-through processing, the total amount of feed solution was 500 mL and the system flow rate was 600 mL/min. On the other hand, during batch processing, the total amount of water was limited to 300 mL (CDI stack

internal volume). The flowing water was stopped when the electrode was saturated with ions and the electrode regeneration process was executed. As expected, the bi-polar connection exhibited higher ion adsorption capacity. Hence, the ion adsorption capacities of uni-polar and bi-polar connections in flow-through processing were 0.083 mol/m^2 and 0.091 mol/m^2, respectively. The electrode regeneration was executed in batch processing whereas the ion desorption capacities of uni-polar and bi-polar connections were 0.117 mol m^2 and 0.131 mol/m^2, respectively. It is noteworthy that the ion desorbed capacity was higher than the ion adsorbed capacity regardless of the polar circuit connection. This discrepancy comes from the difference in the operating conditions. As mentioned earlier, the ion adsorption process was conducted in flow-through processing and the amount of processed water was 500 mL. On the other hand, when the electrode was regenerated (ion desorption process), the amount of processing water was limited to 300 mL. Ideally, the amount of ion desorbed capacity should be 1.67 times [0.091 mol/m^2 * (500/300)] higher than the processed water, therefore the amount of ion desorbed with the bi-polar connection should be 0.151 and with the uni-polar connection 0.138 mol/m^2. In this aspect, the ion desorbed capacities for uni-polar and bi-polar connections were less than 15 % and 13 %, respectively, due to a fraction of water with ions that were not collected in the CDI stack.

The combination of processing operations was particularly effective in the capacitive deionization process. For instance, during the ion adsorption process, flow-through processing should be utilized, since it can process a large amount of water. In addition, the ionic solution resistance in flow-through processing is essentially constant, therefore voltage loss (*IR* drop) would be minimal. Although batch processing exhibited high ion adsorption capacity with respect to the processed solution, the ion desorbed capacity was lower compared to combined flow-through and batch processing condition.

4.3.5 Energy recovery of the CDI system

One of the key advantages in capacitive deionization is that the energy recovered in the charged electrodes could be utilized for another ion adsorption process. In the deionization process, energy is required to separate the ions from the solution and those adsorbed into the porous electrodes. Here, the energy was stored. During the regeneration process, the energy was recoverable by regulating the flowing voltage and current; otherwise this stored energy would be unused[8]. In this study, the energy was defined as the integral of the power with respect to time[9], whereas the energy recovery ratio was defined as the ratio of the energy recovered by the charge side and the energy stored at the discharge side.

Here, using the designed circuits and choosing a sequence for optimum energy operation, we were able to determine the most suitable processing technique, wherein the energy was recovered and reused for another ion adsorption process. The main reason why these circuits were designed was to control the flow of current going to the charging cells, therefore lessening the loss of energy. Fig. 4.16 demonstrates the voltage-current profiles of energy recovery processing. It is clear that the energy recovery process of the CDI system primarily depends on its circuit structures. For example, according to eq. (4.2), the ideal energy recovery ratio with respect to the number of unit cells when using only circuit [v]

for the energy recovery process would be 94 %. However, based on the experimental results, only 8 % of the energy was recovered. As can be seen in Fig. 4.16(a), as the energy recovery process began and discharge cells were shifted from parallel to series circuit [see Fig. 4.8(v)], the current fluctuated around 2.4 A, then gradually decreased to 0.0 A. This feature implies that loss of energy was high due to the abrupt circuit shifting. Although it was considered that each component in the CDI system such as electrodes, circuit connectors, switches, and measuring devices contains ohmic resistance that may contribute to the loss of energy recovery due to the voltage drop[9], it is imperative to determine the most efficient energy recovery process. With regard to this aspect, in order to lessen the loss of energy recovery by using the designed circuits, various circuit sequences were used. Even though it appears that the transfer of voltage for all the circuit sequences shows the same pattern wherein the voltage was increasing, the current profiles present different trends, which indicates that the energy recovered varied with the circuit sequence processing.

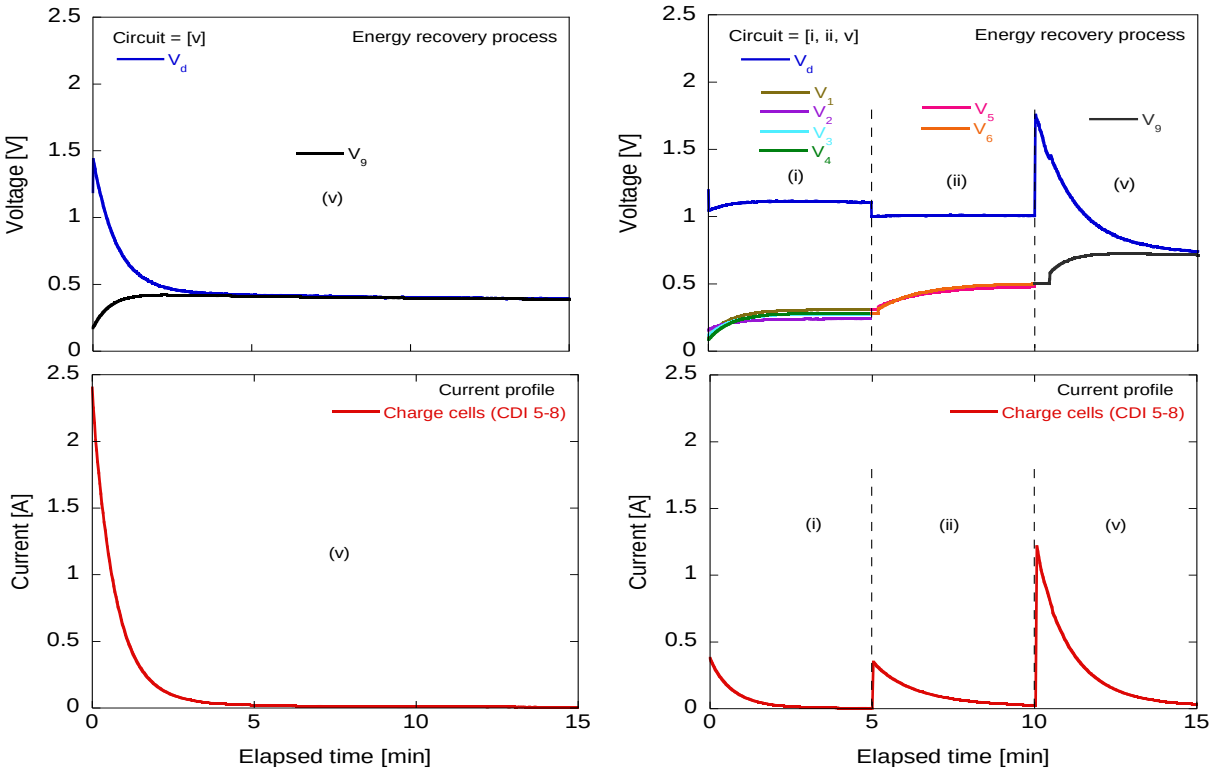

(a) Circuit [v]

(b) Circuit [i,ii,v]

Fig. 4.16 - Energy recovery processing on CDI depending on the circuit sequence.

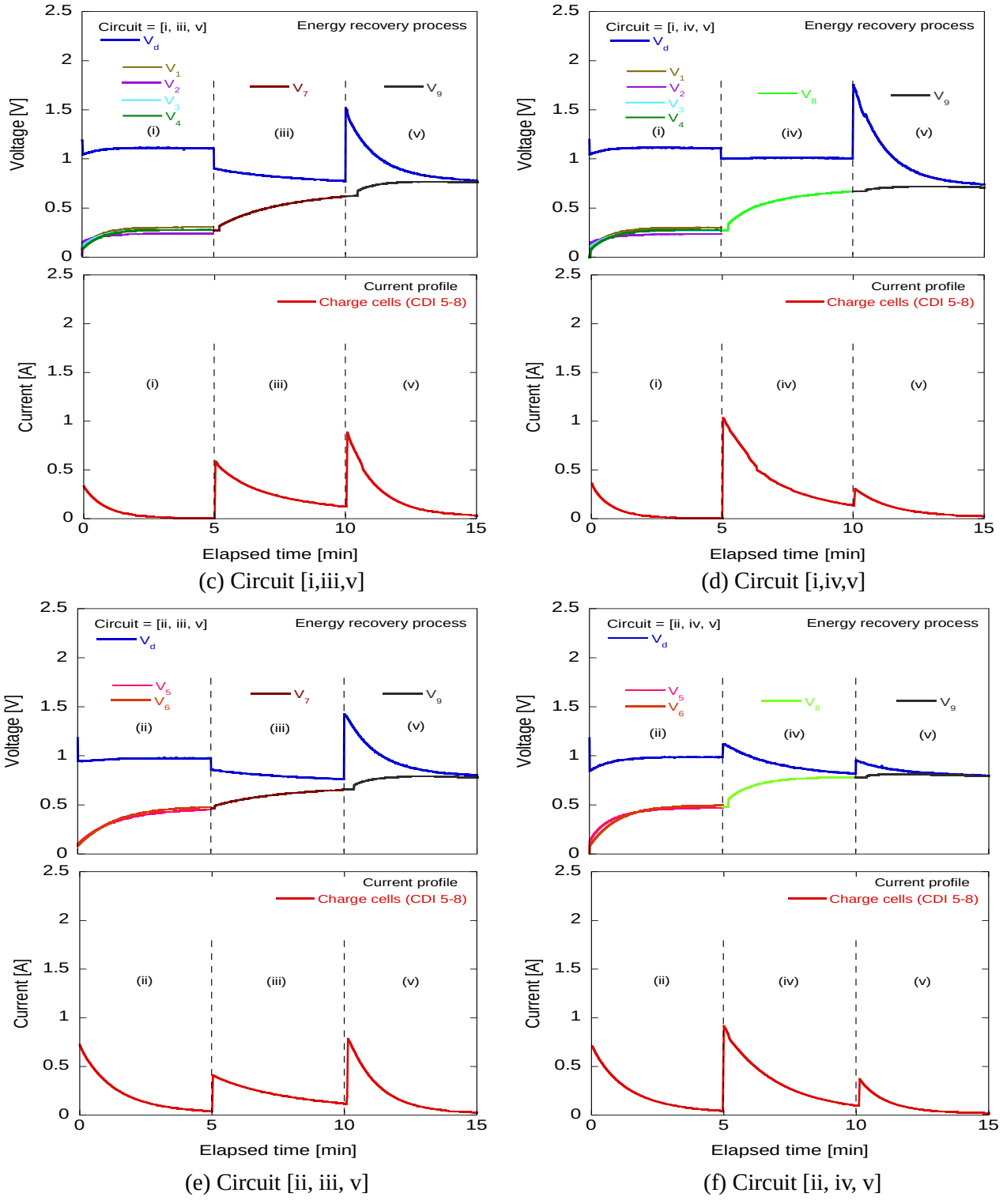

(c) Circuit [i,iii,v]

(d) Circuit [i,iv,v]

(e) Circuit [ii, iii, v]

(f) Circuit [ii, iv, v]

Fig. 4.16 - Energy recovery processing on CDI depending on the circuit sequence.

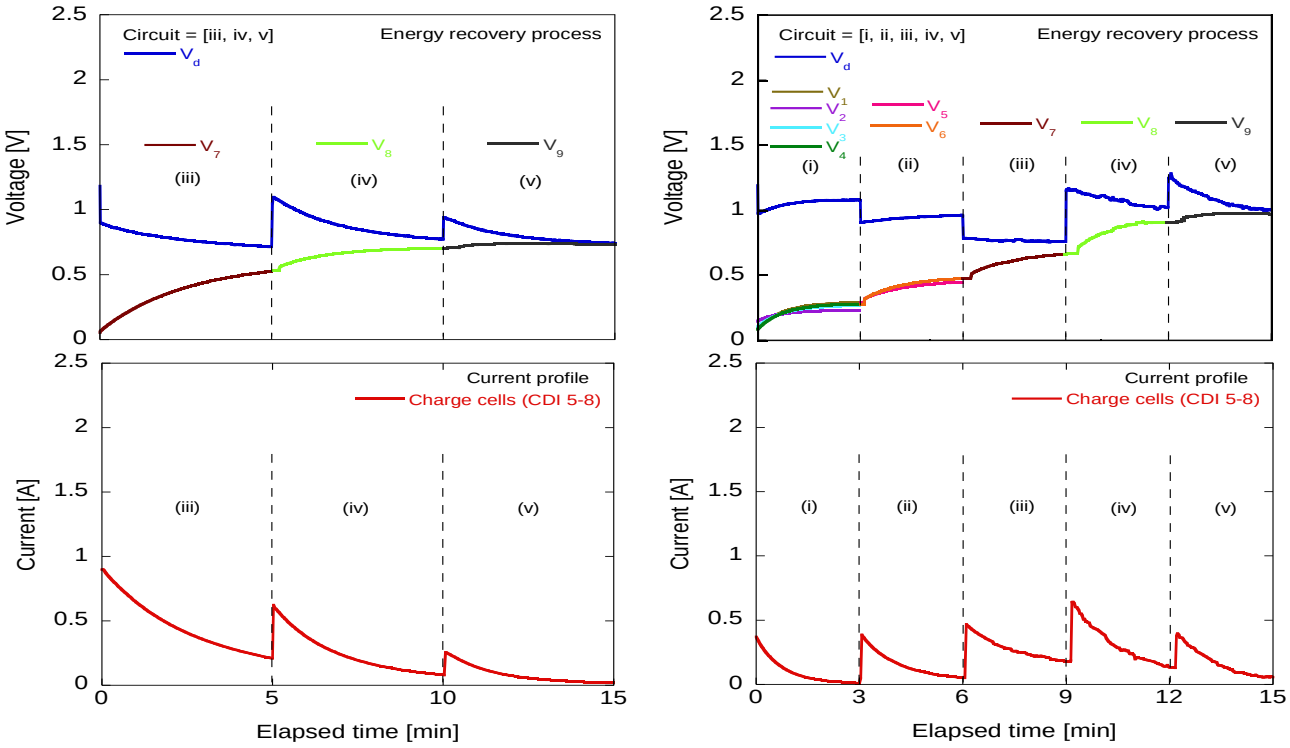

(g) Circuit [iii, iv, v] (h) Circuit [i, ii, iii, iv, v]

Fig. 4.16 (continued) - Energy recovery processing on CDI depending on the circuit sequence.

Fig. 4.17 presents the summary of the energy recovery ratios depending on the circuit processing sequence. For the energy recovery circuit sequences [v], [i, ii, v], [i, iii, v], [i, iv, v], [ii, iii, v], [ii, iv, v], [iii, iv, v], and [i, ii, iii, iv, v], the energy recovery ratios were 8, 33, 40, 42, 57, 70, 57 and 81 %, respectively.

It is obvious from this evaluation that the circuit sequence plays a significant role in recovering the stored energy. Furthermore, the highest energy recovery ratio of 81 % was achieved using circuit sequence [i, ii, iii, iv, v]. Judging from these results, it was clear that regulating the circuit sequence, which leads to high efficiency energy recovery, could control the energy recovery process.

For further analysis, the ion adsorption performance of the charge cells was executed by only using the recovered energy and by measuring the change of the feed water ion conductivity. All experiments were carried out with the use of the prepared NaCl solution having initial ion conductivity of 5.5 mS/cm in a constant flow-through ion adsorption and desorption process. Each CDI cell internal volume was approximately 42 mL (42 mL * 4 cells = 168 mL) and the amount of feed water flowing in the system was around 132 mL. A gear pump with a constant flow rate of 30 mL/min was used, taking less than 2 min to re-circulate the solution from each CDI cell, and the change of feed water ion conductivity was measured accurately.

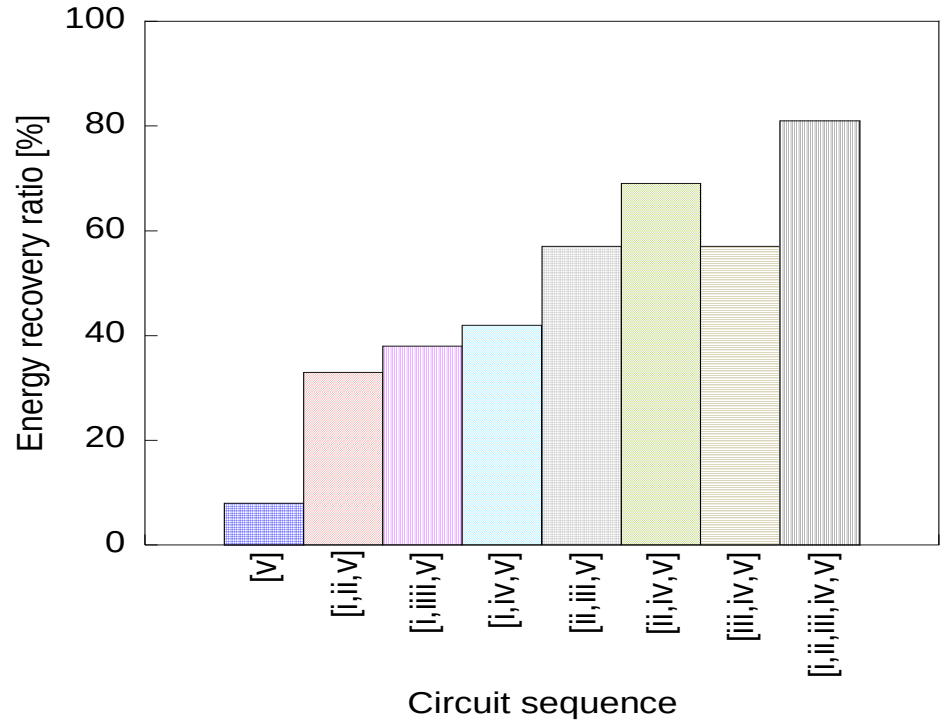

Fig. 4.17 - Energy recovery ratio.

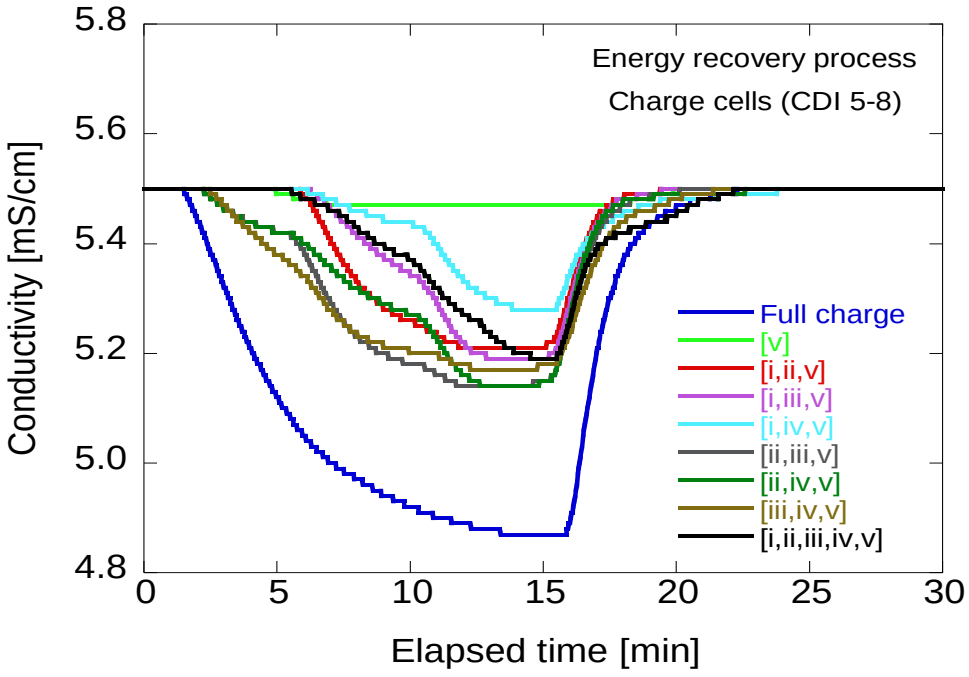

Fig. 4.18 - Comparison of ion conductivity changes during energy recovery and in the case that the CDI stack was fully charged.

Fig. 4.18 shows the changes of ion conductivity depending on the processing circuit sequence. Before execution of the energy recovery evaluation, the CDI cells were fully charged so as to measure the ion adsorption recovery ratio using solely the recovered energy. Ideally, the ion adsorption recovery ratio of the charged cell should be proportional to the energy that was recovered. The ion adsorption recovery ratios of the charged cells were 5, 46, 49, 35, 56, 56, 51 and 49 % with the circuit sequences [v], [i, ii, v], [i, iii, v], [i, iv, v], [ii, iii, v], [ii, iv, v], [iii, iv, v], and [i, ii, iii, iv, v], respectively. Amongst these circuit sequences, [ii, iii, v] and [ii, iv, v] exhibited the highest ion adsorption recovery ratio. As presented in Fig. 4.19, the ion adsorption recovery ratio is generally in proportion to the energy recovery ratio in the range up to 70 %. It was observed, however, that the ion adsorption ratio decreases in spite of the higher energy recovery ratio, particularly in the case of [i, ii, iii, iv, v] switching sequence. The reason for the fluctuation, observed in the proportional range, is that the interval time for each circuit switching was fixed at 5 min. The stepwise voltage change accompanied by the inrush of current at each switching has different relaxation times based on the voltage change, the density of ions at the electrode and other factors.

By taking this into account, it is noted that optimizing the energy recovery process could elevate the ion adsorption recovery ratio. On the other hand, the time interval of energy recovery processing in the [i, ii, iii, iv, v] sequence was limited to only 3 min per circuit change, which was not enough for sufficient relaxation to effectively use the recovered energy for ion adsorption. In this latter case, the [i, ii, iii, iv, v] sequence having 5 steps or 4 switching times, is twice as high in comparison to a 3-step sequence with 2 switching times such as [ii, iii, v], in which an inrush current flows during every circuit change. This signifies that the inrush current affects the energy recovery ratio due to circuit conversion, and high current fluctuation may result in a low energy recovery due to the large energy loss. This is mainly attributed to the ohmic resistance of the CDI system and the voltage drop caused by circuit conversion. In particular, the energy recovery of the circuit sequence [i, ii, iii, iv, v] was 81 % and its ion adsorption recovery ratio was only 49%. In this case, even though increasing voltage was observed for the first two circuits, no significant change of ion conductivity was observed. This effect was mainly caused by abrupt circuit shifting and resulted in inefficient energy transfer.

In these energy recovery experiments, we used the SSR to control the circuit switching by taking the experimental scale into account. The electricity loss of a diode in the SSR is in proportion to the forward voltage as it turns on. Since this forward voltage is approximately constant regardless of the power supply, the electricity loss becomes larger with increasing electric current. Therefore, it may be possible to realize higher ion adsorption recovery by using a point contact relay in place of the SSR. Furthermore, optimization of the charge/discharge interval is also important. Thus, further study is vital in this matter.

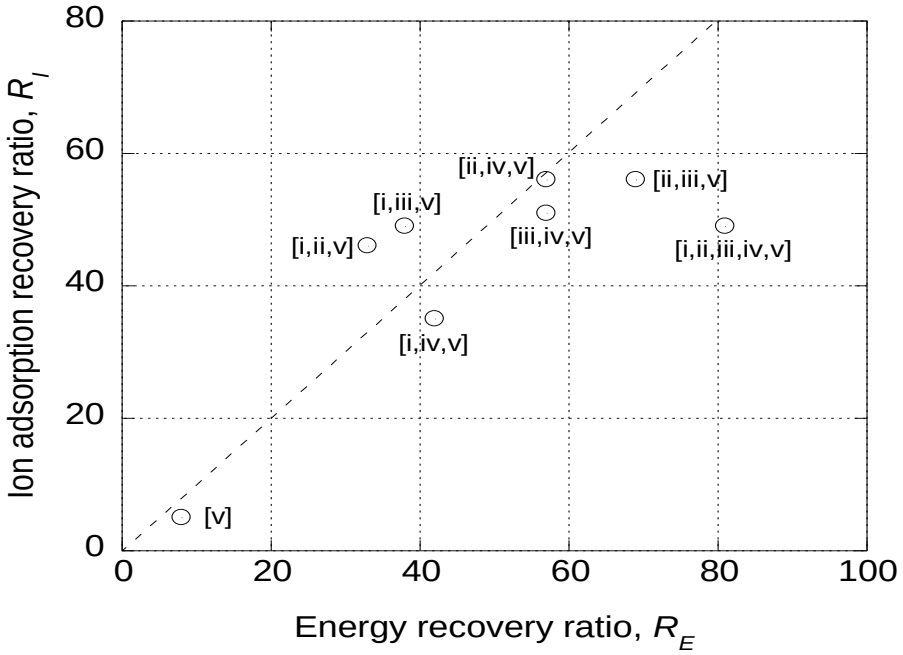

Fig. 4.19 - Relationship between ion adsorption recovery ratio and energy recovery ratio.

Although the recoverable energy from the discharge cells to the charge cells could be increased by regulating the circuit of the CDI system, the ion adsorption recovery was not always in proportion to the recovered energy. Nevertheless, this process could be improved by varying the experimental conditions, such as system flow rate, feed water ion concentration, time interval of circuit switching and constant current operation, which will be studied further in our laboratory.

References

1. Andres G. L., Yano N., Shiyoukei Y., Yoshihara Y. and Tanahashi M. (2014) *Journal of Water and Environment Technology*, **12**(3), 261-276.
2. Lee J. K., Kim Y. E., Kim J., Chung S., Dukjin J. and Lee J. (2012) *Journal of Industrial and Engineering Chemistry*, **18**(2), 763-766.
3. Bouhandana Y., Ben-Tzion M., Soffer A. and Aurbach D. (2011) *Desalination*, **268**, 253-261.
4. Andres G. L., Tanahashi M., Tanahashi S. and Yoshihara Y. (2014) *Journal of Chemical and Pharmaceutical Research*, **6**(8), 118-124.
5. Tanahashi M., Matsumura S., Yoneda H. and Umeda J. (1985) *Institute of Telecommunications Engineers*, CPM85-99, 19-24 (in Japanese).
6. Andres G. L., Shiyoukei Y., Yoshihara Y. and Tanahashi M. (2013) *Sustainability of Water Resources and Environmental Solutions to Climate Change*. Philippine Water Works Association, March 20-22, 2013, Manila, Philippines, pp. 98-104.
7. Andres G. L., Yano N., Shiyoukei Y., Yoshihara Y. and Tanahashi M. (2013) *The 5th IWA*

ASPIRE Conference and Exhibition, International Water Association, September 8-12, 2013, Daejeon, South Korea, 09A3-1.
8. Porada S., Bryjak M., van der Wal A. and Biesheuvel P. M. (2012) *Electrochimica Acta*, **75**, 148-156.
9. Dlugolecki P. and van der Wal A. (2013) *Environmental Science & Technology*, **47**, 4904-4910.

CHAPTER 5

DEVELOPMENT OF AN ION REMOVAL TECHNIQUE BASED ON CAPACITIVE DEIONIZATION FOR TREATMENT OF RINSING WATER OF INCINERATION ASH

5.1 Introduction

Incineration of household wastes has been utilized as an effective way to reduce its mass and volume. Currently, there are about 1,800 incineration plants in Japan incinerating approximately 50 million tons of household wastes or municipal solid wastes (MSW) per year to maintain sanitation and to reduce those volume and mass. The mass reduction in incineration is about 90 %, while 10 % of residual incineration ashes are buried in landfills hence only a small fraction of it are being recycled and reused. In recent years, recycling and reuse of incineration ashes have caught attention due to its increasing amount and limited available landfill spaces. Additionally, part of incineration ashes classified contain hazardous elements such as, heavy metals, toxic halogens and dioxins which could cause serious impact to the environment and ultimately to human health.

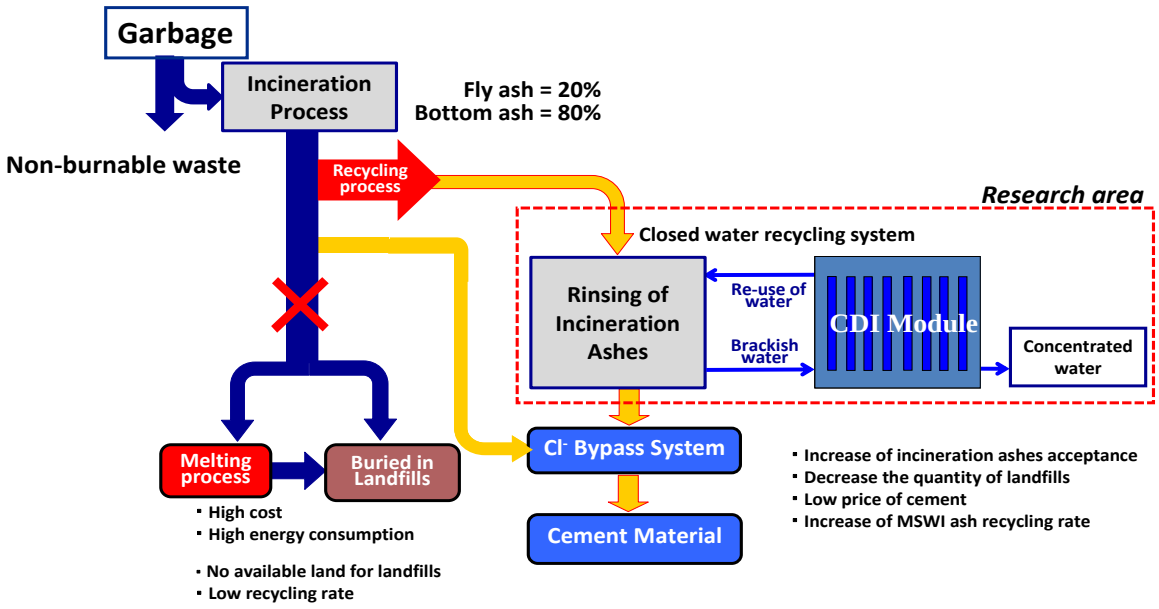

Fig. 5.1 - Schematic illustrations of the research background.

The schematic illustration of the research background of this study is shown in Fig. 5.1. At present, in some municipal waste treatment plants, incineration ashes are melted to make a molten slag to promote recycling as construction materials or aggregates. However, the energy cost to heat up ashes to around 1,700 K is preventing it from becoming popular. The molten slag also has the problem in strength as the aggregate materials. Another way to promote recycling is to use the incineration ash as a raw material for cement manufacturing. Since the chemical composition of incineration ashes is similar to cement, the quantity going into landfills can be reduced. Nonetheless, incineration ashes usually have high chloride ion content, which causes metal erosion especially in reinforced concrete. Therefore, the amount of incinerated ashes accepted is limited by the high cost and huge consumption of energy of the chlorine bypass system typically used for controlling the chloride content of the cement material. An alternative method to remove chloride is by rinsing the incineration ashes with water. Reverse osmosis (RO) is the most popular water treatment technology for this purpose. However, RO requires the pretreatment of its membrane to prevent clogging by the sludge in the liquid. The process also uses a large quantity of energy and the high cost of the fabrication as well as the maintenance can be prohibitive. In this regard, our research aims to develop a carbon electrode using inexpensive activated charcoal powder and construct a closed water re-circulating CDI treatment system for dechlorination of incineration ashes by water rinsing using the capacitive deionization technique. By utilizing this technology, the recycling rate of the residual ashes generated though incineration of municipal solid wastes will increased and the quantity of ashes going into landfills will be minimized. In this study, using the developed CDI stack system and the prepared bottom ash rinsed water was used as the aqueous electrolyte. The capacitive deionization performance was examined based on the Cl^- ion adsorption capacity.

5.2 Materials and Methods

5.2.1 Preparation of extracted ash sample (soluble and non-soluble chloride analysis)

The incineration ash samples were supplied by different incineration plants in Japan having different incineration capacity. The specifications of the ash samples is presented in Table 5.1. The chloride content of the ashes gathered from a stoker type incinerator, with a rating capacity ranging 400 - 700 t/day in spring, was measured and analyzed. The sample was dried in a constant-temperature oven for several hours to evaporate the moisture in the ash. It was then crushed into small particles and all visible metals were removed using a magnet. The desired amount of the prepared ash was washed with water. The ash and water were mixed vigorously for 1 h before separating the rinsed ash from the water using porous filter paper (5A, Advantec, φ = 300 mm). The amount of soluble chloride in the aqueous solution was measured using a chloride ion electrode (Horiba, Japan). The washed ash was dried for 12 h at 105 °C, then placed into a PTFE cylinder and subsequently washed with pure water and HNO_3 (nitric acid) solution. A dilution liquid was prepared in a ratio of 1:1 (HNO_3:pure water). Nitric acid was used to dissolve the non-soluble chloride, after which,

it was placed on a hot plate and heated for 1 h at 130 °C. It was then cooled at room temperature for 12 h before filtering and placed directly into a 250 mL container. Finally, the solution was analyzed by a Cl electrode to measure the amount of non-soluble chloride[2,3]. The soluble chloride removal efficiency with respect to the mass ratio of the washed water to the mass of ash was calculated using eq. (5.1).

$$Rr = \left(1 - \left(\frac{1}{x}\right)\left(\frac{a}{1-a}\right)\right) \times 100[\%] \quad (5.1)$$

where x is the mass ratio of washed water as a function of the ash moisture content a after washing.

Table 5.1 - Sample name, incinerator type and incineration rating capacity.

Facility	Sample		Type	Incinerator capacity	Cooling process
	Incineration ash	Fly ash/Melting fly ash			
A	Export ash A		Stoker	400t/day	Wet-type
	Pit ash A				
B	Export ash B			600t/day	
	Pit ash B				
C	Bottom ash C-1	Fly ash C		700t/day	Semi-wet type
	Bottom ash C-2	Fly ash C			
	Bottom ash C-3				
D	Bottom ash D			600t/day	
E		Fly ash E		400t/day	
F		Fly ash F		400t/day	
G		Fly ash G		400t/day	

5.2.2 Preparation of extracted ash samples for alkali metal, alkali earth metal, and heavy metal ions analysis

The elemental concentrations of extracted incineration ash, particularly heavy metal ions were analyzed using an inductively coupled plasma atomic emission spectrometer shown in Fig. 5.2 (ICP-9000, Shimadzu, Japan). Ash samples were prepared with given mass ratios of rinse water to incineration ash. After washing, the mixture was carefully filtered using a porous filter paper to separate the solid from the liquid. Because the concentration of ions from the solution varied, different volume ratios using the prepared dilution liquid (HNO_3: pure water = 1:500) were used for accuracy of the measurements. The pH of the solution was maintained at <2 to prevent scaling at a nano-sized nozzle of the ICP instrument (Japan Standards Association, 2010).

Fig. 5.2 - Inductively Coupled Plasma Atomic Emission Spectrometry Analyzer (ICP-AES).

5.2.3 Removal of calcium (Ca) by carbon dioxide (CO_2) treatment

Fig. 5.3(a) demonstrates the schematic drawing of the pilot scale micro-bubble generator system fabricated in our laboratory. Nitrogen (N_2) gas was used to dilute the carbon dioxide (CO_2) to control the amount of CO_2 gas. In this experiment, a sample labeled as C-3 was utilized to study the effect of carbon dioxide treatment. The treatment was executed by immersing a porous ball filter at a bottom of the cylinder and generated micro-bubbles as shown in Fig. 5.3(b).

Each 50-mL sample was treated while the concentrations of carbon dioxide, 5 % and 10 %, were used. The summary of the dilution ratio is presented in Table 5.2. After, the treated water was filtered using porous filter paper 5B before elemental concentration analysis using the ICP-AES instrument. Furthermore, the filtered precipitates (Fig. 5.3(d)) acquired from the treated water were analyzed by an EDAX (Energy Dispersive Analysis X-ray) instrument.

Table 5.2 - Dilution ratio of carbon dioxide to nitrogen gas.

	5% CO_2 gas		10% CO_2 gas	
	Ratio [mL/min]	%Ratio [%]	Ratio [mL/min]	%Ratio [%]
Gas mixture	130	—	130	—
CO_2	6.5	5	13	10
N_2	123.5	95	117	90

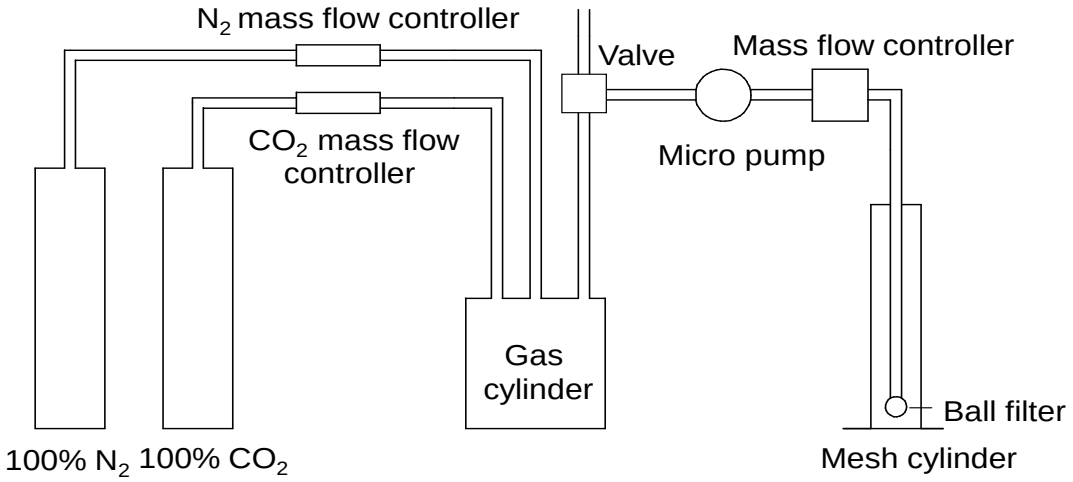

(a)

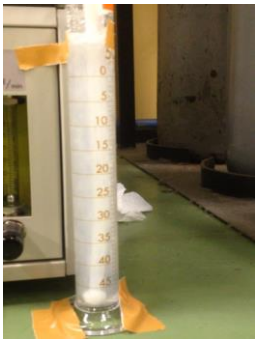

(b)

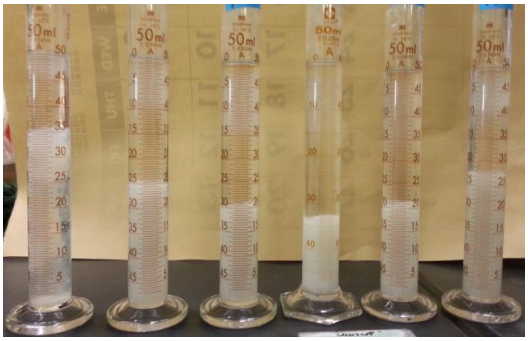

(c)

(d)

Fig. 5.3 - (a) Schematic drawing of CO_2 dilution system (micro-bubble generator system), (b) CO_2 treatment reaction process in mesh cylinder, (c) After CO_2 treatment images and (d) dried precipitates collected in the filter paper.

5.2.4 CDI using incineration ash rinsed water

The ion adsorption/desorption performance of the developed CDI stack system[1] comprising of a four-pair activated charcoal electrodes was evaluated using the prepared bottom ash rinsed water (C-3, S:L=1:4 mass ratio). The internal volume of the CDI stack was measured to be 100 mL including the electrode adsorbed water. The evaluation was carried out using a combination of flow-through and batch processing. The 300 mL bottom

ash rinsed water was constantly re-circulated at a flow rate of 20 mL/min whilst the change of ion conductivity, chloride concentration and pH of the feed solution was analyzed using the ion conductivity probe, chloride ion electrode and pH probe (pH/conductivity meter, Laqua F-74, HORIBA, Japan). The ion adsorption/desorption performance of the developed electrode was evaluated according to eq. (4.1)

The power consumed $P_{consumed}$, during ion adsorption process, was analysed according to the following equation:

$$P_{consumed} = \frac{\int_0^t V_c i_c dt}{v} \tag{5.2}$$

where, V_c is the applied potential [V] and i_c current [A] at a given time t, v volume of the processed solution [L].

5.3 Results and Discussion

5.3.1 Analysis of Soluble and Non-soluble Chloride

To evaluate the required specification of the CDI system for the treatment of rinsed water of incineration ash, the chloride content has been monitored. The mass ratio of rinsed water to incineration ashes was investigated to realize the most efficient removal of chloride from rinsed water so as to minimize its regeneration load. It is said that approximately 1 – 2 % of chlorides is included in the incineration bottom ash. In addition, the chlorinity is known to change by difference in incinerator type and in quality of garbage by the season. In this evaluation, it shows that the total amount of chloride in the ash sample was around 1 %. Fig. 5.4 shows the removal efficiency of the mass ratio of rinsed water to bottom ash. The moisture content after washing was found to be 35 %. Measuring the moisture content of the ash after washing plays an essential role particularly in analyzing the soluble chloride. It could cause serious problems when used as aggregates for cement manufacturing. In the case of soluble chloride removal efficiency shown in Fig. 5.4, the chloride removal rate was calculated to be 90 % for a solid: liquid ratio of 1:4. Non-soluble chloride is believed to exist together with other compounds such as calcium oxide (CaO) and aluminum oxide (Al_2O_3) or Friedel's salts. Utilizing eq. (5.1), the calculated removal rate for a solid: liquid ratios of 1:2, 1:4, 1:6, 1:8 and 1:10 are 78, 90, 92, 92, and 96 %, respectively. The chloride removal efficiency of the experimental data was measured to be most likely identical to the calculated one as shown in Fig. 5.4. This specifies that soluble chloride was dissolved perfectly while the residual chloride with rinsed ash are non-soluble chloride and some soluble chloride exists in the residual water in ash. Meanwhile, as rinsed water increases, the rate of soluble chloride increases, which implies that almost all chlorides were dissolved. The mass ratio of rinsed water to bottom ash appears to be ideal within the range of 1:3 and 1:4 for effective analysis and economical for brackish

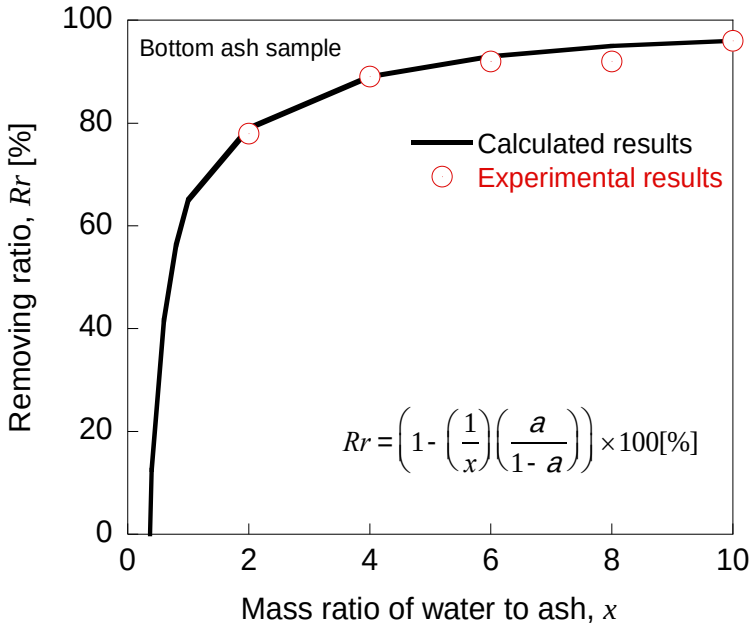

Fig. 5.4 - Soluble Chloride removal efficiency as a function of mass ratio of rinsed water to dry bottom ash (using sample C-3).

water purification. This result signifies that the analysis is accurate when soluble and non-soluble chlorides exist in the rinsed water sample.

On the other hand, analyzing the incineration fly ash, it shows that a total of chloride was 29.6 %. As shown in Table 5.3, 99.6 % of chloride in the incineration fly ash-C was soluble chloride where non-soluble chloride (Friedel's salt) indicated 0.4 %. Majority of the chlorides contained in the fly ash were water soluble and could be dissolved by just washing process. Moreover, no significant effect was found on the removal rate of the soluble chloride even by changing the weight ratio of the wash water as can be seen in Fig. 5.5, and even by lowering the weight ratio because it can also remove nearly 90 % of chlorine. Analyzing the suitable ratio for removing soluble chloride in incineration bottom ash and fly ash, could be cost effective since increase of the processing liquid volume could also elevate the total processing cost. Therefore, the results obtained in this study is reasonable and can be a useful guide for designing efficient incineration facility.

Table 5.3 – Chloride content of incineration fly ash-C.

Sample	Chloride	Cl content %	Rate %
Fly ash C	Total	29.6	-
	Soluble	29.5	99.6
	Non-soluble	0.1	0.4

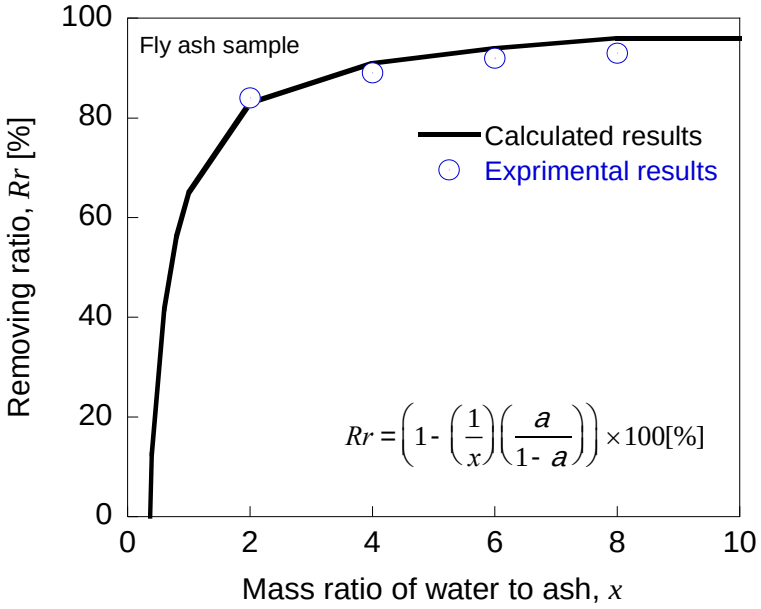

Fig. 5.5 - Soluble Chloride removal efficiency as a function of mass ratio of rinsed water to dry fly ash (using sample fly ash-C).

5.3.2 Elemental analysis of the incineration ash rinsed water

Heavy metal concentrations in incineration ash vary depending on the volatility and boiler combustion conditions during the incineration process. Bottom ash usually does not need to be treated due to its low level of heavy metal concentrations. However, there are standards that must be considered since heavy metals from incineration ash could cause negative effects on the environment and especially to human health. Therefore, it is highly critical to determine the concentration of heavy metals in incineration ash and control their amounts. Bottom ash samples A, B, C and D were obtained from stoker type incineration plants having different rating capacities. Table 5.4 presents the elemental analysis of extracted bottom ash samples with a 1:4 mass ratio of bottom ash to rinsed water (S: L).

The pH values of all ash samples indicate high alkalinity when alkali metals such as Na and K are abundant. Alkaline earth metal Ca is present in significant amounts whereas the Mg average content varies. Heavy metal ions are present in a minimal amount except for Pb and Cu with concentrations ranging 0.2 - 0.6 mg/L and 0.04 - 0.89 mg/L, respectively. Generally, chloride concentration included in an incineration bottom ash is known to change with difference in incinerator type and in quality of garbage by the season. Hence, the chloride content of the bottom ash in a stoker type incinerator was measured and

analyzed in spring. In this evaluation, it shows that the average amount of chloride in the bottom ash rinsed water varied depending on the ash sample. Moreover, since the analysis is likely in a good agreement with the total DS (dissolved solid), if it is calculated from the concentration of Na, K, Ca and Cl ions, it is presumed that many of such compounds exist as chlorides and these have mostly dissolved in the rinsed water. Furthermore, chloride concentration in samples labeled as A-1 and B-1 were relatively high as compared to the C-3. This is because A and B samples were both used as cooling water in the respective incineration plants, and thus based on the analysis it was found to have a high level of chloride ion. These samples were analyzed in a liquid form and analyzed as it is. On the other hand, powder C and D samples were washed with distilled water and the dissolved components were analyzed.

Table 5.4 - Elemental analysis of the bottom ash rinsed water.

Unit : mg/L

	Sample	Ba	Ca	Cd	Cr	Cu	K	Mg
Rinsed Bottom Ash	A-1	-	1900	ND	1.4	0.04	850	-
	B-1	-	1300	ND	0.12	0.69	530	-
	C-1	0.13	200	0.01	0.12	0.07	90	0.022
	C-2	0.03	70	0.01	0.16	0.35	140	0.004
	C-3	-	20	ND	0.31	0.06	190	-
	D-1	0.03	150	0.02	0.09	0.89	60	0.116

Unit : mg/L

	Sample	Na	Pb	Sr	Zn	pH	Cl (Cl Electrode)	TDS
Rinsed Bottom Ash	A-1	4800	ND	-	0.20	12.2	11000	21200
	B-1	1300	ND	-	0.10	12.3	6760	12800
	C-1	90	0.5	0.44	-	10.3	1790	3380
	C-2	790	0.2	0.22	0.04	11.8	1350	3650
	C-3	580	ND	0.03	ND	11.8	1200	3540
	D-1	60	0.6	0.31	0.08	10.1	1080	3810

TDS: Total dissolved solids

Table 5.5 shows the washing liquid elemental analysis results of the incineration fly ash. For any of the incineration fly ash, chlorine concentration is higher compared to incineration bottom ash. It is understood that the chlorine is immobilized by blowing lime in incinerator exhaust gas treatment process. This is obvious since Ca concentration was in a significant amount. Similarly, the concentrations particularly, Na and K has become high. For heavy metals, unlike incineration bottom ash, heavy metals concentration in the incineration fly ash are higher, such as Pb, Cu and Zn. Although it seems that high concentration of heavy metals were in fly ash, it can be reduced by coagulation-sedimentation process.

Table 5.5 - Elemental analysis of the fly ash rinsed water.

Unit : mg/L

	Sample	Ba	Ca	Cd	Cr	Cu	K	Mg
Rinsed Fly ash	E	3.7	10000	0.1	1.0	0.5	10100	0.1
	C	3.3	8700	0.2	1.6	0.3	13500	1.4
	F	3.2	14100	0.1	1.3	0.6	8800	0.2
	G	1.0	4200	0.1	2.4	0.3	11800	2.1
	C	2.3	4800	0.1	0.8	1.1	33700	0.1

	Sample	Na	Pb	Sr	Zn	pH	Cl	TDS
Rinsed Fly ash	E	7400	2.1	13.2	1.9	11.8	44000	78600
	C	9900	1.0	7.8	0.2	7.3	62200	91200
	F	4900	-	29.6	3.2	11.7	57400	104400
	G	7400	6.2	7.5	0.1	7.6	43700	54000
	C	32500	11.9	9.4	0.5	7.3	123000	156500

TDS : Total dissolved solids

5.3.3 Removal of calcium (Ca) by carbon dioxide (CO_2) treatment

As can be seen in the elemental analysis of the incineration ash rinsed water in Table 5.4 and 5.5, calcium (Ca) ions are present in a significant amounts. In addition, Ca compounds exist in the incineration ash rinsed water, which could cause the scaling problem on the porous electrode since these compounds usually attached permanently when flowed through the CDI system. This may cause degradation of ion adsorption/desorption performance of the electrode. Fig. 5.6(a) shows the photo of the activated charcoal electrodes before and after capacitive deionization experiments, using the bottom ash rinsed water sample C-3. Fig. 5.6(b) illustrates the EDAX analysis results on the anode and cathode surface layer. It is noticeable that extensive amount of calcium was attached on the cathode after ion adsorption process, which was confirmed with the EDAX analysis. Wherein, a fraction of calcium was impregnated on the electrode surface layers as can be seen (after ion adsorption/desorption process (cathode) in Fig. 5.6(a).

In consideration to this effect, calcium compounds from incineration ash rinsed water needed to be removed before capacitive deionization process. And this could be done by carbon dioxide (CO_2) treatment using the fabricated micro-bubble generator. Meanwhile, chemical reactions may be generated during the treatment process. It is known that calcium compounds for instance, calcium hydroxide ($Ca(OH)_2$) exists in the rinse water therefore when CO_2 gas was employed, then the water becomes cloudy (milky liquid) and coagulation of compounds takes place. Here, calcium carbonate ($CaCO_3$) was produced as defined from the chemical eq. (5.4). Another reaction might take place when excessive amount of CO_2 gas was incorporated. In this case coagulated compounds (milky liquid)

will be dissolved and converted into ions in a form of aqueous calcium bicarbonate ($Ca(HCO_3)_2$). The chemical eq. (5.5) shows the chemical reaction of this phenomenon.

$$Ca(OH)_2 + CO_2 \rightarrow CaCO_3 + H_2O \quad (5.4)$$

$$CaCO_3 + CO_2 + H_2O \rightarrow Ca(HCO_3)_2 \quad (5.5)$$

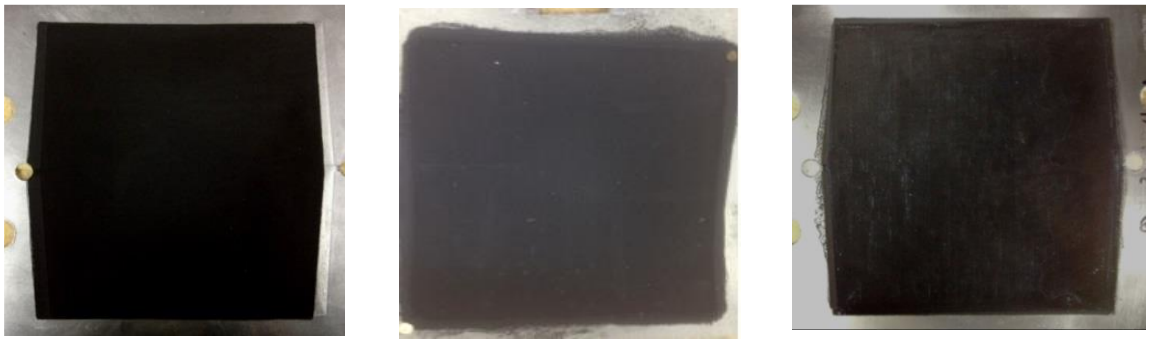

Before CDI process | After ion adsorption/desorption process (anode) | After ion adsorption/desorption process (cathode)

(a)

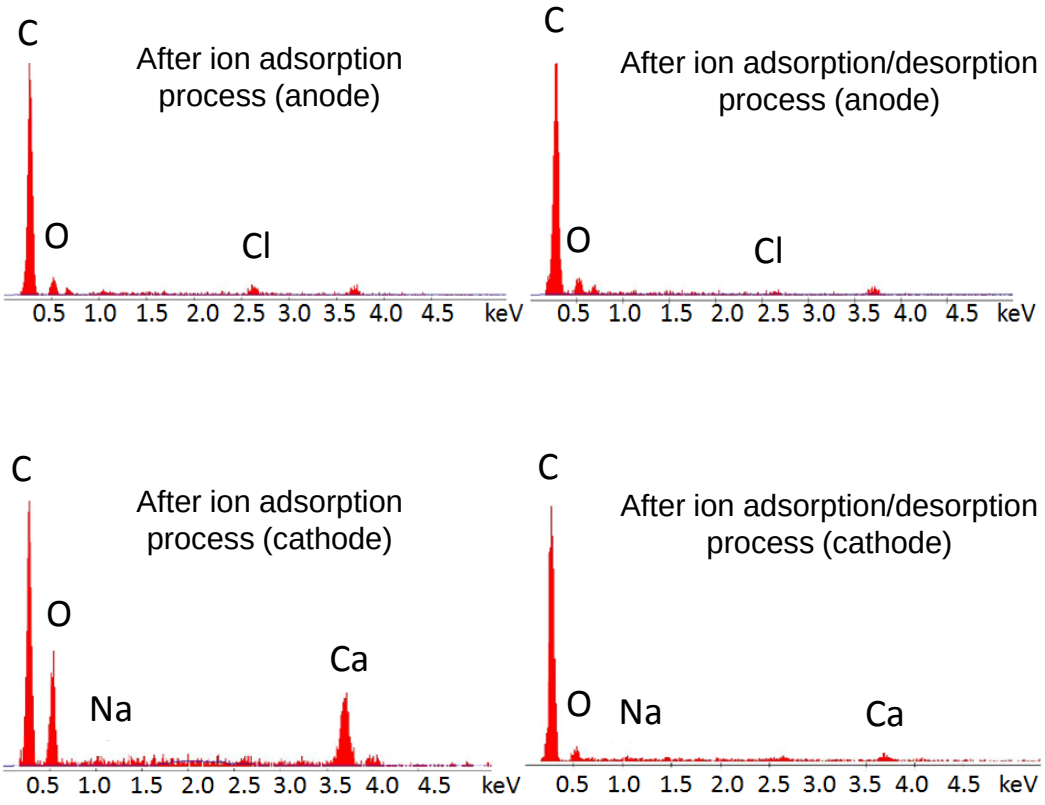

(b)

Fig. 5.6 - (a) Carbon electrode surface layer and (b) EDAX analysis results on the anode and cathode surface layers before CDI process, after ion adsorption process and after ion adsorption/desorption process.

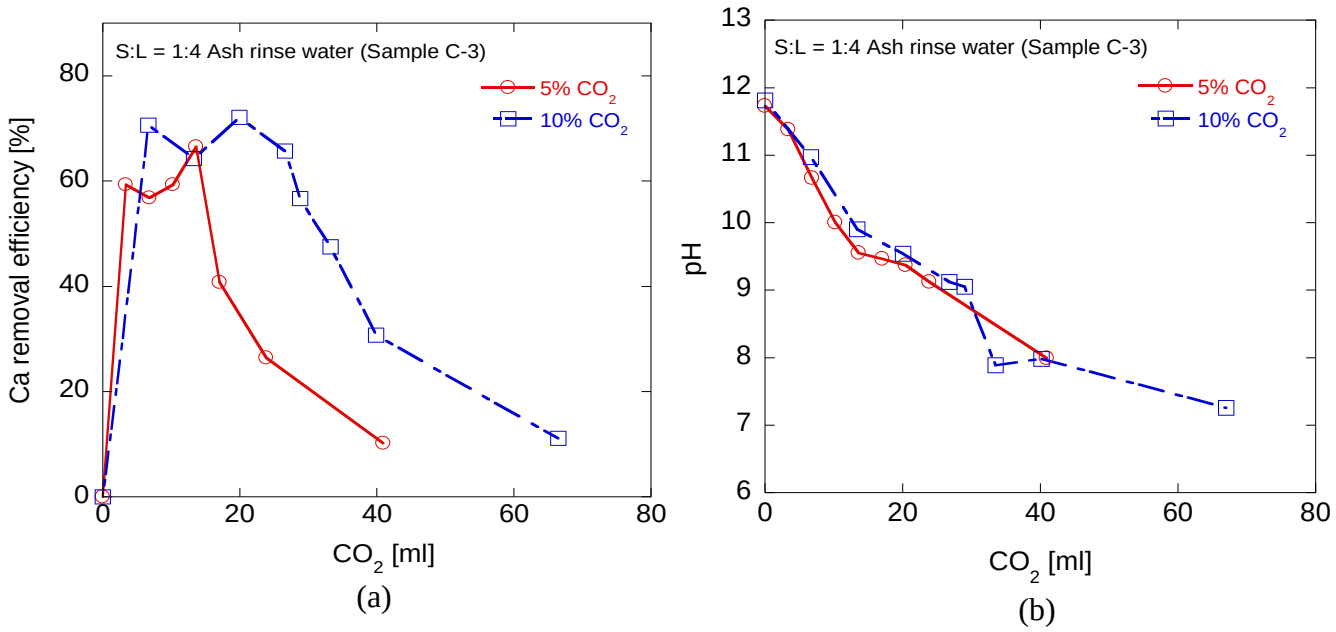

Fig. 5.7 - (a) Calcium removal efficiency to the amount CO_2 gas used and (b) pH change of the rinse water to the amount CO_2 gas used.

Consequently, the results obtained from CO_2 gas treatment of the sample C-3 are shown in Fig. 5.7. The amount of Ca removal with respect to the amount of CO_2 gas used is shown in Fig. 5.7(a). The Ca concentration decreased significantly when the CO_2 gas was incorporated with the amount of 6.65 and 3.41 mL for 10 % and 5 % CO_2 gas, respectively. Hence, the removal rate in the case of 10 % CO_2 gas indicated 72 % while 59 % in the case of 5 % CO_2 gas. In both cases, the removal of Ca was efficient enough to make chemical reactions. In the same graph, one can see that the removal efficiency was gradually decreased as the amount of CO_2 gas increased. This indicates that chemical reaction in eq. (5.5) has taken place. Moreover, although in this experiment the chemical reaction in rinsed ash water depending on the difference between the amounts of CO_2 gas was revealed, however controlling the chemical reaction was not taken into account. Therefore, it is suggested to increase the gas-liquid contact interfaces so as to control the chemical reactions. This could be done by increasing the effective area of the porous filter to generate finer bubbles (micro-bubbles). Accordingly, the change of pH with respect to the amount of CO_2 gas is shown in Fig. 5.7(b). Although the Ca removal efficiency was decreasing as the amount of CO_2 gas was increasing, the pH of the rinsed water was constantly decreasing. This is caused by continuous decomposition into hydrogen ion (H^+), wherein water reacting with carbon dioxide changes to unstable carbonic acid, and followed by decomposition into the hydrogen ion and hydrogen carbonate ion therefore converted the rinsed water into a slightly acidic. The chemical equations for these reactions are shown in eqs. (5.6) and (5.7).

$$H_2O + CO_2 \rightarrow H_2CO_3 \quad (5.6)$$

$$H_2CO_3 \rightarrow H^+ + HCO_3^- \quad (5.7)$$

The results from the carbon dioxide treatment at different concentrations justified that hydroxide like calcium hydroxide exists in the ash rinsed water, which is then removable by carbon dioxide treatment wherein 72 % Ca removal efficiency for the sample C-3 in a form of calcium hydroxide (10 % CO_2 gas) was achieved. However, possibility that other forms of compound such as calcium chloride exists in the rinsed water was not removable. In such a case, this could be treated during CDI process.

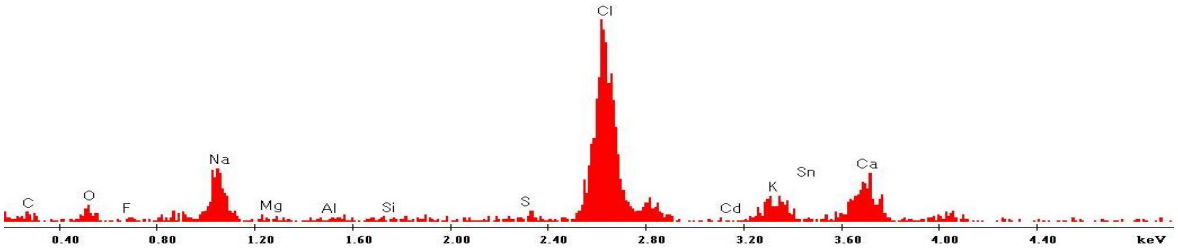

(a)

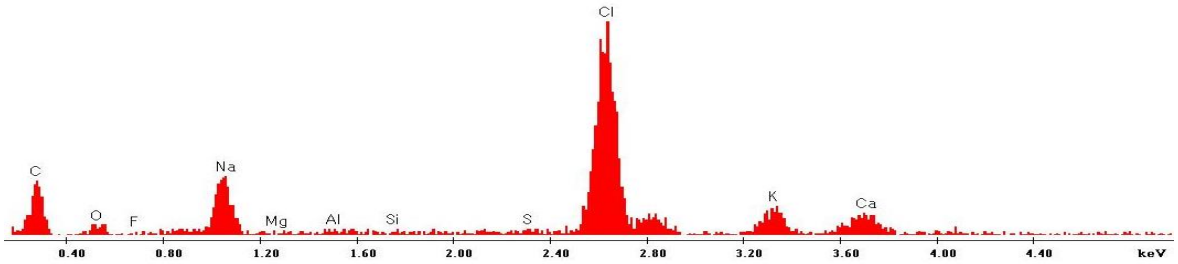

(b)

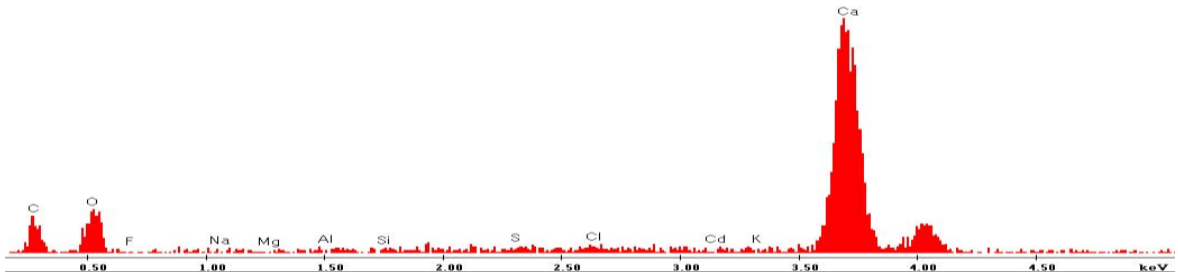

(c)

Fig. 5.8 - Precipitates (DS) EDAX analysis (a) Original water before CO_2 treatment, (b) After CO_2 treatment and (c) Filtered precipitates.

For deeper understanding about the elemental concentrations in the incineration ash rinsed water and the effect of carbon dioxide treatment, EDAX analysis was performed. A fraction of water sample before and after carbon dioxide treatment was dried in a drying oven. The precipitates acquired from the filter paper was gathered and dried for several hours until all samples became powder. The EDAX analysis results are shown in Fig. 5.8. If we compare the TDS of the rinsed water before (Fig. 5.8(a)) and after (Fig. 5.8(b)) CO_2 treatment, basically one would think that the intensity rate of the Ca would drop, since it was removed by CO_2 treatment. Apparently, the results from EDAX analysis revealed that Ca still exists in the rinsed water, which it was thought to be due to chloride compounds as mentioned earlier. In line with this, the analysis result of the precipitate as shown in Fig. 5.8(c) demonstrates that the intensity rate of Ca, C and O was high, which implies that it was deposited as calcium carbonate ($CaCO_3$).

5.3.4 Capacitive deionization using incineration ash rinsed water

Fig. 5.9 presents the ion adsorption capacity evaluation of the developed CDI stack system. Upon polarization, the ion conductivity of the flowing bottom ash rinsed water was decreased from 4.81 to 4.09 mS/cm corresponding to 15 % ion adsorption efficiency and equivalent to 0.067 mol/m^2 ion adsorption capacity. The chloride ion adsorption capacity was also measured and exhibit a 30 % ion adsorption efficiency, corresponding to ion adsorption capacity of 0.093 mol/m^2. Ideally, chloride concentration should at least reduce to ~50 % so that the rinsed water could be recycled for another washing process. Accordingly, in the case of recycling incineration ash for production of ordinary portland cement (OPC), cement manufacturer required that chloride content in the incineration ash is less than 0.1 % (1000 ppm)[4]. Thus, the proposed CDI process in this study is a closed re-circulating system wherein the amount of water used for washing to control the chloride concentration would be minimal. On the other hand, the condensed solution produced when the electrodes were regenerated could be used for another application such as salts for melting snow by chemical reaction process. From the same figure, as soon as the potential was applied, the current flowing in the CDI system dramatically decreased from 12 to 0.04 A, indicating that electrodes were saturated with ions. Whereas, the apparent power consumption was calculated based on the current measured at the same applied potential with respect to time. The consumed power during ion adsorption process after 10 min was 25.6 mWh/L. Table 5.6 presents the summary of CDI stack ion adsorption/desorption performance. One can see that the ion conductivity and chloride ion desorbed was 2 times higher than the adsorbed ions. This is because, the regeneration process was executed in batch processing by halting the flowing solution. By this time, the processed solution (4.09 mS/cm, 780 mg/L) remained inside the CDI stack and was reused as electrolyte to regenerate the electrodes. Here, the amount of ion desorbed solution was two times lower (100 mL) than the processed water during ion adsorption process (300 mL). The disproportion of the amount of desorbed ions denotes that the electrodes were regenerated ineffectively due to a fraction of uncollected solution having low resistance. Hence, ionic solution having low resistance may influence the ion adsorption capacity of the CDI system due to the loss of energy caused by a high voltage drop.

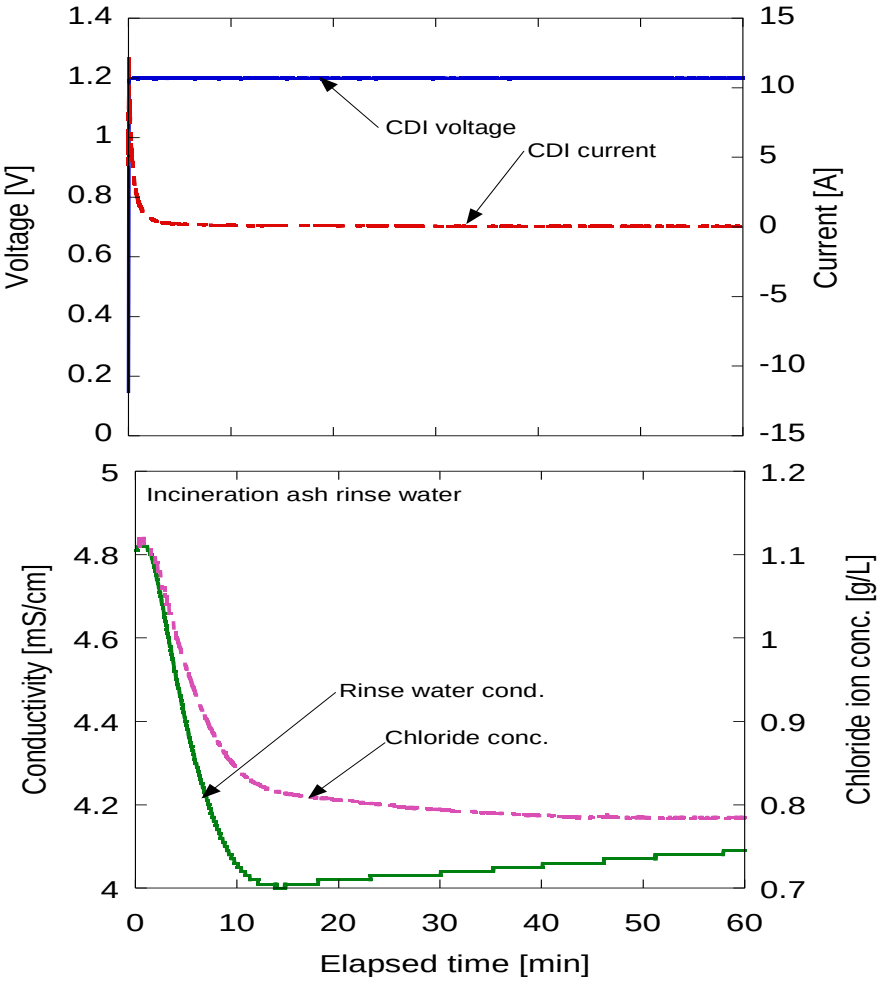

Fig. 5.9 - Voltage-current profile and ion adsorption performance of the CDI stack in flow-through processing condition using the prepared bottom ash rinsed water.

Table 5.6 - Summary of ion adsorption/desorption of PVA-bonded electrode.

Adsorbed ions					
Ion conductivity [mS/cm]			**Cl- ion concentration [g/L]**		
Initial	Final	Ion-adsorbed	Initial	Final	Ion-adsorbed
4.81	4.09	0.72	1.120	0.78	0.34
Desorbed ions					
Initial	Final	Ion-desorbed	Initial	Final	Ion-desorbed
4.09	5.77	1.68	0.78	1.340	0.56

Furthermore, the ion adsorption/desorption performance and durability of the prepared carbon electrode were evaluated at various voltages ranging from 0.8 to 1.4 V. The ion adsorption/desorption performance of the CDI stack is presented in Fig. 5.10. The ion adsorption time was 15 min and the electrode regeneration was executed with a desorption potential of 0.0 V while short-circuiting the electrodes. It is obvious that the ion conductivity of the incineration ash rinse water decreased as the applied voltages increased. The summary of the ion adsorption capacity is depicted in Fig. 5.11.

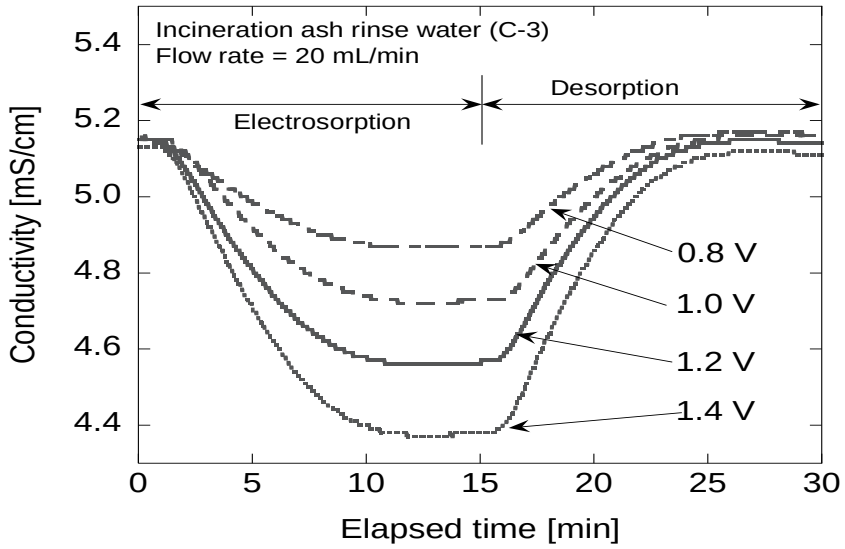

Fig. 5.10 - Change of ion conductivity with respect to the applied voltages.

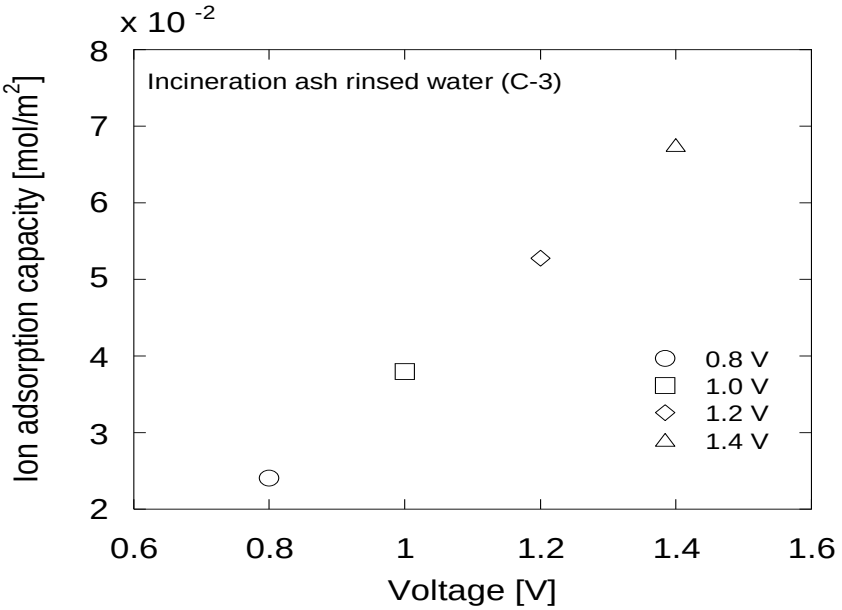

Fig. 5.11 - Summary of ion adsorption capacity.

Here, the decrease of ion conductivity depends on the voltage applied on the electrodes, therefore the ion adsorption capacity exhibited in a linear form. This indicates that the voltage supplied on the electrode was effectively utilized for ion capturing. In addition, the carbon electrode shows high durability even in a high electric field since the experiments were done one after another. Fig. 5.12 shows the pH of the solution during ion adsorption/desorption process. One can see that the final pH of the solution was increased simultaneously with the decrease of ion conductivity, when the electrode was charged, then the pH returns to about its initial value after capacitive deionization process.

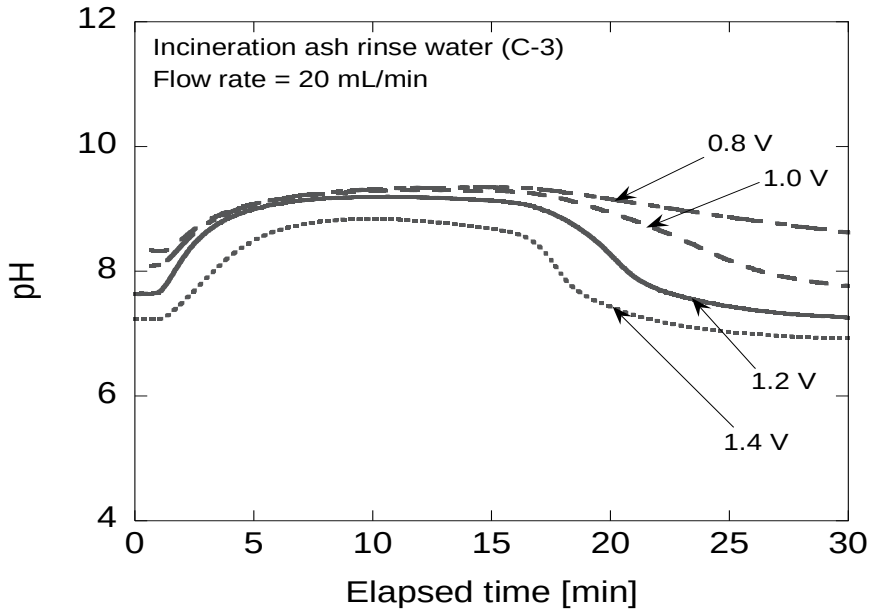

Fig. 5.12 - pH change of the rinsed water at various voltages.

Accordingly, the pH increased simultaneously with increasing voltages even at a low voltage of 0.8 V. This is caused by the reactions at the electrodes at the time the ions are being electrosorbed. Also, the ionic reactions must be considered since the electrolyte (incineration ash rinses water) used in this experiment is consisted of various ions with different equilibrium constants for hydrolysis. In this experiment, the similar pH patterns were observed from the work of *Lee et al.* (2010)[5]. In the case of 0.8 V, the pH was increased from 8 and remained constant at pH 9.3. This means that generation of OH^- at the cathode is in constant rate and therefore reduction of dissolved oxygen (DO) from the influent is also in constant rate. Dissolved oxygen is known to undergo reduction reactions on the cathode surface layer through two pathways, as demonstrated in the following chemical equations.

(1) Direct four-electron pathway:

$$O_2 + 2H_2O + 4e^- \rightarrow 4OH^- \qquad E^o = 0.401\ V \qquad (5.8)$$

(2) Peroxide pathway:

$$O_2 + H_2O + 2e^- \rightarrow HO^-_2 + OH^- \qquad E^o = -0.065\ V \qquad (5.9)$$

followed by the reduction of peroxide:

$$HO^-_2 + 2H_2O + 2e^- \rightarrow 3OH^- \qquad E^o = 0.867\ V \qquad (5.10)$$

As shown in eq. (5.8), due to continuous reduction of dissolved oxygen on the cathode, OH^- is produced. While in the eq. (5.9), neither DO nor OH^- is reduced. Regardless of the pathways, OH^- is produced which lead to the increase in pH during ion adsorption process. Despite of these slight reactions, the ion conductivity of the solution goes back from its original value when the electrodes were regenerated, which indicates that the capacitive deionization process was efficient.

5.3.5 A closed re-circulating CDI washing system

For the purpose of further recycling promotion of the incineration ashes for cement raw material, the closed washing system of incineration ashes for regulating its chloride concentration was investigated by applying the developed CDI system. Additionally, even though only incineration bottom ash is an ideal component as cement raw material, for further study, we also considered the use of fly ash.

5.3.6 Utilization of incineration ash

In a stoker-type incinerator, the most popular type in Japan, incineration ashes are cooled by water to prevent explosion and dust generation. As for ash cooling equipment system, there are wet and semi-wet cooling systems. A wet system comprises a water bath and a flight conveyor. On the other hand, a semi-wet system comprises an ash extractor. In this study, an incineration system having wet type ashe cooling equipment is evaluated since a closed-chloride washing system could be built easily by installing a CDI system. The analysis for ion extraction by washing incineration ashes had been conducted in previous experiments. As shown in Fig. 5.13, is the wet process ash cooling method. The drain area which located at the bottom of the stoker-type incinerator is continuously draining the ashes. The ashes are then cooled and washed in a scraper conveyor with cooling water. This cooling water tank could serve as a deionization washing tank. Table 5.7 shows the plant specifications that we examined.

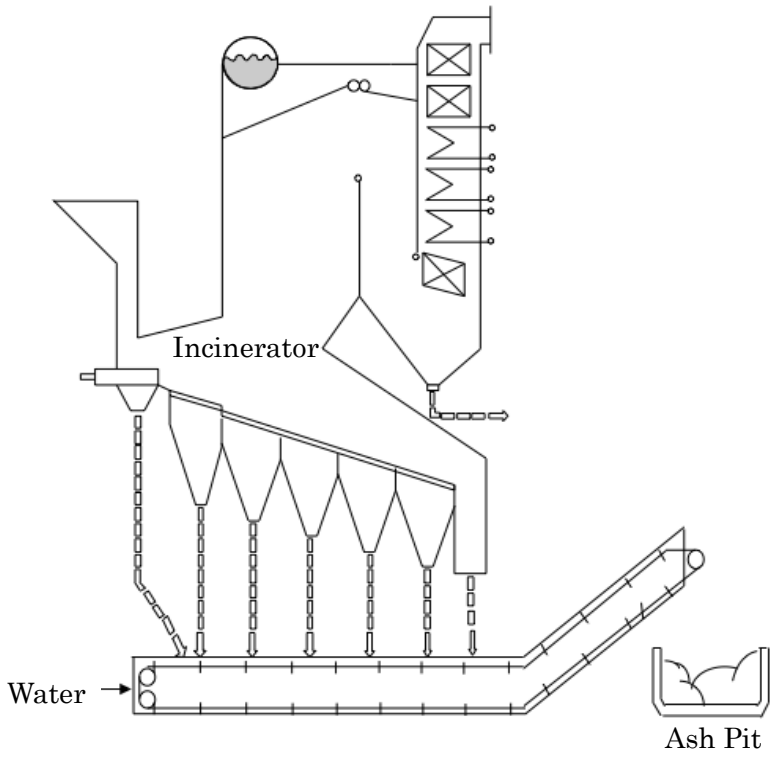

Fig. 5.13 - Typical wet ash-cooling system.

Table 5.7 - Target waste processing facility specifications.

	Stoker type
Exhaust gas cooling system	Water spray type
Incineration rating capacity	37 t/day * 2 incinerator, (74 t/day)
Ash removal system	Wet type

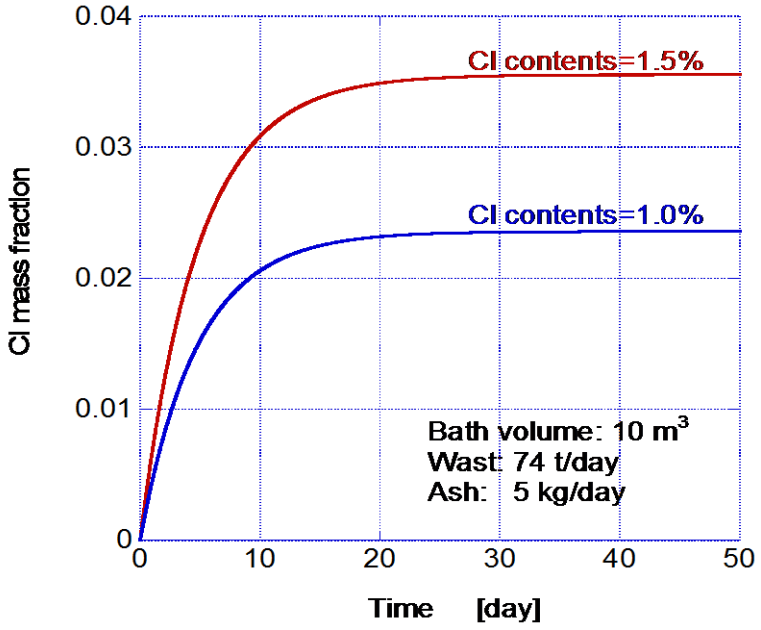

Fig 5.14 - Chloride concentration changes of washed ash in the cooling water tank.

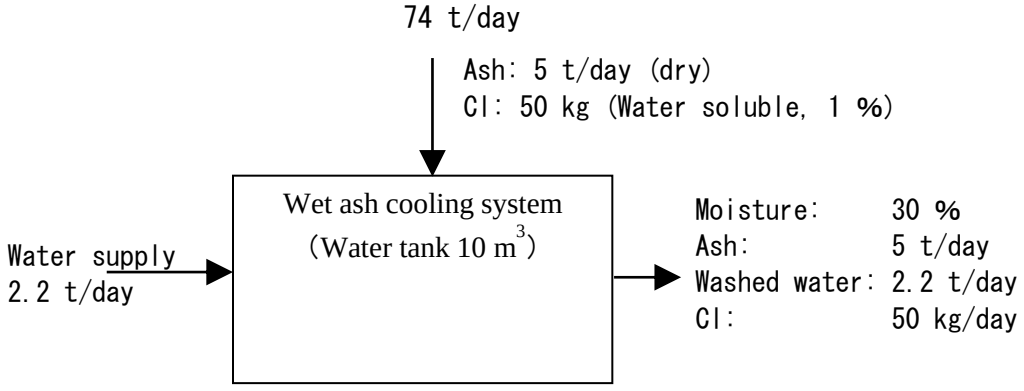

Fig 5.15 - The material balance in equilibrium state.

Generally, in the wet ash cooling system, the level of the water tank is kept constant and the water is conveyed along with the ash. Therefore, the chloride and heavy metals components included in ashes are concentrated, and eventually reached in equilibrium state. The concentrations of chloride and heavy metals that are supplied in the water tank and the mass exiting are balanced.

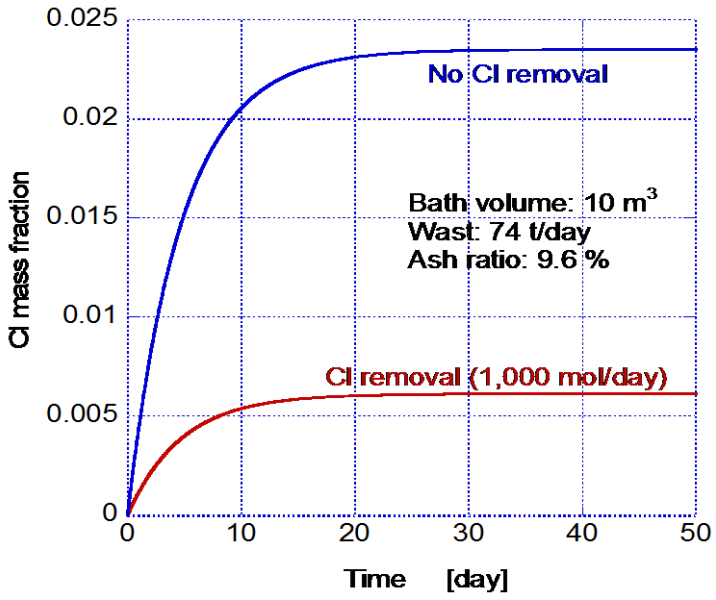

Fig. 5.16 - Chloride concentration changes in the cooling water tank when doing chloride removal.

The simulated changes of chloride concentrations in the water tank and the specification of the incinerator plant are presented in Fig. 5.14 and Table 5.4, respectively. The changes of chloride concentrations in the water tank is the calculation results obtained when water-soluble chloride concentration in the ash were 1 % and 1.5 %, whilst the water outlet rate from the water reservoir was 30 %, when the volume of the tank was 10 m^3. As can be seen in the Fig. 5.14, the chloride concentration in the water reservoir becomes equilibrium state with respect to time. Additionally, the chloride concentration in the water tank in equilibrium state is found to be proportional to the chloride content in the ash. A material balance at this time is shown in Fig. 5.15. The concentration of chloride contained in the ashes in equilibrium did not change before and after entering the water tank. This phenomenon could also be applied for heavy metal analysis, provided that the heavy metals do not precipitate in the water bath.

Fig. 5.16 indicates the changes of the chloride concentration in the water reservoir when sending a certain quantity of water to CDI ion removal system and removing a certain amount of chloride from the feed water, a water-soluble chloride contained in ash indicated the amount of 1 %, equivalent to 36 kg/day (1,000 mol/day) chloride removal amount. Thus, the equilibrium concentration was reduced to approximately 1/3 as compared in the case without the removal of chloride. Presented in Fig. 5.17, after washing, the water-soluble chloride included in the ash was found to be 0.27 %. If the concentration of the non-soluble chloride was 0.4 % and the total chloride was 0.6 %. Therefore, the chloride concentration in the water bath was about 0.7 %.

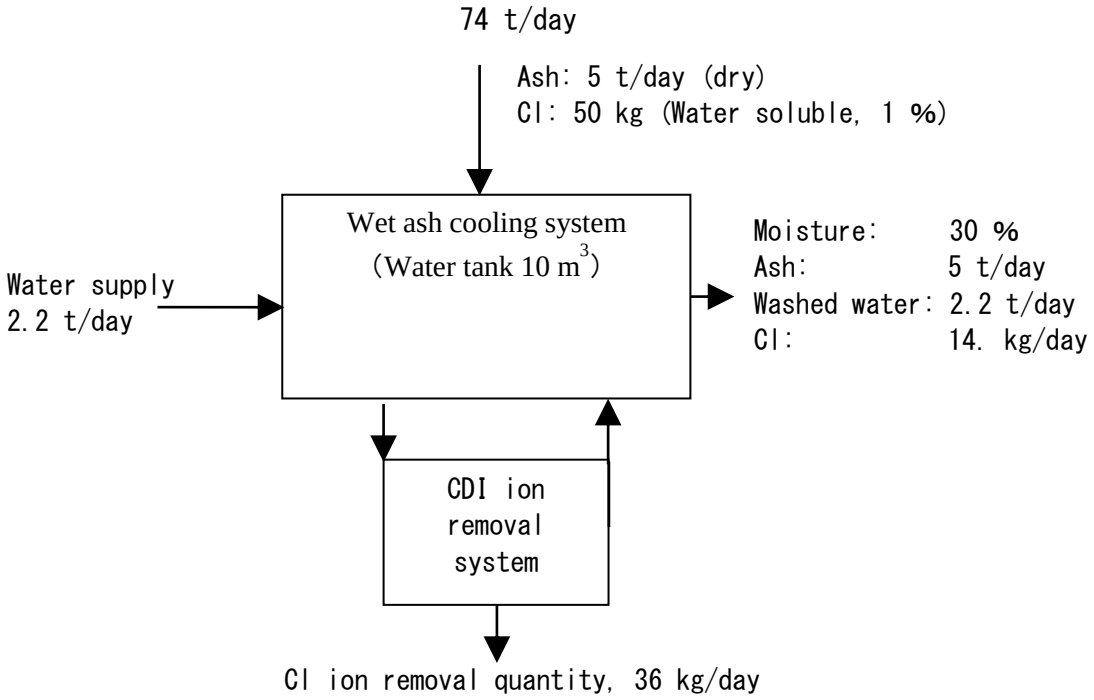

Fig. 5.17 - Material balance at the time of chloride removal.

The details of a material balance when applying a CDI system to an incineration facility with rating capacity of 74 t/day are indicated in Fig. 5.17. Ashes discharged from incinerators will fall into a wet ash-unloading device and cooled in water held in the device. The incineration bottom ash where it containing water moisture of about 30 －40 % is led directly to the ash pit via a conveyor. After removing the solids from the rinsed water using a screen, the water was then led to the CDI ion removal system. Here, a predetermined amount of salts (ions) was removed. Then, the treated water was re-used for another washing process.

For each incinerator having a rating capacity of 37 t/day is equivalent to 2.5 t/day ash (dry) generation. Based on the results obtained from the laboratory experiments, solid:liquid ratio of 1:4 is an enough quantity of water to extract soluble chloride in the ash, therefore the water quantity required was 10 t/day. With 2.5 t/day ash (dry) and the rinsed ash having 30 % water moisture content, the apparent amount of water therefore in the water bath is 1.1 t/day. Consequently, a 1.1 t/day quantity of water is needed to maintain the 10 t/day of water in the water bath, re-circulating the remaining 8.9 t/day to the CDI ion removal system. Furthermore, the chloride ion concentrate produced during the CDI processing could be converted into hypochlorous acid (HClO) for sewage sterilization.

When water-soluble chloride content of incineration bottom ash is 1 % and keeping the chloride concentration of the water bath constant, 0.7 %. A daily chloride ion removal of CDI ion removal system should be 1,000 mol/day so as to maintain the 0.2 % amount of chloride in the rinsed ash.

Table 5.8 – Estimated capital costs and utility costs.

	Expenses	Remarks
Capital costs	20,000,000 JPY	Equipment, pipes and installation costs
Utility costs	140,000 JPY/year	Electricity cost and chemicals

Excluding the maintenance and labor costs as shall be shared with the incineration facility.

The estimated introductory expenses (capital cost) and utility costs are shown in Table 5.8. Using the developed technology, it is possible to control the chloride concentration of the incineration ash. If the production cost of cement raw material could be reduced from 25,000 to 15,000 JPY/ton, the cost reduction of 20,160,000 JPY a year could be achieved. Accordingly, it is possible to recover both building expenses and the utility cost in a span of 1 year.

5.3.7 Using incineration bottom ash and fly ash

When both incineration bottom ash and fly ash were considered for washing and dechlorination process with incinerator rating capacity of 74 t/day shown in Fig. 5.19. The bottom ash and fly ash were washed separately. The fly ash generation rate including other chemicals is 1.8 t/day and having a chloride content of 10 %. Therefore, the mass of chloride will be 1.8 t/day x 10 % = 180 kg/day. Obviously, the ratio of the chloride concentration of the fly ash to that of the bottom ash is about 1-fold higher, where the chloride concentration of the bottom ash in the water tank is 1.1 %. If the fly ash having 50 % moisture content, the amount of chloride removed from fly ash was 1.8 t/0.5 x 0.5 x 0.011 = 0.02 t = 20 kg. Therefore, the amount of chloride which should be removed from the fly ash washing water is 180 - 20 = 160 kg/day, 160/35.5 x 1,000 = 4,507 mol/day (188 mol/h). Furthermore, it is economically desirable if the bottom and fly ashes could be processed in the same cement plant wherein the chloride concentrations of both ashes are comparable. Hence, if the chloride concentrations of both ashes are at the same degree where the chloride concentration of the water reservoir is 1.1 %. Therefore, the required chloride removal of the washed water in the water tank is 26 kg/day, corresponding to 26/35.5 x 1,000 = 732 mol/day (30.5 mol/h). Details for the material balance are indicated in Fig. 5.17. Moreover, heavy metal treatment by condensation precipitation processing is needed in addition to the installation of washing wastewater of fly ash. When we assumed that it is proportional to the chloride removal amount to the capital costs and utility costs,

which is estimated to be 100,000,000 JPY and about 700,000 JPY, respectively.

The above study is a consideration for a water spray type waste incineration facility, and the application to a boiler system waste incineration facility is also possible, we assume that the wastewater from CDI system could be used for cooling towers or could be dispose the wastewater into a waste drainage for further treatment to an existing wastewater treatment facility.

The proportionality ratios of washing water to incineration ashes were evaluated. The design and implementation of washing process to the actual incineration facility are attributed with its advantages and cost effectiveness and impact to society was systematically elaborated. With the involvement of cement companies, national and local government, this research and development will be possible. The engineering data they provided helps the analysis of the present study more accurate and reliable. We hope that in the near future, the present study could be a useful tool for further research and development. The analysis of the present study suggests that the fabricated CDI system could treat and control the ionic species present in the incineration ash wastewater.

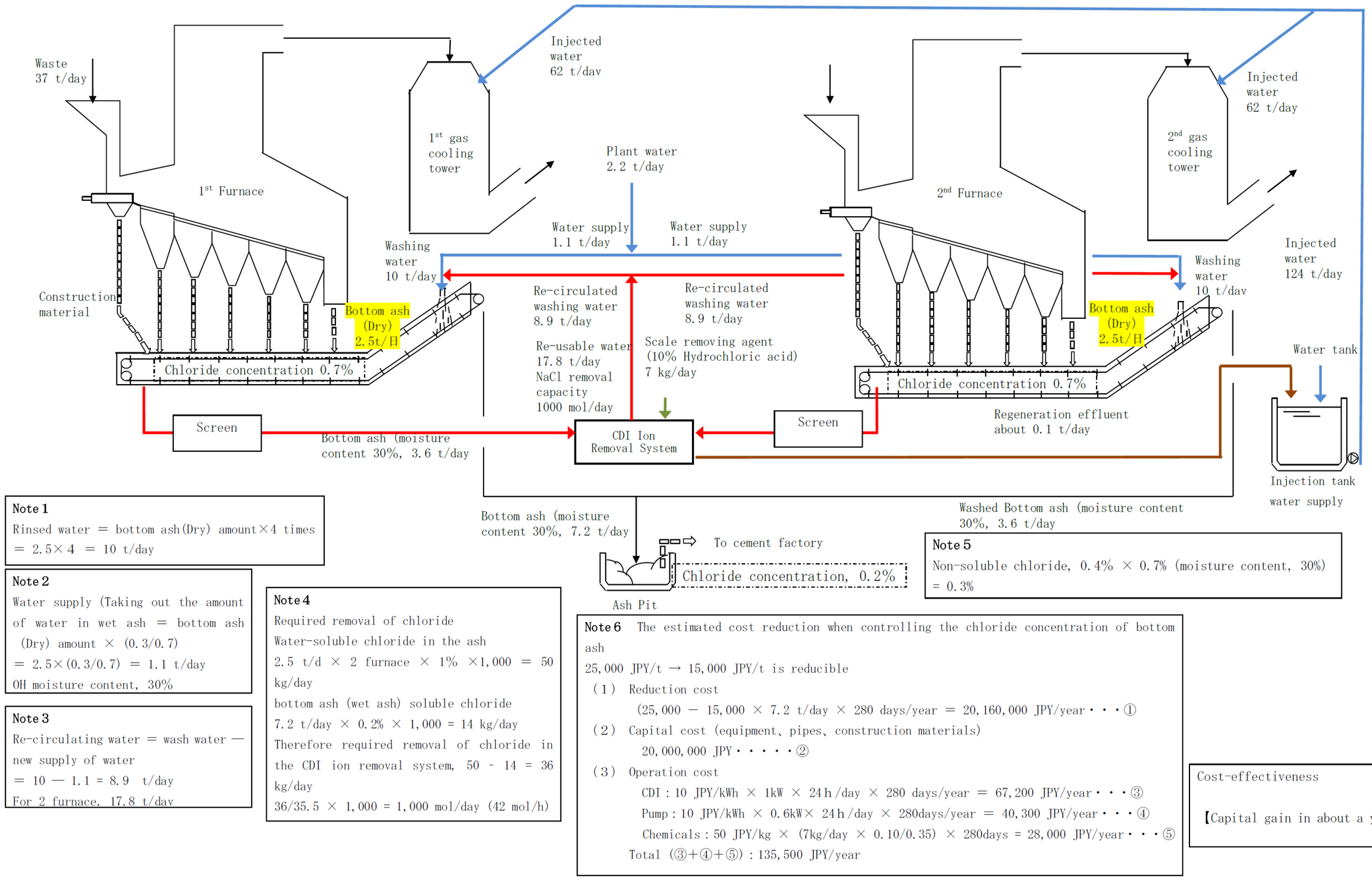

Note 1
Rinsed water = bottom ash(Dry) amount×4 times
= 2.5× 4 = 10 t/day

Note 2
Water supply (Taking out the amount of water in wet ash = bottom ash (Dry) amount × (0.3/0.7)
= 2.5×(0.3/0.7) = 1.1 t/day
OH moisture content, 30%

Note 3
Re-circulating water = wash water — new supply of water
= 10 — 1.1 = 8.9 t/day
For 2 furnace, 17.8 t/day

Note 4
Required removal of chloride
Water-soluble chloride in the ash
2.5 t/d × 2 furnace × 1% ×1,000 = 50 kg/day
bottom ash (wet ash) soluble chloride
7.2 t/day × 0.2% × 1,000 = 14 kg/day
Therefore required removal of chloride in the CDI ion removal system, 50 - 14 = 36 kg/day
36/35.5 × 1,000 = 1,000 mol/day (42 mol/h)

Note 5
Non-soluble chloride, 0.4% × 0.7% (moisture content, 30%) = 0.3%

Note 6 The estimated cost reduction when controlling the chloride concentration of bottom ash
25,000 JPY/t → 15,000 JPY/t is reducible
（1） Reduction cost
(25,000 — 15,000 × 7.2 t/day × 280 days/year = 20,160,000 JPY/year・・・①
（2） Capital cost (equipment、pipes、construction materials)
20,000,000 JPY・・・・・②
（3） Operation cost
CDI：10 JPY/kWh × 1kW × 24h/day × 280 days/year = 67,200 JPY/year・・・③
Pump：10 JPY/kWh × 0.6kW× 24h/day × 280days/year = 40,300 JPY/year・・・④
Chemicals：50 JPY/kg × (7kg/day × 0.10/0.35) × 280days = 28,000 JPY/year・・・⑤
Total (③+④+⑤)：135,500 JPY/year

Cost-effectiveness
【Capital gain in about a year】

Fig. 5.18 – An example of bottom ash waste incineration facility (Incineration capacity, 37 t/day x 2 furnace)

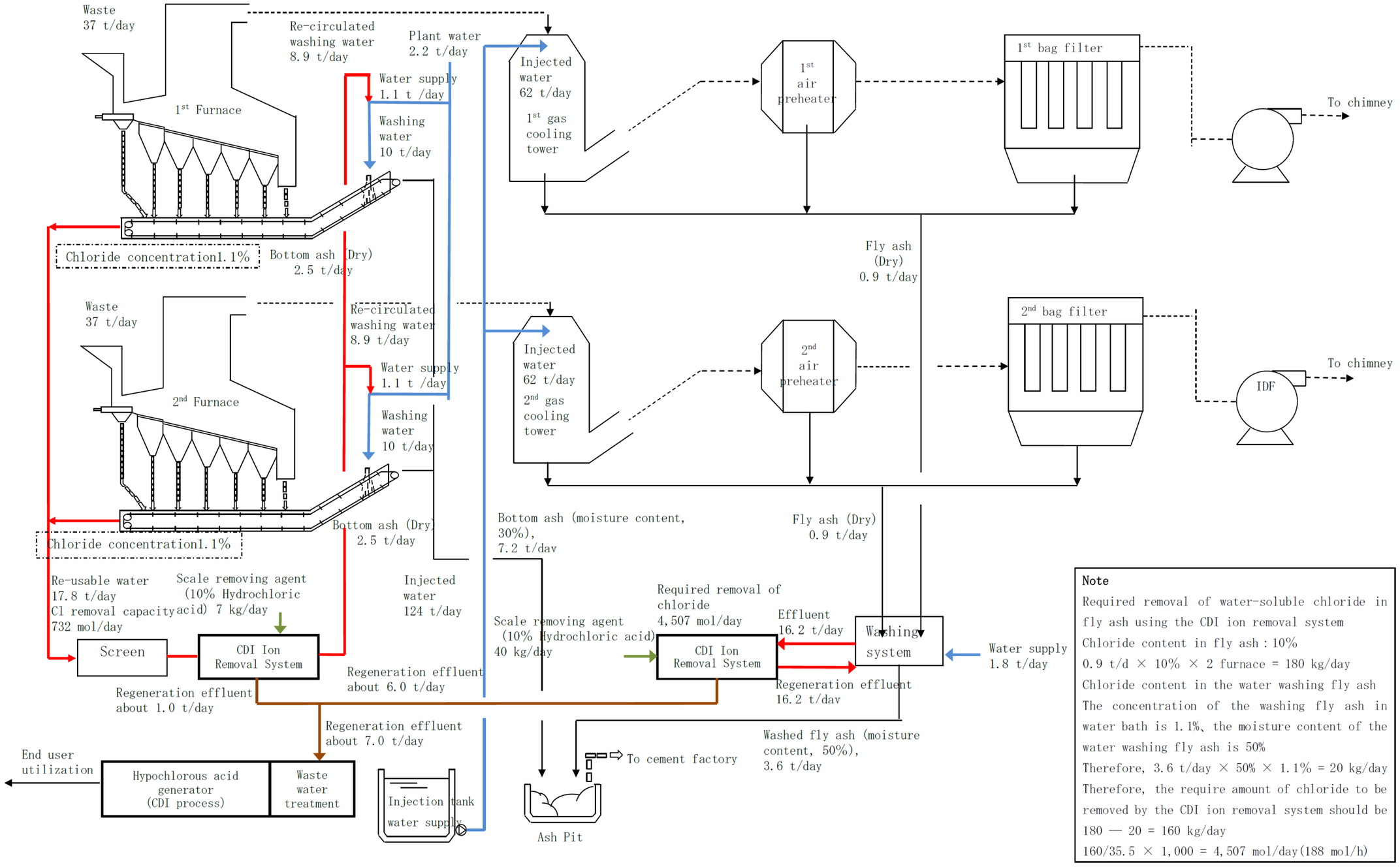

Fig. 5.19 – An example of bottom ash and fly ash waste incineration facility (Incineration capacity, 37 t/day x 2 furnace)

References

1. Andres G. L., Yano N., Shiyoukei Y., Yoshihara Y. and Tanahashi M. (2014) *Journal of Water and Environment Technology*, **12**(3), 261-276.
2. Japanese Standards Association (2010) Methods for chemical analysis of cements (JISR5202). Japanese Standards Association, Tokyo, Japan. (in Japanese).
3. Japanese Standards Association (2012) Methods of test for chloride ion content in hardened concrete (JISA1154). Japanese Standards Association, Tokyo, Japan. (in Japanese).
4. Ito R., Dodbiba G., Fujita T. and Ahn J. W. (2008) *Waste Management*, **28,** 1317-1323.
5. Lee J. H., Bae W. S. and Choi J. H. (2010) *Desalination*, **258**(1-3), 159-163.
6. Andres G. L., Tanahashi M., Tanahashi S. and Yoshihara Y. (2014) *Journal of Chemical and Pharmaceutical Research*, **6**(8), 118-124.
7. Andres G. L., Shiyoukei Y., Yoshihara Y. and Tanahashi M. (2013) *Sustainability of Water Resources and Environmental Solutions to Climate Change*, Philippine Water Works Association, March 20-22, 2013, Manila, Philippines, pp. 98-104.
8. Andres G. L., Yano N., Shiyoukei Y., Yoshihara Y. and Tanahashi M. (2013) *The 5th IWA-ASPIRE Conference and Exhibition*, International Water Association, September 8-12, 2013, Daejeon, South Korea, 09A3-1.
9. Yano N., Nakajima T, Andres G. L., Ando Y., Yoshihara Y. and Mukai A. (2014-2) *The 35th National City Cleaning Meeting*, pp.148-150. *(in Japanese)*
10. Yoshimasa A., Andres G. L., Yano N., Okuda T., Yoshihara Y. and Mukai A. (2013) *The 24th waste resource management society research presentation meeting*, pp.255-256. *(in Japanese)*

CHAPTER 6

SUMMARY AND CONCLUSIONS

Activated charcoal-based carbon electrodes were fabricated and evaluated. The developed carbon electrodes possessed high hydrophilic properties and high mechanical strength. For effective capacitive deionization, an asymmetrically paired capacity carbon electrode was determined to be ideal. Consequently, electrochemical reaction between the electrode and the electrolyte interface was prevented, effectively utilizing the supplied potential. For the developed electrodes, a suitable thickness ratio (δ_{anode}: $\delta_{cathode)}$ was 2.5:1. The hydrophilic property of the carbon electrode was enhanced by chemical modification.

In this study, we investigated the ion adsorption performance of the fabricated CDI stack system with regard to its polar circuit connections. It is revealed that the CDI stack having bi-polar connection shows more favourable capacitive deionization performance in comparison with the CDI stack with uni-polar connection. Although there is minimal difference in the ion adsorption performances of the connections, it was confirmed that the energy consumption with the bi-polar connection was 70 % less than the uni-polar one. This is because the bi-polar connection could be operated in a shorter period of time.

Considering the practical point of view and for optimization of the capacitive deionization process, various processing conditions were used and their effects on the CDI stack ion adsorption performance were examined. It is found that a combination of batch and flow-through processing is the ideal operation in the capacitive deionization process. In addition, the manufactured CDI stack has proven its ability and flexibility when used in different operations without degradation of its capacity, indicating a long electrode life cycle. Moreover, activated charcoal electrodes are reproducible and can be utilized according to the purpose of this research.

The energy recovery experiment, in contrast to other published papers, was not focused on the energy requirement for desalination but rather on the energy recovery processing of the CDI system. To regulate the energy recovery process, different circuit switching sequences was used. The energy recovery by discharging the stored energy of the ion desorbing electrode pair to another pair for ion adsorption by switching four-CDI cells for both the discharge and the charge sides was 81 % at the maximum. Slight discrepancies between the energy recovery ratio and the ion adsorption recovery ratio were observed. The discrepancies can be attributed largely to ohmic resistance of the CDI system and voltage drop caused by abrupt circuit conversion using the SSR, which controls the circuit switching.

Our paper demonstrates, for the first time, how the sequestered energy of the charge cells could be effectively reused for another ion adsorption process by controlling the circuit sequence of the CDI system. The energy recovery process we describe in this study can be a useful guide in optimizing the operation of a CDI device. While improvements on the operating conditions for the effective capacitive

deionization process are required, the results of these experiments prove that the developed activated charcoal-based electrode could be used to reduce or control the ion species present in the ionic electrolyte. The proportionality ratio of rinse water to incineration bottom ash was evaluated. Although there were several other ions present in the bottom ash, sodium and chloride ions were abundant. The analysis suggests that the fabricated CDI system could be used to treat or control the concentration of the ionic species present in the incinerator ash wastewater.

ACKNOWLEDGEMENTS

My sincere thanks and appreciation to all the persons and institutions who made this study possible. A special word of appreciation to the following:

- My Heavenly Father that blessed me with the capability to complete this study.
- Prof. Yoshihara Yoshinobu for his patience and encouragement to complete this research.
- To my mother, Erlinda and father, Gerardo – this work is dedicated to you.
- To my wife, Abigail Cid-Andres and my daughters, Sophia Sachi Andres and Kaoru Yzabelle Andres – you were my inspiration.
- To my teammates, Yuki Shiyoukei, Nobuyuki Yano, Hiroyuki Nakajima, Yoshimasa Ando and Kosuke Ito for the exchange of ideas and hard work in completing this research.
- To my labmates, all Yoshihara-lab students especially to Nobuyuki Higa and Shoin Fujiwara.
- To all my friends in Japan who helped me- Kyoto Association of Pinoy Scholars, my host family and my International Student Batchmates.
- To Ritsumeikan University Graduate School of Science and Engineering and Foreign Student Division.
- To President Masakazu Tanahashi for accepting me as an intern to his company.
- To Dainen Corp. for providing the activated carbon powders and instruments.
- To Kankyosho (Japan Ministry of Environment) for the grant and financial support for my doctoral study in Japan.
- To all people who helped me whom I may forget to mention.

Thank you very much

Ginno